



**Michigan
Technological
University**

Michigan Technological University
Digital Commons @ Michigan Tech

Dissertations, Master's Theses and Master's Reports

2018

FIRST-PRINCIPLES INVESTIGATION OF THE INTERFACIAL PROPERTIES OF BORON NITRIDE

Kevin Waters


Michigan Technological University, kwaters@mtu.edu

Copyright 2018 Kevin Waters

Recommended Citation

Waters, Kevin, "FIRST-PRINCIPLES INVESTIGATION OF THE INTERFACIAL PROPERTIES OF BORON NITRIDE", Open Access Dissertation, Michigan Technological University, 2018.
<https://digitalcommons.mtu.edu/etdr/760>

Follow this and additional works at: <https://digitalcommons.mtu.edu/etdr>

 Part of the [Biological and Chemical Physics Commons](#), and the [Quantum Physics Commons](#)

FIRST-PRINCIPLES INVESTIGATION OF THE INTERFACIAL PROPERTIES
OF BORON NITRIDE

By

Kevin Waters

A DISSERTATION

Submitted in partial fulfillment of the requirements for the degree of

DOCTOR OF PHILOSOPHY

In Physics

MICHIGAN TECHNOLOGICAL UNIVERSITY

2018

© 2018 Kevin Waters

This dissertation has been approved in partial fulfillment of the requirements for the Degree of DOCTOR OF PHILOSOPHY in Physics.

Department of Physics

Dissertation Advisor: *Dr. Ravindra Pandey*

Committee Member: *Dr. Ranjit Pati*

Committee Member: *Dr. Max Seel*

Committee Member: *Dr. Loredana Valenzano*

Department Chair: *Dr. Ravindra Pandey*

Contents

List of Figures	xi
List of Tables	xxiii
Acknowledgments	xxvii
List of Abbreviations	xxix
Abstract	xxxiii
1 Introduction	1
1.1 Overview	1
1.2 Nanomaterials	2
1.2.1 0-D Materials	4
1.2.2 1-D Materials	5
1.2.3 2-D Materials	7
1.3 Predictive Power	9
1.4 Applications	13
1.4.1 Toxicity	14

1.4.1.1	Experimental Research	15
1.4.1.2	Theoretical Investigations	17
1.5	Conclusion	18
2	Methodology	21
2.1	Theoretical Foundation	22
2.2	Schrödinger Equation	23
2.3	Approximations	26
2.3.1	Born-Oppenheimer Approximation	26
2.3.2	Independent-Electron Approximation	27
2.3.3	Slater Determinants	28
2.3.4	Hartree-Fock Approximations	30
2.3.5	Post-Hartree-Fock Methods	33
2.4	Roothaan-Hall Equations	33
2.5	Basis Sets	34
2.5.1	LCAO Type Orbitals	35
2.5.2	Plane-Wave Basis	37
2.5.2.1	Pseudopotentials	39
2.6	Density Functional Theory	40
2.6.1	Thomas-Fermi Model	41
2.6.1.1	Thomas-Fermi-Dirac Model	44
2.6.2	Hohenberg-Kohn Theorems	44

2.6.3	Kohn-Sham Equations	46
2.7	Functionals	47
2.7.1	Local Density Approximations	48
2.7.2	Generalized Gradient Approximation	48
2.7.3	Hybrid Methods	49
2.7.4	Jacob's Ladder	50
2.8	Variational Principle	52
2.9	Add-ons	54
2.9.1	van der Waals Corrections	54
2.9.2	Solvent Model	55
3	Boron Nitride	57
3.0.1	Nanotube Chirality	59
3.0.2	Computational Details	62
3.0.3	Pristine Boron-Nitride	63
3.0.3.1	Periodic Model	63
3.0.3.2	Cluster Model	67
3.0.4	Defects	69
3.0.5	Defect Investigation	71
4	Stability and Electronic properties of of Gold Quantum Dots on Boron Nitride Nanotubes	79
4.1	Introduction	80

4.2	Computational Details	81
4.3	Results and Discussion	82
4.3.1	Au _n Clusters	82
4.3.2	Supported Au Clusters: 2D-Au _n and 3D-Au _n clusters on h-BN monolayer	87
4.4	Summary	91
5	Amino Acid Analogue-Conjugated BN Nanomaterials	93
5.1	Amino Acids and Proteins	94
5.2	Conjugated Systems	100
5.3	BNNT with Amino Acids	103
5.4	Computational Model	106
5.5	Results & Discussion	111
5.6	Summary	120
6	AIMD Investigation of Boron Nitride Nanotubes	123
6.1	Introduction	124
6.2	Computational Details	125
6.3	Results and Discussion	126
6.4	Summary	131
7	Stability, Elastic and Electronic Properties of a novel BN₂ sheet with extended hexagons with N-N bonds	133

7.1	Introduction	134
7.2	Computational Model	136
7.3	Results and Discussion	142
7.3.1	Monolayer	142
7.3.2	Stability	144
7.3.3	Electronic Properties	146
7.3.4	Elastic Properties	148
7.3.5	Bilayer	151
7.4	Summary	152
8	Conclusion	153
	References	157
A	Bra-ket Notation	217
B	Units	219
B.1	Unit Conversions	219
B.2	Atomic Units	220
C	List of Selected Publications	223
D	Permission for Chapter 4 Manuscript	227
E	Permission for BN2 Manuscript	229

List of Figures

2.1	The real wave function (blue) and the pseudopotential (red) in the potential of a nucleus (Z/r). The wave functions will match at a point r_c . The smooth of behavior near the center of the nucleus reduces the needed cutoff energy for the plane-wave basis set. The image taken from Wikipedia [357]	41
2.2	A flow chart visualizing the self-consistent-field iterative process that implements the variational principle for a density functional theory calculation. An initial density is calculated, from which the total energy exchange-correlation energy will be calculated. Then the Kohn-Sham matrix is calculated followed by diagonalized through which updated wave function coefficients are obtained. The new density and then energy are calculated, if it is within a determined threshold it iterative process is terminated. Repeat until convergence is achieved.	53

2.3 The long-ranged dispersion energy correction (Grimme-D2) vs distance for carbon-carbon, nitrogen-nitrogen, carbon-nitrogen and neon-neon interactions. Equation was used along with the values in reference [111]. The C_6 is traditionally given in units of Jnm/mol , but they were converted to give the final units in eV. 56

3.1 A sheet of h-BN with the lattice vectors of the unit cell, \vec{a}_1 and \vec{a}_2 , where both are equal to 2.50 Å. The sheet can be rolled up with the labeled hexagons to form the corresponding (n,m) nanotube. The zig-zag nanotube have a chiral angle of 0° , so for a (7,0) nanotube only the strip of (n,0) is needed. For an arm-chair nanotube a chiral angle of 30° is needed, for reference, the angle between \vec{a}_1 and \vec{a}_2 is 60° . . 60

3.2 The band gap of selected zig-zag (n,0) and armchair (n,n) nanotubes. The gray area covers nanotubes sizes that have not yet been observed. The smallest sized that has been observed has a radius of around 7.5Å[175]. The arm-chair nanotubes all have indirect gaps and the most of zig-zag nanotubes and h-BN have a direct gap 3.4. 65

3.3	The strain energy (top) and average bond length (bottom) of selected zig-zag (n,0) and armchair (n,n) nanotubes. The gray area covers nanotubes sizes that have not yet been observed. The smallest sized that has been observed has a radius of around 7.5Å[175]. The strain energy is defined by the difference in energy from a pristine monolayer of h-BN (Equation 3.5). As the radius of the nanotube decreased the bond lengths increase and bonds tend toward a sp ₃ configuration.	66
3.4	The band structures and projected density of states (PDOS) and total density of states (TDOS) of the unit cell of h-BN, where s(blue), in-plane p _x and p _y (green), out-of-plane p _z (blue) and total(grey) are shown.	67
3.5	The boron nitride cluster (with 5 concentric rings), it contains 75 boron (green) atoms 75 nitrogen (white) atoms and 30 hydrogen (tan) atoms passivating the edges.	68
3.6	The HOMO-LUMO gap (eV) is given for the cluster approximations of boron-nitride monolayer. The smallest ring (borazine) with 12 atoms and the largest is constructed of eight rings consisting of 432 atoms. The corresponding periodic calculations are done with VASP and are given as solid lines.	69

3.7 The unit cells used to calculate the formation energies for the vacancies for boron. A similar structure was used to calculate the nitrogen vacancies, but the boron (green) and nitrogen (white) atoms were switched. The concentrations are 3% (1 of 32 total atoms), 6% (1 of 16), and 12% (1 of 8). The black outline is the shape and size of the unit cell. 73

3.8 The projected density of states (PDOS) and total density of states (TDOS) of the different concentrations of boron vacancies of h-BN, top plots are the PDOS projected onto the atoms (boron (red), nitrogen (blue) and total(grey)), the bottom is the PDOS projected on the orbitals where s(blue), p(green), d(blue) (none in the system) and total(grey) are shown for both spin-up and down. 76

3.9 The projected density of states (PDOS) and total density of states (TDOS) of the different concentrations of nitrogen vacancies of h-BN, top plots are the PDOS projected onto the atoms (boron (red), nitrogen (blue) and total(grey)), the bottom is the PDOS projected on the orbitals where where s(blue), p(green), d(blue) (none in the system) and total(grey) are shown for both spin-up and down. 77

3.10	A series of cartoons given to present the cluster model structures and bond lengths of the localized effects of the defects, the boron atoms are red and nitrogen atoms are blue. All defects were generated in a pristine BN finite model with 180 atoms (75 boron, 75 nitrogen, 30 hydrogen) (top left) and the same cluster with a boron-nitrogen bond rotated by 90° (top right) in the center of the cluster created a 5-7-7-5 Stone-Wales defect and a defected BN cluster formerly of 180 atoms with a boron vacancy (bottom left) and a nitrogen vacancy (bottom right) representing possible defects.	78
4.1	Calculated structural configurations of the isolated Au ₆ , Au ₁₀ , Au ₁₂ , Au ₁₄ and Au ₁₆ clusters. The top 5 are the 2D structures and the bottom 5 are the 3D structures.	84
4.2	The total energy/atom as a function of cluster size (n). The plot indicates that after about nine atoms the 3D structures are more stable than the 2D structures when they are isolated. The 2D structures are given in red (squares) and the 3D structures are given in blue (circles).	85
4.3	A top view of the equilibrium configuration of the supported 2D-Au ₆ cluster.	88
4.4	A side view of the equilibrium configurations of the supported 3D-Au _n clusters.	88

4.5	Supported Au_n clusters: Variation in the binding energy/Au atom as a function of cluster size, n. The 2D structures are given in red (squares) and the 3D structures are given in blue (circles).	89
4.6	Projected density of states (PDOS) and total density of states (TDOS) of the supported 2D- Au_n clusters. Color code: grey-TDOS, red-PDOS of 2D- Au_n cluster, blue-PDOS of h-BN monolayer.	90
5.1	Amino acid table containing 20 proteinogenic α -amino acids with a legend in the bottom right hand corner. The common backbone is in faded gray and the unique R-groups are in black. Each amino acid is grouped, acidic, basic, aromatic, polar and non-polar, by color. The table concept was adapted from a table from bio-connect.nl [18] . . .	95
5.2	Each group in an amino acid has a pK_a associated with it, pK_1 is for the carboxyl group, pK_2 is for the amine group and pK_R is for the R-group. The tiles are colored to represent how acidic (red) or basic (blue) the environment is, with white representing a neutral pH. The labels are inserted between the tiles, because at the specific pH the structures have an equal probability of existing.	97
5.3	An atomic representation of a BSA protein based from experimental x-ray diffraction data.[213] The hydrogen atoms are omitted, missing due to the experimental technique with highlighted each type of amino acids having its own color.	99

5.4	An atomic representation of a BSA protein based from experimental x-ray diffraction data. [213] Each peptide chain in the protein has a unique color, one red and the other blue.	100
5.5	A ribbon representation of a BSA protein, with one peptide chain colored blue and the other red, interacting with several boron nitride nanotubes. For a complete simulation this would also need the additional a large amount of water molecules. This would drastically increase the cost of the simulation.	102
5.6	Chemical structures of the amino acids considered. The first column is the amino acid in its zwitterionic form, followed by the analogues in different protonated states. In the analogues, the backbone is replaced by a $-CH_3$ group.	110
5.7	Cluster models of BN nanomaterials: (left) BNML represented by the $(B_{49}N_{49}H_{22})$ cluster and (right) (5,0) BNNT represented by the $(B_{50}N_{50}H_{10})$ cluster. The cluster edge atoms are passivated with H atoms (atomic symbols: N (blue), B (pink), and H (white)).	111
5.8	Calculated equilibrium configurations of Arg- and Asp-conjugated BNML (atomic symbols: N (blue), B (pink), C (black), and H (white)).	114

5.9	Calculated equilibrium configurations of Arg- and Asp-conjugated BNNT (atomic symbols: N (blue), B (pink), C (black), and H (white)).	115
5.10	Physisorbed vs chemisorbed configurations in the solvated phase: adsorption energy vs near-neighbor distance of amino acid- conjugated BN complexes. The red triangles are the BNML systems and the blue circles are the (5,0) nanotube.	117
5.11	Deprotonated Arg interacting with BNML (left) and (5,0) BNNT (right) in the presence of several water molecules (atoms: H (white), B (pink), C (gray), N (blue), and O (red)).	118
6.1	The last snapshot of the AIMD simulation containing a (5,0) boron nitride nanotube with water molecules surrounding it. The simulation cell has periodic boundary conditions implemented, leading to an infinite tube. The small radius tube has large amount of strain leading to the hydrolyzation of the nanotube as seen by formation of chemical bonds with water.	127

6.2	The last snapshot of the AIMD simulation containing a (8,0) boron nitride nanotube with water molecules surrounding it. The simulation cell has periodic boundary conditions implemented, leading to an infinite tube. Due to the solvation conditions some water molecules are present on the inside of the nanotube for the large size nanotube. The small radius tube has large amount of strain leading to the hydrolyzation of the nanotube as seen by formation of chemical bonds with water.	128
6.3	The last snapshot of the AIMD simulation containing a monolayer h-BN sheet with water molecules surrounding it. The simulation cell has periodic boundary conditions implemented, leading to an infinite sheet. The flat surface reduces any strain to zero and the hydrolyzation of the sheet nanotube does not occur, all of the water interactions are long-ranged.	129
6.4	The density of water for a QM/MM model where the substrate, boron-nitride, is treated with DFT and the water molecules are simulated using the SPC/E potentials.	130
6.5	The density of water for AIMD calculations, the peaks around two Å are water molecules bonding to the surface of the (5,0) and (8,0) nanotube.	131

7.1	The structure of BN_2 (Top left). The unit cell consisting of two B atoms (red) and four N atoms (blue) is outlined with the dashed (-) lines. The lattice parameters, bond lengths and bond angles together with Bader charges on each atom are also listed (Table 7.1). Directions for the applied strain ϵ_{11} and ϵ_{22} are shown. The AA stacked bilayer structure (Bottom) is shown with the interlayer distance (c) of 3.17 Å.	144
7.2	Charge density of BN (left), BN_2 (middle), graphene (right) with an isovalue = 0.2e. The metallic, graphene and BN_2 structures show a delocalized electronic cloud as opposed the localized electronic cloud of the semiconducting h-BN	145
7.3	Calculated phonon dispersion (Left) and the associated phonon density of states (Right) of BN_2	147
7.4	Calculated band structure and density of states of the BN_2 monolayer. (Left) orbital projected Color code: blue- s states, green -in-plane p_x and p_y states, blue - out-of-plane p_z states, grey- total density of states. (Right) atomic projected Color code: blue - $N_{1,3}$ states, green - $N_{2,4}$ states, red-B states, and grey- total density of states.	148

7.5 Calculated band structures and density of states of the AA BN₂ bilayer.

(Left) orbital projected Color code: blue- s states, green- in-plane p_x and p_y states, blue: out-of-plane p_z states, grey-total density of states.

(Right) atomic projected Color code: blue - N_{1,3} states, green- N_{2,4} states, red- B states, grey - total density of states. 152

List of Tables

2.1	Selected values of the C_6 ($eV \text{ \AA}^6 / atom$) parameters and the R_0 (\AA), the vdW radii, for the D2 vdW corrections used in this work. The values are taken from the original publication [111] and converted to units below, the Au values were taken from the VASP 5.3.5 source code.	55
3.1	Chirality and diameters of nanotubes that were considered in the initial investigation. The diameters were calculated using Equation 3.3 with a lattice vector magnitude of $a = 2.50 \text{ \AA}$.	61
3.2	Cluster models generated to model a periodic boron nitride monolayer. The clusters contain n concentric rings that create 2-D hexagonal flake shapes, an example is shown in Figure 3.5.	68
3.3	Formation energies of a monolayer of h-BN and a (10,0) nanotube. The formation energies are calculated in a B-rich and N-rich environment as explained in the text.	72
3.4	Formation energies for defects in a periodic sheet of boron nitride, where the following values were used $\mu_B = -6.65 \text{ eV}$, $\mu_N = -8.32 \text{ eV}$, and $\mu_{BN} = -17.58 \text{ eV}$.	74

3.5	The magnetic moment and band gap for the h-BN sheet with 3%, 6% and 12% vacancies of either boron (V_B) or nitrogen (V_N).	74
4.1	Calculated structural properties of the isolated and supported 2D Au_n clusters.	86
4.2	Calculated structural properties of the isolated and supported 3D Au_n clusters.	86
4.3	Supported Au clusters: the nearest distance between the cluster atom and h-BN monolayer (R_{Au-BN}) and the binding energy/Au atom (B.E/Au).	87
5.1	Amino Acid-Conjugated BN Nanomaterials in the Solvated Phase: Adsorption Energy ($E_{ads.}$), Nearest-Neighbor (N.N.) Distance, Mulliken Charge Transfer (ΔQ), and Dipole Moment (D.M.) Obtained Using the Polarizable Continuum Model (PCM) at the DFT (PBE-D2) Level of Theory	113
7.1	The calculated lattice parameters of graphene, h-BN, BN_2 and bilayer BN_2 . Due to symmetry graphene and h-BN have reduced unique parameters. The Atom/Bond/Angle numbers correspond to Figure 7.1. The interlayer distance for the bilayer is 3.17 Å.	146

7.2	Calculated elastic constants (C_{xx}), in-plane Young's modulus defined in Equation 7.10 ($E_{arm/zig}$), and Poisson's ratio (ν) defined in Equation 7.12 for graphene and monolayers of h-BN and BN ₂ . C_{66} is computed using strain and stress data. Units are in N/m, except for ν which is unitless. 1) [353] 2) [258]	149
B.1	Common conversions for units of energy in chemistry and physics. The values were obtained from the Atoms and Molecules by Karplus and Porter [162]	219
B.2	Description of the four fundamental constants of Atomic Units (set to unity) and their SI equivalent. Many sources are available, but this table was adapted from Wikipedia.[356] with the units significant figures reduced to the third decimal place. all other Atomic units can be derived from the stated changes in value.	221

Acknowledgments

The work that has been done in this dissertation rests on a foundation that has been laid by a few revered celebrities and countless individuals whose names have been forgotten. Everyone of us has within us a contribution to weave into the tapestry of the human experience. Each thread is a lifetime filled with failures and mistakes decorated with islands of success. Without the blues and the blacks there cannot be contrast to the yellows and greens. To everyone that has chosen to be a part of my life, I hope I was able to bring as much color to your life as you have brought to mine. As this chapter of my life closes, all I can do is embrace the future and leave with gratitude.

Thank you.

List of Abbreviations

AIMD	Ab Initio Molecular Dynamics
BN	Boron-Nitride
BNML	Boron-Nitride Monolayer
BNNT	Boron-Nitride Nanotubes
B3LYP	Becke, three-parameter, Lee-Yang-Parr
BSA	Bovine Serum Albumin
BSSE	Basis Set Superposition Error
CBM	Conduction Band Minimum
CNT	Carbon Nanotube
CGTO	Contracted Gaussian Type Orbitals
CPU	Central Processing Unit
DNA	Deoxyribonucleic Acid
DFT	Density Functional Theory
eV	Electron Volts
GGA	Generalized Gradient Approximation
GTO	Gaussian Type Orbitals
h-BN	Hexagonal Boron-Nitride

HOMO	Highest Occupied Molecular Orbital
HSE06	Heyd-Scuseria-Ernzerhof
LCAO	Linear Combination of Atomic Orbitals
LDA	Local Density Approximation
LUMO	Lowest Unoccupied Molecular Orbital
MD	Molecular Dynamics
ML	Monolayer
NBO	Natural Bond Orbitals
NT	Nanotube
PAW	Projected Augmented-Wave
PBE	Perdew-Burke-Ernzerhof
PDOS	Projected Density of States
PCM	Polarizable Continuum Model
pH	Potential of Hydrogen
pKa	Acid Dissociation Constant
QM	Quantum Mechanics
QMMM	Quantum Mechanics/ Molecular Mechanics
RPA	Random Phase Approximation
RNA	Ribonucleic Acid
SCF	Self-consistent-field

STO Slater-type Orbitals
TDOS Total Density of States
VASP Vienna Ab-initio Simulation Package
VBM Valence Band Maximum
vdW van der Waals

Abstract

The interactions of nanomaterial surfaces with biological compounds, e.g. proteins, DNA, etc., unites the biological regime and nanomaterial world. Hybrid systems of boron-nitride nanotubes (BNNTs) and biological compounds are well-suited for a broad range of applications. First-principles methods are used to characterize the interface of these hybrid systems. Previous work has shown that the sensing capabilities of pristine BNNT are limited by long-ranged interactions. In this study the surfaces of pristine and functionalized BNNTs are investigated. The surfaces of the functionalized BNNTs give new properties to the tubes, which may enhance their sensing capabilities, while retaining their stability and chemical inertness. These simulations provide a fundamental understanding of these interaction. During the course of the investigation, two related projects were pursued.

The first tangent characterized a new material that was found during the investigation of defects of BNNTs. The material is a B-N monolayer material (BN_2) consisting of a network of extended hexagons. The distinguishable nature of the 2-D material is the presence of bonded N atoms (N-N) in the lattice. Analysis of the phonon dispersion curves suggests this phase of BN_2 to be stable. The calculated elastic properties exhibit anisotropic mechanical properties that surpass graphene in the armchair direction.

The second project investigated the effects of boron nitride substrates on the properties of gold clusters. Experimentalists have deposited gold quantum dots onto boron-nitride nanotubes and were interested in a theoretical explanation for the different 2D and 3D structures. For the calculations 2D and 3D, Au₆, Au₁₀, Au₁₂, Au₁₄ and Au₁₆ clusters were selected. Their properties were analyzed in a free-standing configuration and on a substrate of h-BN.

Chapter 1

Introduction

1.1 Overview

Nanomaterials have been the subject of research since the 1960s however, since the discovery and synthesis of C_{60} [184] the field has come center stage. Researchers are predicting new materials, discovering new methods of synthesis and finding novel applications on a daily basis. A prime example of the rapid rate of research and publication in the nanomaterials realm is graphene. In 2013 it was shown that there were about 9000 articles published[271] since the original experimental announcement in 2004[243]. With this speed of innovation, studies investigating the risks of these new materials to our health and environment are falling behind. [125, 279, 366]

1.2 Nanomaterials

A nanomaterials is any material with at least one dimension whose size is in the sub-micron range. At this scale macroscopic laws breakdown and quantum effects dominate. This allows for unique phenomena to be utilized, however, there are additional challenges. Each method of growth, top-down or bottom-up, possesses obstacles. Researchers are trying to achieve consistent growth conditions and mass production.[42] These materials will impact many aspects of society; including the computing[90], construction[190], health care[64], food and agriculture[149] industry.

The use of nanomaterials is not new, but the use of nanotechnology is. The difference being that nanotechnology is the explicit manipulation of atoms to create nanomaterials. Throughout history nanomaterials have been used, but their practitioners did not have the tools needed to understand or manipulate the structures and molecules at the individual atom or molecular level. To date, researchers have discovered their use in weapons and decorative objects.[167, 281]

In the modern era, nanotechnology started in the 1960s[129] with research being conducted on clusters and nanoparticles. Since then, the field has grown from a niche field in physics to a subject that spans biology, chemistry, engineering, material science, medicine, and physics. [42, 282] The popularization can be attributed to

three ground-breaking discoveries, all of which resulted in new carbon based nanomaterials. The materials are the buckminsterfullerene[240], carbon nanotubes[145] and graphene[243]. Carbon nanomaterials are the most studied materials and they catalyzed the next generations variants. Some of the novel materials share similar topologies[154] with different constituent atoms, while others have drastically different atoms, shapes, sizes and properties [217].

The discoveries started with zero-dimensional materials, followed by one-dimensional and then rounded out with two-dimensional materials. The dimensionality of nanomaterials describes not the atoms, but the directions in which electron can travel. Fullerenes, clusters or nanoparticles are molecular, which leads to the localization of electrons within the structure, when the materials are in an isolated environment. Another way to picture this is by looking at the number of directions that the material can be modeled with an infinite amount of images or periodic boundaries. A three dimensional material would not be considered a nanomaterial but would be a "traditional" bulk materials and would not have any dimension in the sub-micron range.

1.2.1 0-D Materials

The initial investigations of clusters were done in the 1960s. The clusters existed in a gas phase and they were only composed of a handful of atoms (≈ 12). [129] It was assumed that the properties of the clusters, if they contained only a few more atoms, would reach the bulk material limits. [129] However, in 1984 two groups discovered that larger clusters (≈ 100) still had properties that deviated from their bulk counterparts. These structures had ordered electronic structures, now called superatoms, that could be predicted and extrapolated to clusters containing thousands of atoms. [78, 79, 172] This lead scientists to believe that the possibilities of cluster were much larger than previously expected.

The best known 0-D material is the buckminsterfullerene (C_{60}). It is the first material of the "big" three and it was discovered in 1985. [184] This project lead to the Nobel Prize being awarded to the lead researchers of the project in 1996 [240] and lead to a research frenzy into fullerenes. [3]

Other notable 0-D structures are; clusters, nanoparticles and quantum dots. At times these names are used interchangeably, which can lead to some confusion. The difference between clusters and nanoparticles is that nanoparticles are metallic leading to plasmonic properties while clusters are semiconducting. Clusters and quantum

dots (large clusters), due to the limited amount of atoms and/or their chemical structures (quantum confinement), the electronic states are discretized leading to semi-conducting behaviors. [323] This leads to unique optical and electronic properties, such as fluorescence and phosphorescence.[370] Clusters (nanoclusters or quantum clusters) tend to be in the range of tens of atoms and under 2 nm. Researchers wish to utilize their physical and chemical properties. However, to utilize them, precise control over the number of atoms must be obtained. [43, 156, 368] Some examples of clusters that have been studied to date include: gold [129, 155, 252, 299, 323, 376], silver[49, 69], copper[106, 152, 351], platinum[308, 329, 333], palladium[81, 144], Their alloys[163, 199, 228] and many others [250].

In the recent decades more 0-D materials have been discovered, predicted and synthesized. [157] More names are invented to describe the topologies, some of these include quantum dots, nanospheres, nanorods, nanofibers, and nanocups.[167] With the search for novel structures, more complex stoichiometries and varying growth conditions have been used to explore the limitless configuration space.[342]

1.2.2 1-D Materials

The structures in one dimension are typically called nanotubes, nanowires[140] or nanoribbons[76], with nanotubes being the traditional and most researched. The

first published discovery of nanotubes was in 1952. Radushkevich and Lukyanovich published images of 50 nm diameter tubes made of carbon in the Soviet Journal of Physical Chemistry.[275] Due to the nature of the political climate during the Cold War and the language barrier, the publication went unnoticed in the West.[229] There have been a few other papers that were published on carbon nanotubes that flew under the scientific radar.[2, 32, 135, 245] In 1991, the paper that started the nanotube craze was published. [145] Iijima, typically is incorrectly given credit for the discovery of carbon nanotubes[229], they used similar techniques that were previously established in the discovery of the C₆₀ fullerene.

A few years later, researchers took this knowledge and predicted a boron and nitrogen analogue to carbon nanotubes. [289] Soon after in 1995, the synthesis of boron nitride nanotubes occurred. [50] Since their discovery many other tubes have been discovered and investigated.[325] Some examples of synthesized nanotubes are boron-carbon-nitrogen nanotubes[375], gallium nitride [103], silicon [56], tungsten disulfide [324] and boron [208, 274].

Nanoribbons, in theory, are analogues to 2-D materials, they are in principal "cut" into ribbons from a periodic 2-D sheet of the material, resulting in a 1-D material. The edge atoms of the ribbons undergo reconstruction with either other edge atoms or they are passivated by external atoms, such as hydrogen fluoride.[150, 280] There has been a keen interest into graphene nanoribbons, due to the edge effects, there is

a finite gap introduced into the material.[211]

1.2.3 2-D Materials

Early investigations into 2-D materials indicated that they were unstable. The instability was suggested to be caused by thermal lattice fluctuations that would occur at any finite temperature. [257]. However, it was known that there were 3-D layered structures that existed, such as graphite, that are only bonded through van der Waals interactions. If one of these layers could be isolated it could be the first 2-D material. There were theoretical investigations into a single layers of graphite dating back to 1984[74], it would take another 30 years to be seen inside the laboratory. In 2004, researchers isolated one layer of graphite (graphene) with simple scotch-tape exfoliation. [243] The simplicity of this method and ground-breaking properties of graphene spurred a massive search for other 2-D nanomaterials.

The leading researchers of the project were awarded the Nobel Prize for their work in 2010. [238] The template for future 2-D materials was established with their work on graphite. Exfoliation methods become more sophisticated and more layered materials started to be isolated.[54, 236]

The time it takes from initial theoretical discovery to synthesis/isolation is shrinking with the latest materials. Hexagonal boron-nitride is a structure similar to graphene.

The structure looks identical, but it is composed of boron and nitrogen pairs instead of carbon. It was predicted in 2006 [359] and then synthesized a few years later [104, 154]. More detail of boron-nitride is given in Chapter 3. For Borophene, it was predicted in 2014 [267] and then synthesized a year later [217]. Other materials that continue this phenomena are silicene [89, 338], phosphorene [203] and germanene [62]. [354] Recent investigations are looking into transition metal oxides and transition metal dichalcogenides, which have type of dual layered structure. [227] They have atoms within each layer are held together by covalent bonds, while van der Waals (vdW) interactions hold the layers together in their bulk phase.

There are also more exotic morphologies that have been proposed from the same atoms that make up the more traditional structures. Some examples for graphene and boron nitride are α -Graphyne/BNyne [248], 6-6-12 Graphyne hetero-structures [214], and Graphdiyne [204]. These materials, theoretically, may also form pentagonal structures, penta-graphene [384], penta-BN and penta-BN₂ [200]. Many of these structures are meta-stable and have not been experimentally investigated or seen, most will probably will not be seen. Materials are now being designed and tailored through theoretical means to maximize certain properties, all before even being seen in the laboratory. An example of this is the recently proposed material Graphamid [296], it was designed to utilize the strength of graphene, but avoid its brittleness.

The possibilities with 2-D materials are limitless. In the past decade numerous new

materials have been predicted and researched. Some examples are NiTe₂ and VSe₂, which are semi-metals, WS₂, WSe₂, MoS₂, MoSe₂, MoTe₂, TaS₂, RhTe₂ and PdTe₂ which are semiconductors and h-BN, and HfS₂ which are insulators. There are even some 2-D materials, NbS₂, NbSe₂, NbTe₂ and TaSe₂, which are superconductors. [227] This is only a small sample of the published materials.

1.3 Predictive Power

There has been a funding push by the US government, that was initiated in 2011, under the administration of President Obama.[107] This project is a multi-agency initiative designed to accelerate the discovery, manufacture and application of advanced materials. The project has invested over \$250 million dollars into R&D, which has spurred many aspects of materials design, one of which is the prediction of materials. [107]

A powerful tool that has enabled this initiative is the growth of computation power. A fundamental component to material prediction is electronic structure theory. It is the foundation of this dissertation and it has lead to a large fraction of publications in materials research. [128] Many other materials methods (molecular dynamics, coarse-grain methods...etc) have grown alongside electronic structure theory. The theoretical foundation was discovered back in the 1920's with the work of Paul Dirac

and Erwin Schrödinger. They were awarded the Nobel Prize in 1933 "for the discovery of new productive forms of atomic theory".[239] Schrödinger greatest work was on the, now named, non-relativistic Schrödinger Equation.[301] Dirac has a similar, but relativistic equation, also named after the discoverer, the Dirac Equation. [70] Both of these equations are wave-equations that, within the correct framework, accurately describe tiny particles (electrons). More discussion is given in the next chapter, is dedicated to the theory.

Already in the 1930's during the theory's establishment, Dirac and others understood that the theoretical framework was "done".[70]

The underlying physical laws necessary for the mathematical theory of a large part of physics and the whole of chemistry are thus completely known, and the difficulty is only that the exact application of these laws leads to equations much too complicated to be soluble. It therefore becomes desirable that approximate practical methods of applying quantum mechanics should be developed, which can lead to an explanation of the main features of complex atomic systems without too much computation.

The topic of computation will only be covered briefly, it is vital aspect to the field and necessary to conduct these studies, but in this dissertation only the scientific conclusions of the work will be discussed. To gain the insights from the established

theory, numerics and computation is needed to solve the many body problem. Two decorated individuals who took up the numerical challenge were Walter Kohn and John Pople. They were awarded the Nobel Prize in 1998 "for his development of the density-functional theory" and "for his development of computational methods in quantum chemistry".[241] Over the last 80 years, due to their work and many others, the theories grew into powerful tools that are now used daily in physics, biology, chemistry, material science, and mechanical engineering. The methods and theories will be outlined in the next chapter, Chapter 2.

In the current paradigm, nation's governments are pushing for supercomputers to break the exascale barrier. [27] Supercomputers with exascale capabilities will enable more involved and complex simulations with more resolution. Researchers are already working on developing the next generation of density functional theory codes for the future computing environment. [344] This dissertation does not delve into the specifics of supercomputers and the tools necessary to utilize them, but they are worth mentioning due to their necessity.

To tackle the large conformational spaces generated by materials and nanomaterials, researchers have designed novel computational methods. These methods look to effectively and efficiently utilize computation power using different searching strategies to predict novel materials. They typically use density functional theory in the back-end as the driver to calculation the energetics, which are then used to determine the

absolute and relative stability of the material. Programs like Calypso [345] and General Utility Lattice Program (GULP) [94] use particle swarm methods optimization to find local minimum structures. Using these methods can reduce the manpower and computation power needed to find the next ground breaking materials.

For material discovery, high-throughput calculations [60, 304] can also be used. Researchers can generate a large batches of structures by following rules and they can calculate all the structure permutations. After the calculations are complete, metrics can be generated that can grade the results. These metrics can be written by researchers themselves or generated by machine learning algorithms. Some groups have taken to machine learning algorithms to reduce the amount of electronic structure calculations necessary.[268] They can utilize data bases and use learning algorithms to construct rules that can extrapolate these to new materials with minimal computation. By creating and using these tools, researchers are fulfilling a part of the the goal of the Materials Genome Initiative ”to discover, manufacture, and deploy advanced materials twice as fast, at a fraction of the cost.”[107] With the progress made in computation power in the recent decades, materials prediction and analysis has become a standard research tool for researchers of all fields.[233]

1.4 Applications

One of the original documented ideas of the impact and possibilities of working at the nanoscale was in 1959. The concept was introduced in a talk to the American Physical Society by Richard Feynman titled "There's Plenty of Room at the Bottom". [88] The lecture predicted two major areas of research that are present in the nanotechnology field today. The first topic was the miniaturization of computers and the second was the use of nanomaterials in the medical field. While there are numerous other fields that have and will be impacted by nanotechnologies, only a few applications pertaining to biology will be covered.

The idea of scaling materials down opens a new realm of possibilities. In his presentation Feynman mentions that biology operates at the nanoscale level. Biology has also been able to store complex human information (DNA) in a condensed framework contained in bits made up of only tens of atoms (nucleotides). Giving each cell the ability to store all the genetic information needed to reproduce its much more complex host.[88] Life shows researchers that nanotechnology is possible, however, humans are still trying to understand and effectively integrate the technologies with society. Some of the applications of nanomaterials are for imaging[137, 201], biosensing[46, 246, 380], drug delivery[254, 273, 290, 352], cancer therapy[196, 295], tissue engineering[77] and storing data in DNA[52]. When it comes to these applications, it is important to

determine how these nanomaterials interact with their human hosts.

1.4.1 Toxicity

For biological applications an important property must be determined, whether the material is toxic or not. With the growing number of nanomaterials, humanity will have contact with them whether it be through direct or indirect means. Materials that have deemed toxic can still find ways to come into contact with humans, this can occur, for instance, through improper disposal. There have already been documented events, where nanomaterials have caused adverse effects on human health.[209, 361]

For in vitro applications, researchers need to have a thorough understanding of most of the interactions before continuing to human trials. It needs to be understood if the material can cause cell death, cytotoxicity, or lead to other undesired effects. The concentration, the size, the potential chemistries, physical interactions and exposure time of the materials needs to be considered. A material's toxicity can change depending on the exposure times, materials can degrade if it is in the system for an extended period of time. All of these properties have the potential to change with varying temperature and pH.[198] To answer the question of toxicity, a large and complex parameter space must first be explored.

Studies over the years have started to tackle this challenge. [6, 158, 315] Currently, in

vivo or in vitro experiments must be conducted to gain a understanding of this property. This will remain an expensive and time consuming process until the theoretical community has the computational power and predictive models. While the proof is in the experiment, theory can guide experimentalists and reduce these costs. Some of the work in this dissertation attempts to continue chipping away at the theoretical problem. While there are hundreds of articles with specific studies on nanomaterial toxicity[5, 6, 68, 158, 223], a brief overview will be given to demonstrate the efforts of researchers to a complex problem.

1.4.1.1 Experimental Research

Experimentalists have the benefit of having "preconstructed" (real) cells to work with. However, they must approach the problem from a top down approach, while theorists may start from a bottom up approach. Experimental methods have been developed to test for cytotoxicity[198], but it is still a difficult property for theory to determine. Theory currently can only look at small fractions of the potential interactions and it must do so one interaction at a time.

Many 0-D and 1-D nanostructures suffer from surface oxidation and surface reconstruction, which can alter their physical behavior.[325] Quantum dots challenged researchers for biological studies due to the cytotoxicity of some of their

components.[201] For example, in cadmium-based quantum dots it had been discovered that cadmium can leak from the particle and lead to toxicity.[45] This hampers efforts and requires researchers to discover novel methods to generate dots that can work around such issues. Most functions of 0-D and 1-D nanomaterials are due to their core structure, however their surface coating defines much of their bioactivity. A "simple" solution was to generate cadmium free quantum dots, researchers developed silicon and carbon based quantum dots.[201, 317] In a similar method, silicon quantum dots were functionalized using carboxylic acids[205, 297], amines[347], allylamine[328] and other groups[82]. These groups stabilize the materials and they are considered biologically favorable.

For carbon nanotubes and graphene, there have been numerous studies that have shown the materials to be cytotoxic.[116, 126, 141, 372, 374]. These materials can still be used for biological applications, but the scope is limited. However, for boron-nitride, experiments show contrasting results in terms of the toxicity effects of BNNTs.[67, 86, 87, 373] Boron-nitride is still relatively new and the research on the topic is still limited, when compared to graphene and carbon nanotubes.

To address the complex space that is needed to investigate toxicity, researchers have proposed new methods to generate and approach data sets. Scientists have started to automate the researcher process by investigating toxicity by creating high throughput experiments.[235] Using their data and data of groups investigated toxicity in rodents,

they construct machine learning algorithms in an attempt to find patterns and predict toxicity of materials not yet test.[98]

1.4.1.2 Theoretical Investigations

There have been numerous studies investigating the interactions between biological molecules with carbon-based materials. [108, 109, 192, 341, 392] Similar studies have been done with boron-nitride materials. [7, 83, 231, 232, 283, 311] All these studies limited their scope to pristine materials, whose interactions are all long-ranged vdW interactions and $\pi - \pi$ stacking for aromatic molecules. Other materials of interest include noble metal clusters [1, 40, 121, 148, 221, 228, 369], other nanotubes and monolayers[83, 232, 285, 291, 292, 349, 349], 2-D layered transition-metal dichalcogenides, transition metal oxides, and others[186].

In most cases either the inherent defects of the materials can be used or the surface can be modified to enable stronger interactions to occur.[65] These modifications range from binding more sensitive molecules on the surface through $\pi - \pi$ stacking [189] or through permanent chemical bonds[293, 294]. The covalent modifications will alter the structural and electronic properties of the nanomaterials, while the non-covalent maintain the intrinsic properties of the materials. Carbon based nanomaterials have been heavily investigated over the past decades for fundamental research, industrial production and potential applications. [383] For graphene the most

effective approach, so far, has been with graphene oxide. The modified material has found a number of uses in the the biological community.[168] Boron-nitride materials have also seen its share of modifications to enhance its properties for applications. [59, 95, 189, 293, 294]

There are theoretical investigation studying the peptide-nanomaterial interface. Researchers are also interested in the interaction due to the potential to grow nanomaterials using peptides. [313] Some of the topologies that have been investigated as substrates for these applications include nanotubes[46, 48, 161, 251, 364] nanowires[58], nanoparticles[138], nanorods[38], and two-dimensional (2-D) sheets[309]. Boron nitride nanotubes[50], one of the emerging nanomaterials, have a morphology similar to that of the well-established carbon NTs (CNTs). Boron nitride nanotube are recognized as viable candidates for conjugation with biomolecules[101], showing a strong affinity toward proteins[389]. Some researchers have started to investigate larger scale interactions. Hilder et. al. have studied periodic cell membranes with boron-nitride nanosheets through different interaction schemes.[133]

1.5 Conclusion

These are a few avenues of research that are currently being pursued, but the possibilities are limitless.[186] Some problems of society are being actively addressed by

state-of-the-art methods, with the next innovation just around the corner. There are still many challenges that need to be overcome in the manufacturing process to harness the potential of nanotechnology. In this dissertation, only a fraction of the nanomaterial machinery was investigated.

In Chapter 2 a brief history and overview of the theoretical methods of Hartee-Fock Theory and density functional theory is presented. In Chapter 3, shows the initial investigations on boron-nitride monolayers and nanotubes. It discusses some of the approximations that were made to model large nanotubes and it shows the cluster model that were used for some studies. Chapter 4 investigates the potential changes in structures of gold cluster in the gas-phase and clusters deposited on BNNTs. In Chapter 5, the first published work on the interactions of select amino acids with boron-nitride is presented. The study was the first boron-nitride study to introduce amino acids structures that are present in physiological conditions. Chapter 6 AIMD studies investigating the water boron-nitride interface is presented. As a continuation of the previous work, the study was going to look at similar interactions in the presence of defects, but during that investigation a new structure was discovered. This structure is presented in Chapter 7, along with the materials's electronic and mechanical properties. The last chapter, Chapter 8, an overview of the work is given and the potential future studies are given.

Chapter 2

Methodology

In this chapter a brief summary of the fundamentals of electronic structure will be presented. It will start with the original problem that was encountered in classical physics that spurred the creation of quantum mechanics. There will only be a discussion of the theoretical framework, not the numerical framework that makes these many body problems calculable. The numerical methods are out of the scope of the dissertation.

2.1 Theoretical Foundation

In 1900, physicist encountered a problem now known as the "ultraviolet catastrophe". The classical theory, Rayleigh-Jeans law predicted low wavelength behavior of blackbody radiation correctly but the short wavelengths drastically diverged from the experimental observations. This problem was being tackled by an individual who is now known as the "founder" of quantum physics. In his solution to the problem, Max Planck was the first to quantize electro-magnetic energy. He achieved this by following the statistical work of the second-law of thermodynamics. The law was previously published by Boltzmann, which received a large deal of skepticism from the community. Planck's newly derived black-body radiation law postulated that electro-magnetic energy was quantized in the following manner

$$E = h\nu \tag{2.1}$$

where h is Planck's constant and ν is the frequency of radiation, where ν takes on discrete values. The consequences of Equation 2.1 were radical. At the time Planck proposed this novel solution, he, along with the community, were skeptical of the consequences. After two decades of experiments by others in the laboratory, it earned him the Nobel Prize in Physics in 1918.[237] Since that law was proposed, skepticism

has trailed almost every idea in quantum physics. Many more times theory and experiments conflicted during the evolution of quantum mechanics and when they agreed it was typically perceived with a similar trepidation.

2.2 Schrödinger Equation

In 1926, Erwin Schrödinger introduced the wave equation, that now bears his name.[19] The paper "An Undulatory Theory of the Mechanics of Atoms and Molecules" was based off of work previously done in de Broglie Thesis on phase-waves.[63, 301] His work on the wave-equation earned him the Nobel Price in Physics in 1933, which was shared with Paul Dirac. [239]

The non-relativistic electronic structure of any material can be solved by using the Schrödinger equation. [301] In its time-dependent format the equations is typically presented as

$$\hat{H} |\Psi(t)\rangle = i\hbar \frac{\delta}{\delta t} |\Psi(t)\rangle \quad (2.2)$$

where \hat{H} is the Hamiltonian operator, Ψ is the wave function of the system, and \hbar is the reduced Planck's constant. This formula uses Dirac notation, for additional information see Appendix A. The \hat{H} term in the equation can be expanded into a more "traditional" form, which describes a single particle evolving in a electric field

(i.e. electron and a nucleus.) (For the rest of the theory section atomic units will be used, it will simplify the equations. For additional information see Appendix B.)

$$\left[-\frac{1}{2}\nabla^2 + V(\mathbf{r}, t)\right]\Psi(\mathbf{r}, t) = i\hbar\frac{\delta}{\delta t}\Psi(\mathbf{r}, t) \quad (2.3)$$

Where $-\frac{1}{2}\nabla^2$ is the kinetic energy of the system and $V(\mathbf{r}, t)$ is the potential energy of the system. Typically, when solving for the properties of atoms and molecules the time-independent Schrödinger Equation is taken into consideration. The time-independent simplifies from Equation 2.2 to the following

$$\hat{H}\Psi(\mathbf{r}) = E\Psi(\mathbf{r}) \quad (2.4)$$

which, when expanded, turns into the recognizable Schrödinger equation.

$$\left[-\frac{1}{2}\nabla^2 + V(\mathbf{r}, t)\right]\Psi(\mathbf{r}) = E\Psi(\mathbf{r}) \quad (2.5)$$

For a many body problem with Coulombic interactions, the Hamiltonian (\hat{H}) expands to

$$H_e = - \sum_i \frac{1}{2} \nabla_i^2 - \sum_{i,A} \frac{Z_A}{r_{iA}} + \sum_{i < j} \frac{1}{r_{ij}} + \sum_{B < A} \frac{Z_A Z_B}{R_{AB}} - \sum_A \frac{1}{2M_A} \nabla_A^2 \quad (2.6)$$

Where i, j are indices representing the electrons, A, B represent the nuclei, r_{ij} is the distance between particle x and y (i & j are electrons and A & B are nuclei), and M_A is the mass of nuclei A . This equation is usually reduced and presented with the following operators.

$$\hat{T}_N(\mathbf{R}) = - \sum_A \frac{1}{2M_A} \nabla_A^2 \quad (2.7)$$

$$\hat{T}_e(\mathbf{r}) = - \sum_i \frac{1}{2} \nabla_i^2 \quad (2.8)$$

$$\hat{V}_{Ne}(\mathbf{R}, \mathbf{r}) = \sum_{i,A} \frac{Z_A}{r_{iA}} \quad (2.9)$$

$$\hat{V}_{NN}(\mathbf{R}) = \sum_{A < B} \frac{Z_A Z_B}{R_{AB}} \quad (2.10)$$

$$\hat{V}_{ee}(\mathbf{r}) = \sum_{i < j} \frac{1}{r_{ij}} \quad (2.11)$$

$$\hat{H} = \hat{T}_N(\mathbf{R}) + \hat{T}_e(\mathbf{r}) + \hat{V}_{Ne}(\mathbf{r}, \mathbf{R}) + \hat{V}_{NN}(\mathbf{R}) + \hat{V}_{ee}(\mathbf{r}) \quad (2.12)$$

Where \mathbf{R} is the nuclear coordinates and \mathbf{r} is the electron coordinates. In this form the wave functions of the nuclei and electrons are not separable due to the cross-term $\hat{V}_{Ne}(\mathbf{r}, \mathbf{R})$. A method to relieve this coupling is presented in the next Section 2.3.1

2.3 Approximations

2.3.1 Born-Oppenheimer Approximation

To solve Equation 2.12, the Born-Oppenheimer or adiabatic approximation can be implemented. This will work around the difficult cross term $\hat{V}_{Ne}(\mathbf{r}, \mathbf{R})$. The approximation assumes the nuclei are in fixed positions relative to the electrons.[33] This is typically a conservative assumption, due to the fact that the electron mass is about $1/1000^{\text{th}}$ of a nucleus. A more rigorous derivation can be found in the following reference [307]. The interaction between the electron and nuclei under this assumption

are strictly classical and the wave function can be decoupled.

$$\Psi(\mathbf{r}, \mathbf{R}) = \Psi_{ele}(\mathbf{r}, \mathbf{R})\Phi(\mathbf{R}) \quad (2.13)$$

Here the nuclear wave function is $\Phi(\mathbf{R})$ and the electronic wave function is $\Psi_{ele}(\mathbf{r}, \mathbf{R})$. \mathbf{R} in the wavefunctions is now a constant. Now there is a simpler, but still difficult, form of Equation 2.4, where the electrons are under the influence of external electrostatic field produced by fixed nuclei.

$$H_{ele}\Psi_{ele}(\mathbf{r}, \mathbf{R}) = E_{ele}\Psi_{ele}(\mathbf{r}, \mathbf{R}) \quad (2.14)$$

2.3.2 Independent-Electron Approximation

The greatest challenge in the electron many-body problem is presented by the electron correlation. Due to the impossible task of solving the n-body problem, approximations must be applied to make the problem approachable.

For the electron correlation there exist two regimes, weakly correlated and strongly

correlated. The traditional theories that have been developed over years work relatively well within the weakly correlated regime, typically associated with most chemical phenomenon. In the weak regime the kinetic energy is the dominate term and the non-interacting electron gas approximations tend to do well. The electron correlation can be generally be described through the Pauli exclusion principle and the interactions through an average potential. To calculate qualitatively accurate descriptions additional care needs to be taken to capture the additional correlations in localized bonded systems.[92, 219]

Strongly correlated systems tend to appear in condensed matter phases and lead to phenomenon such as Mott insulators[120], superconductivity[20], etc. When it comes to these systems the potential energy term dominates and the electron exhibit collective behaviors in the systems. Only weakly correlated systems were investigated, but it is worth mentioning the shortcomings of the independent electron approximation.

2.3.3 Slater Determinants

The Hatree product does not take into account the indistinguishability of electrons. The antisymmetric principle states that upon switching the electron spin and space coordinates the sign of the wave function must change.

$$\Psi_{1,2}(\mathbf{r}_1, \mathbf{r}_2) = \Phi_1(\mathbf{r}_1)\Phi_2(\mathbf{r}_2) \quad (2.15)$$

upon switching the electron the Hartree product will become

$$\Psi_{2,1}(\mathbf{r}_1, \mathbf{r}_2) = \Phi_1(\mathbf{r}_2)\Phi_2(\mathbf{r}_1) \quad (2.16)$$

The wave functions distinguishes between electrons. To introduce the indistinguishability of electrons, the linear combination of the two products can be taken.

$$\Psi_{1,2}(\mathbf{r}_1, \mathbf{r}_2) = \frac{1}{2^{1/2}}(\Phi_1(\mathbf{r}_1)\Phi_2(\mathbf{r}_2) - \Phi_2(\mathbf{r}_1)\Phi_1(\mathbf{r}_2)) \quad (2.17)$$

where the factor of $2^{1/2}$ is a normalization constant and the minus sign gives the wave function antisymmetry upon interchange of electron.

$$\Psi(\mathbf{r}_1, \mathbf{r}_2) = -\Psi(\mathbf{r}_2, \mathbf{r}_1) \quad (2.18)$$

This new form of the wave function also provides another benefit, the Pauli exclusion principle is now present. If two electrons are to occupy the same orbital ($i=j$), the wave function would vanish. The previous Equation 2.18 can be rewritten into a more

compact form called a determinant.

$$\Psi_{1,2}(\mathbf{r}_1, \mathbf{r}_2) = \frac{1}{2^{1/2}} \begin{vmatrix} \Phi_1(\mathbf{r}_1) & \Phi_2(\mathbf{r}_1) \\ \Phi_1(\mathbf{r}_2) & \Phi_2(\mathbf{r}_2) \end{vmatrix} \quad (2.19)$$

the Slater determinant can be generalized to an N-electron system.

$$\Psi(\mathbf{r}_1, \mathbf{r}_2, \dots, \mathbf{r}_N) = \frac{1}{\sqrt{N!}} \begin{vmatrix} \Phi_1(\mathbf{r}_1) & \Phi_2(\mathbf{r}_1) & \cdots & \Phi_N(\mathbf{r}_1) \\ \Phi_1(\mathbf{r}_2) & \Phi_2(\mathbf{r}_2) & \cdots & \Phi_N(\mathbf{r}_2) \\ \vdots & \vdots & \ddots & \vdots \\ \Phi_1(\mathbf{r}_N) & \Phi_2(\mathbf{r}_N) & \cdots & \Phi_N(\mathbf{r}_N) \end{vmatrix} \equiv |\Phi_1, \Phi_2, \dots, \Phi_N\rangle \quad (2.20)$$

2.3.4 Hartree-Fock Approximations

The Hartree-Fock approximation assumes that the energy of a system can be minimized using an orthonormal basis of Φ_i using a single determinant and using a single-particle Hamiltonian where the interaction between electrons is calculated using an average potential (mean-field).

$$E_{HF} = \langle \Psi_{HF} | \hat{H} | \Psi_{HF} \rangle = \sum_i H_i + \frac{1}{2} \sum_{i,j} (J_{ij} - K_{ij}) \quad (2.21)$$

Where H_i is the single-particle Hamiltonian and the other two terms describe the average potential. Where J_{ij} is the Coulomb integral and K_{ij} is the exchange integral. These terms are given by the following

$$H_i = \int \Phi_i^*(\mathbf{r}) \left[-\frac{1}{2} \nabla^2 + \sum_A \frac{Z_A}{r_{iA}} \right] \Phi_i(\mathbf{r}) d\mathbf{r} \quad (2.22)$$

$$J_{ij} = \int \int \Phi_i(\mathbf{r}_1) \Phi_i^*(\mathbf{r}_1) \frac{1}{r_{ij}} \Phi_j^*(\mathbf{r}_2) \Phi_j(\mathbf{r}_2) d\mathbf{r}_1 d\mathbf{r}_2 \quad (2.23)$$

$$K_{ij} = \int \int \Phi_i^*(\mathbf{r}_1) \Phi_j(\mathbf{r}_1) \frac{1}{r_{ij}} \Phi_i(\mathbf{r}_2) \Phi_j^*(\mathbf{r}_2) d\mathbf{r}_1 d\mathbf{r}_2 \quad (2.24)$$

Where the identity $J_{ii} = K_{ii}$ allows for the sum over $i = j$. With these formulas and orthonormalization conditions for the wave functions, the Fock operator can be constructed

$$\hat{F} = \hat{h} + \hat{j} - \hat{k} \quad (2.25)$$

giving the Hartree-Fock differential equations

$$\hat{F}\Phi_i(\mathbf{r}) = \sum_{j=1}^N \epsilon_{ij}\Phi_j(\mathbf{r}) \quad (2.26)$$

The orbital energies can then be found by multiplying Equation 2.26 by Φ_i

$$\epsilon_{ii} = \langle \Phi_i | \hat{F} | \Phi_i \rangle = H_i + \sum_j (J_{ij} - K_{ij}) \quad (2.27)$$

Using this information, the total energy of the system can be found by summing of all i and adding the nuclear-nuclear interaction constant.

$$E_{HF} = \sum_i \epsilon_{ii} - \sum_{i,j} (J_{ij} - K_{ij}) + \sum_{A<B} \frac{Z_A Z_B}{r_{AB}} \quad (2.28)$$

These formulas will have slight modifications when applied to open versus closed shell systems and when electron spin is taken into consideration. The changes are not trivial, but the previous equations do not undergo large changes. A more detailed derivation with this modifications can be found in the following Reference [253].

2.3.5 Post-Hatree-Fock Methods

An important factor that is omitted from the Hatree-Fock Approximation is the correlation energy. The equations has an exact value for the exchange integral, but no term for the correlation energy. Researchers have presented many methods to remedy this short coming, gaining more accuracy but at an additional computation cost. This dissertation is not focused on many-body perturbation methods[195] or configuration interactions[318], but it is worth mentioning as these theories are more accurate than Hatree-Fock and Density Function Theory (presented later in this chapter).

2.4 Roothaan-Hall Equations

In 1951 Clemens Roothan and George Hall, independently, introduced a matrix representation of the Hatree-Fock equation. The method converted the differential equation 2.4 from a differential equation to a matrix equation in the following form [382].

$$F(\mathbf{C})\mathbf{C} = \mathbf{S}\mathbf{C}\epsilon \quad (2.29)$$

Where $F(\mathbf{C})$ is the Fock Matrix, \mathbf{C} is the coefficients matrix, \mathbf{S} is the overlap matrix

and ϵ is the matrix of orbital energies. This is done by using the antisymmetric product provided by the Slater determinant, equation 2.20, and by introducing the linear combination of atomic orbitals (LCAO) approximation. [287] This allowed standard techniques to be used to solve the Hartree-Fock equations.

$$\Phi_i = \sum_{\mu} \phi_{\mu} C_{\mu i} \quad (2.30)$$

Where ϕ_{μ} are the LCAO and $C_{\mu i}$ are the coefficients. More details for LCAOs can be found in Section 2.5.1.

It can be seen that $\mathbf{F}(\mathbf{C})$ depends on \mathbf{C} , so an initial guess for \mathbf{C} must be given. Then to solve the equation a self-consistent-field calculation must be done. For more details on the procedure see Figure 2.2.

2.5 Basis Sets

The basis set is a set of function that are used to represent the wave function Ψ of the system. There are limitless possibilities when constructing the wave function using functions. However, there are practical and computational consideration to take into account. In the past many different approaches have been used, some examples

are Gaussian type orbitals[34], numerical basis set[147], planewaves[332], Slater-Type Orbitals[312] and Wavelets[276]. Each method can be used to approach the Hartree-Fock limit, the minimum energy possible when using a single Slater determinant, if an infinite basis set is used. This is not possible, so the sets must be truncated. When constructing a basis set there is a balancing act between accuracy and computational efficiency.

Improvements are not straightforward, but by changing the functional form and increasing the bases set size, it is possible to increase accuracy and computational cost. This was seen when Gaussian type orbitals were introduced and replaced Slater type orbitals.[55]

2.5.1 LCAO Type Orbitals

There are many forms these basis functions can take, but originally slater-type orbitals were used. Slater-type orbitals (STO) are analytically solved from a hydrogen-like atom. They take the following form

$$\phi^{STO}(x, y, z) = Nx^a y^b z^c e^{-\alpha r} \tag{2.31}$$

where $L = a + b + c$ is the angular momentum, N is a normalization constant, α is

the effective charge of the nucleus, and r is the distance between the electron and nucleus.[312]

These hydrogen-like orbitals were replaced with linear combination of atomic-orbital self-consistent-field (LCAO-SCF) theory, each molecular orbital is written in the following form [287].

$$\Phi_i = \sum_{\mu} \phi_{\mu} C_{\mu i} \quad (2.32)$$

Where ϕ_{μ} are basis functions, and $C_{\mu i}$ are coefficients. The basis set went from one hydrogen-like function to a linear combination of Gaussian type orbitals (GTO), using only one Gaussian function would give a poor description.

$$\phi^{GTO}(x, y, z) = N x^a y^b z^c e^{-\alpha r^2} \quad (2.33)$$

Although this method introduces more complexity to the wave function, it allows for the use of the Gaussian product theorem.[28] The theorem allows for a 4-5 order of magnitude speedup when evaluating the integrals in the Hamiltonian. For Gaussian basis sets, contracted Gaussian functions (CGTO) are used as basis functions.[73]

$$\phi^{CGTO}(x, y, z) = N \sum_{k=1}^N d_k x^a y^b z^c e^{-\alpha r^2} \quad (2.34)$$

where d_k is a fitted parameter, i is the orbital (1s, 2p...etc.), N is the number of Gaussian functions, x, y, z are the position.

The most popular implementation by was Pople, they are split-valence basis sets. The naming scheme describes the number of primitive Gaussian functions that are used in each basis function. 6-31 G implies that six (6) Gaussian functions (G) are used to describe the core electrons and while the valence electrons are split (-) into to basis of each three (3) and one (1) Gaussian. Having the valence split into two basis is called a split-valence double zeta basis set, a triple zeta basis set could have the notation of 6-311G. Adding more basis functions allow for more flexibility in describing the orbitals, this can also be done by adding polarization and diffuse functions.[278]

2.5.2 Plane-Wave Basis

Plane-waves methods rest on Bloch's theorem. The theorem states that each energy wave function in a crystal can be written using Bloch waves. They are used to represent a wave function in a periodic potential. A wave function takes the form of a Bloch wave has the following form.[14]

$$\Psi(\mathbf{r}) = e^{i\mathbf{k}\cdot\mathbf{r}} u(\mathbf{r}) \quad (2.35)$$

where Ψ is the Bloch wave, \mathbf{r} is the position, \mathbf{k} is the crystal wave vector and $u(\mathbf{r})$ is a periodic function. The periodic function can be expanded using a basis set containing discrete plane-waves represented in reciprocal space.

$$u(\mathbf{r}) = \sum_{\mathbf{G}} c_{i,\mathbf{G}} e^{i\mathbf{G}\cdot\mathbf{r}} \quad (2.36)$$

\mathbf{G} is are the reciprocal lattice vectors that are defined as $\mathbf{G} \cdot \mathbf{l} = 2\pi m$, where \mathbf{l} are the crystal vectors and m is an integer. This allows the wave function to be written as a discrete sum of plane-waves by combining Equation 2.35 and 2.36.

$$\Phi_i(\mathbf{r}) = \frac{e^{i\mathbf{k}\cdot\mathbf{r}}}{\Omega^{\frac{1}{2}}} \sum_{\mathbf{G}} c_{i,\mathbf{G}} \Phi_i e^{i(\mathbf{k}+\mathbf{G})\cdot\mathbf{r}} \quad (2.37)$$

To represent that states correctly an infinite plane-wave basis set would be used, but due to computational limitations only a finite amount are used. Generally the coefficients ($c_{i,\mathbf{k}+\mathbf{G}}$) for small kinetic energy plane-waves

$$\frac{\hbar^2}{2m} |\mathbf{k} + \mathbf{G}|^2 \quad (2.38)$$

are generally more important to represent the states, so the series are truncated to allow for plane-waves below a specific kinetic energy.[256] The convenience of using a plane-wave basis set is that the accuracy, within the framework, of the calculation can be adjusted by increasing the cutoff energy.

It is important to note that core states, when represented by plane-waves, require a high cutoff energy when compared to the outer-shell valence states. While this may improve the accuracy of the calculation, it increases the computational cost by a significant amount and the core states typically do not affect bonding or physical properties of interest. To solve this problem, researchers replaced the core electrons with pseudopotentials, a critical component to plane-wave calculations.

2.5.2.1 Pseudopotentials

Pseudopotentials serve three important functions. They allow for a lower cutoff energy for a plane-wave basis set, they reduce the number of electrons in the calculation and they allow for the addition of relativistic effects within a non-relativistic framework. The potentials are determined before using an atomic reference state, assuming the core electrons behave as if isolated. They were first introduced by Hamann et. al in 1979[123], where they split the potential into an inner region, divided by r_c , as seen in Figure 2.1. The pseudopotential approximation is implemented by splitting the core and valence states[166] and replacing the core electrons with a weaker potential

(pseudopotential). This in turn will generate pseudo-wave function as seen in Figure 2.1. The number of nodes in the wavefunction is reduced, decreasing the cost need to represent the core electrons.

There are two main types of pseudopotentials, norm-conserving[17, 123] and ultrasoft[337]. Norm-conserving pseudopotentials follow two conditions. Within the cut-off radius r_c the norm of the pseudo-wave function must be identical to its corresponding all-electron wave function. The second condition requires the wave functions to be identical outside of the cut-off radius r_c . For ultrasoft potentials these conditions are typically relaxed, allowing for an even further reduction in computational cost. Similar to the ultrasoft potentials, plane augmented waves (PAW)[180] are more accurate due to a higher cutoff value leading a slight increase in computational cost. For the work done in this dissertation the PAW potentials were used. For more information on pseudopotentials see the following review [302]

2.6 Density Functional Theory

Density functional theory allows the N-electron wave function to be replaced with a simpler 3D electron density. This greatly reduces the cost and effort required needed to calculate systems. The pedagogical beginnings of density functional theory is introduced through the statistical models introduced by Llewellyn Thomas in 1927

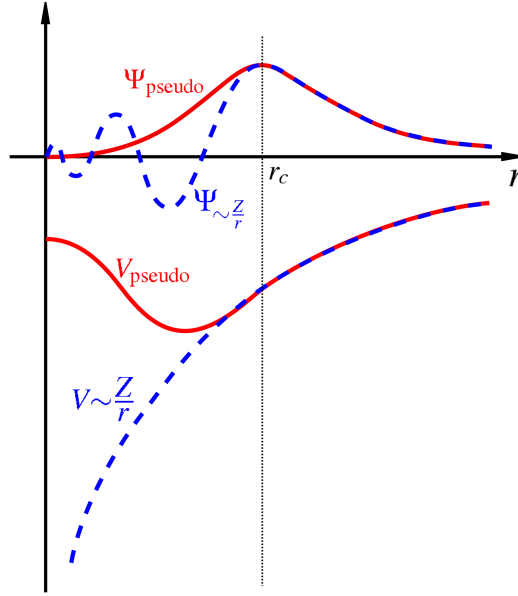


Figure 2.1: The real wave function (blue) and the pseudopotential (red) in the potential of a nucleus (Z/r). The wave functions will match at a point r_c . The smooth behavior near the center of the nucleus reduces the needed cutoff energy for the plane-wave basis set. The image taken from Wikipedia [357]

[327] and a year later by Enrico Fermi [84].

2.6.1 Thomas-Fermi Model

The novelty of the model was treating the ground state electrons using statistical models. The models were used to distribute the electrons around the atom, this changed the complexity of the problem from a N-electron wave functional to a "more tractable" three-dimensional electron density $\rho(\mathbf{r})$.

A crude model but it does tend to correctness in the limit of a nuclear charge of

infinity, as noted by Dirac[71]

Although this model hitherto has not been justified theoretically, it seems plausible approximation for the interior of a heavy atom and one may expect it to give with some accuracy the distribution of electric charge there.

The energy of the system under this model is given by

$$E_{TF}[\rho(\mathbf{r})] = T[\rho(\mathbf{r})] + V_{Ne}[\rho(\mathbf{r})] + V_{ee}[\rho(\mathbf{r})] \quad (2.39)$$

Where $T[\rho(\mathbf{r})]$ is the kinetic energy, $V_{Ne}[\rho(\mathbf{r})]$ is the attractive potential between the electrons and nuclei and $V_{ee}[\rho(\mathbf{r})]$ is the repulsive potential between electrons.

$$T[\rho(\mathbf{r})] = C_F \int \rho(\mathbf{r}) d\mathbf{r} \quad (2.40)$$

Where C_F is a constant from the derivation ($\frac{3}{10}(3\pi^2)^{1/3}$), see Reference [253].

$$V_{Ne}[\rho(\mathbf{r})] = -Z \int \frac{\rho(\mathbf{r})}{r} \quad (2.41)$$

$$V_{ee}[\rho(\mathbf{r})] = \frac{1}{2} \int \int \frac{\rho(\mathbf{r}_1)\rho(\mathbf{r}_2)d\mathbf{r}_1d\mathbf{r}_2}{|\mathbf{r}_1 - \mathbf{r}_2|} \quad (2.42)$$

Assuming the ground state of the system minimizes the functional $[E_{TF}]$, under the constraint

$$N[\rho(\mathbf{r})] = \int \rho(\mathbf{r})d\mathbf{r} \quad (2.43)$$

where N is the total number of electrons in the system. Using Lagrange multipliers the ground state of the system can satisfy the variational principle

$$\delta[E_{TF}[\rho(\mathbf{r})] - \mu_{TF}(\int \rho(\mathbf{r}) - N)] = 0 \quad (2.44)$$

which leads to the following Lagrange equation.

$$\mu_{TF} = \frac{\delta E_{TF}[\rho]}{\delta \rho(\mathbf{r})} = \frac{5}{3}C_F\rho^{2/3}(\mathbf{r}) - \frac{Z}{r} - \int \frac{\rho(\mathbf{r}_2)}{|\mathbf{r} - \mathbf{r}_2|}d\mathbf{r}_2 \quad (2.45)$$

2.6.1.1 Thomas-Fermi-Dirac Model

The Thomas-Fermi model later was adjusted by Paul Dirac in 1930[71] For the updated model the total energy was calculated using an additional exchange term.

$$E_{TFD}[\rho(\mathbf{r})] = T[\rho(\mathbf{r})] + V_{Ne}[\rho(\mathbf{r})] + V_{ee}[\rho(\mathbf{r})] \quad (2.46)$$

The Thomas-Fermi model was a step in the right direction but it lacked accuracy and predictive power when it came to atoms, molecules and solid state calculations. [206, 306, 322] This would be remedied in 1964 with the work of Hohenberg and Kohn.

2.6.2 Hohenberg-Kohn Theorems

The big theoretical breakthrough came from Pierre Hohenberg and Walter Kohn 1964 with the publication of two theorems in their paper that established density functional theory.[136] The theory is build upon finding the minimum energy of a system using the density $\rho(\mathbf{r})$ as a basic variable instead of the wave function Ψ . This "change" of variable greatly reduces the dimensionality of the problem, it changes from $3N$ (using wave functions) to just $3D$. Where the density can be found from the wave function

with following formula

$$\rho(\mathbf{r}) = \sum_n^{occ.} |\phi_n(\mathbf{r})|^2 \quad (2.47)$$

With the second theorem restricts the theory to ground-state of the system, although a limitation it makes the theory possible. In the paper the authors were also able to provide a proof for the previous Thomas-Fermi equations using the new framework. Although the paper did not provide any practical developments, it was the first piece of two to establishing density functional theory for electronic structure calculations.

Theorem 1 *The external potential $v_{ext}(\mathbf{r})$ and total energy if a unique functional of the electron density $\rho(\mathbf{r})$.*

Theorem 2 *The ground-state can be obtained variationally and the obtained density minimizes the total energy of the exact ground state.*

$$E_{HK}[\rho(\mathbf{r})] = F_{HK}[\rho(\mathbf{r})] + \int \rho(\mathbf{r})v_{ext}(\mathbf{r})d\mathbf{r} \quad (2.48)$$

where $\rho(\mathbf{r})$ is the density, $F_{HK}[\rho(\mathbf{r})]$ is the universal functional and $v_{ext}(\mathbf{r})$ is the external potential.

2.6.3 Kohn-Sham Equations

$$\left[\nabla^2 + v(\vec{r})_{eff} \right] \Phi_n(\vec{r}) = \epsilon_n \Phi_n(\vec{r}) \quad (2.49)$$

Where ϵ_n is the energy of KS orbital Φ_n , and $v(\vec{r})_{eff}$ is an effective potential describing the system. It was shown by Hohenberg and Kohn that there is a universal functional that would map the density to the ground-state energy easily. [136] The functional is expanded into three known terms and a unknown terms are placed in E_{xc} . Due to the non-interacting electrons the exchange energy and correlation energy is missed and put into this unknown term.

$$E[\rho(\vec{r})] = T_s[\rho(\vec{r})] + V[\rho(\vec{r})] + U[\rho(\vec{r})] + E_{XC}[\rho(\vec{r})] \quad (2.50)$$

T_s is the non-interacting kinetic energy, V is the external potential (nuclei), and U is the interelectron repulsion term (Hartree energy).

Modeling the E_{xc} term is difficult and over the years more accurate methods have been developed. The exact exchange functional is known, but the correlation functional is unknown. The exact functional is incorporated in Hatree-Fock calculations, however when implemented in DFT, the results were inaccurate and the results improved when both the exchange and correlation energy were approximated [197].

The E_{XC} can be put into the Kohn-Sham effective potential using the following functional derivative

$$v_{xc} = \frac{\delta E_{xc}[\rho(d\vec{r})]}{\delta \rho(d\vec{r})} \quad (2.51)$$

2.7 Functionals

The difficulty with density functional theory is the absence of the exact functional for the exchange and correlation that was introduced by Hohenberg and Kohn in Equation 2.48. Since the introduction of the idea of an exact functional, researchers have been coming up with non-empirical and empirical functionals to increase the accuracy of calculations. Some of these include derived functionals[259, 265] (LDA, GGA), range-separated functionals[153], empirically fit functionals[24, 187, 316, 340], functionals fit by machine learning algorithms[314] and many more[159] (creativity is the only limiting option). Outside of the derived functionals there are hundreds if not thousands of functionals, each tuned for specific systems or to describe select properties.[277] Below are some of the most utilized functionals and a brief description.

2.7.1 Local Density Approximations

The local density approximation (LDA), first introduced by Kohn and Sham[176], uses only the density to calculate the exchange-correlation energy [265]. The correlation energy was obtained from quantum Monte Carlo simulations of jellium (uniform electron gas).[263] The functional tends to underestimate the exchange energy and overestimate the correlation energy, due to approximating a uniform density.[25] This functional was popular in the 70s and 80s in condensed matter systems, but it lacked the accuracy needed for chemical applications.

$$E_{XC}^{LDA}[\rho(\vec{r})] = \int \epsilon_{xc}(\rho) d\vec{r} \quad (2.52)$$

2.7.2 Generalized Gradient Approximation

To improve on the LDA functional, the term was expanded to include the density and the gradient of the density. This allows for the functional to take into account the non-homogeneity of the electron density. The functional was published in the late 80s as a new functional, and it coined as the generalized gradient approximations (GGA). [261]

$$E_{XC}^{GGA}[\rho] = \int \epsilon_{xc}(\rho, \nabla\rho) d\vec{r} \quad (2.53)$$

There are multiple implementations of the GGA functional some include the B88[23], PW91[261], PBE[259, 260] and BLYP[23, 187] functionals. The GGA functional had the ability to describe molecular properties with good accuracy bring DFT in the domain of chemistry.

2.7.3 Hybrid Methods

There were however still know shortcomings of the GGA functional, it lacked the correct longed-ranged behavior that a theory like Hartree-Fock had. This leads to the underestimation of the band gap, incorrect description of reaction barriers and van der Waals interactions and other properties due to the local nature of the functionals. [53] To overcome this, empirical parameters were implemented into the exchange-correlation term mixing a little bit of every theory together. These functionals came about in the 90s and they were called hybrid functionals. They mixed exchange and correlation terms from both the LDA and GGA functionals and they had fraction of the exact exchange used in Hatree-Fock. The most popular hybrid function become known as B3LYP [24, 187, 316, 340] using the exchange term from the GGA B88[23],the correlation from the GGA LYP functional[187] and the LDA VWN[340]

functional for correlation. They were combined in the following formula

$$E_{XC}^{B3LYP} = E_X^{LDA} + a_0(E_X^{HF} - E_X^{LDA}) + a_x(E_X^{GGA} - E_X^{LDA}) + E_C^{LDA} + a_c(E_C^{GGA} - E_C^{LDA}) \quad (2.54)$$

where $a_0 = 0.20$, $a_x = 0.72$, $a_c = 0.81$ are empirically derived parameters. Other popular hybrid functionals include the PBE0[4] functional

$$E_{xc}^{PBE0} = \frac{1}{4}E_x^{HF} + \frac{3}{4}E_x^{PBE} + E_c^{PBE} \quad (2.55)$$

and the HSE[131] functional

$$E_{xc}^{PBEh} = aE_x^{HF,SR}(\omega) + (1 - a)E_x^{PBE,SR}(\omega) + E_x^{PBE,LR}(\omega) + E_c^{PBE} \quad (2.56)$$

where SR and LR represent the short-ranged and long-ranged exchange terms that are separated by an error function parameterized by ω . The empirical values a and ω change depending on the implementation of the functional.

2.7.4 Jacob's Ladder

To convey the hierarchy of accuracy of the levels of density functional theory, it was thought appropriate to compare them the biblical concept of Jacob's ladder.[263] This

base is in the world of Hartree-Fock theory but extends to the "Heaven of Chemical accuracy". Over the years part of the ladder has been successfully implemented into modern density functional theory. The lowest rung on the ladder is the local density approximation containing only density as an input. The next level contains the generalized gradient approximation with the parameters of density and the gradient of the density. This is followed by the meta-GGA which has all of the previous parameters and the Laplacian of density. Popular meta-GGA functionals include the TPSS functional[320] and the suite of hybrid MO6 functionals[387, 388]. The second to last level is hyper-GGA where the addition of exact local exchange would be implemented into the functional. There has been limited work[264] and it has not yet become a "mainstream" level of theory. The last rung is the generalized random phase approximation, which would utilize all occupied and unoccupied Kohn-Sham orbitals. It would not need data from the electron gas and it would take into account long-ranged van der Waals attractions. The theory would be analogous to coupled cluster theory, it would be expensive and require large basis sets.[263] A thorough review of the challenges and triumphs of these functionals can be found in the following references [53, 159]

2.8 Variational Principle

$$E[\Psi] = \frac{\langle \Psi | \hat{H} | \Psi \rangle}{\langle \Psi | \Psi \rangle} \quad (2.57)$$

Following the minimization of equation 2.57, the energy would be the true ground state Ψ_0 with an energy E_0 . However, due to limitations of expressing the wave function and Hamiltonian, the true ground state is impossible to obtain in practice. It is known that the following formula will be true, using the Hartree-Fock equations, if the energy obtained through minimization with an approximate wave function.[253] When using density functional theory, the variational principle may not approach the true ground state. This is due to the additional approximations used in density functional theory that are not present in Hartree-Fock theory.

$$E[\Psi] \geq E_0 \quad (2.58)$$

The variational principle is an iterative process that lends itself well to computation. The process can be visualized using a flow chart seen and described in Figure 2.2.

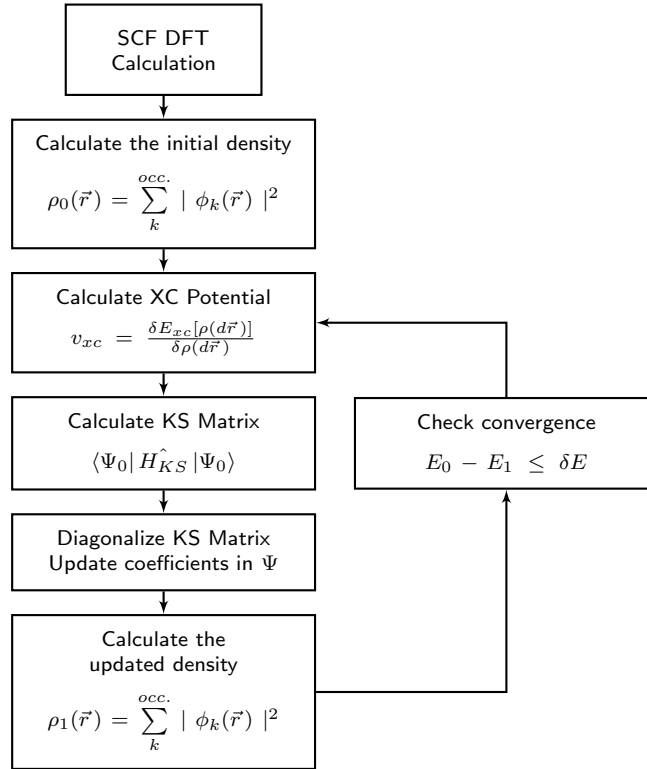


Figure 2.2: A flow chart visualizing the self-consistent-field iterative process that implements the variational principle for a density functional theory calculation. An initial density is calculated, from which the total energy exchange-correlation energy will be calculated. Then the Kohn-Sham matrix is calculated followed by diagonalized through which updated wave function coefficients are obtained. The new density and then energy are calculated, if it is within a determined threshold it iterative process is terminated. Repeat until convergence is achieved.

2.9 Add-ons

2.9.1 van der Waals Corrections

Due to the local nature of the exchange-correlation functionals in DFT mid and long-ranged interactions are poorly described.[171] The ideal solution would be to use a different theory that takes the long-range interactions into account, but these methods are computationally expensive and cannot go beyond tens of atoms. The most tractable solution to this is to add an empirical corrective term from expensive MP2 or CCSD calculations. Stefan Grimme introduced and coined the DFT-D, later called DFT-D1, D2, and D3 (D-version#) [110, 111, 112]. In the calculations, a simple empirical formula, that approximates the vdW energies, is added to the DFT energy [111]. The calculations add a post-SCF correction to the energy using the following formulas.

$$E_{DFT-D} = E_{KS-DFT} + E_{disp} \quad (2.59)$$

The energy corrections is calculated using the following formula:

$$E_{disp} = -s_6 \sum_{i=1}^{N_{at}-1} \sum_{j=i+1}^{N_{at}} \frac{C_6^{ij}}{R_{ij}^6} f_{dmp}(R_{ij}) \quad (2.60)$$

Table 2.1

Selected values of the C_6 ($eV\text{\AA}^6/atom$) parameters and the R_0 (\AA), the vdW radii, for the D2 vdW corrections used in this work. The values are taken from the original publication [111] and converted to units below, the Au values were taken from the VASP 5.3.5 source code.

Element	C_6	R_0
H	$1.35 * 10^{-2}$	1.001
B	$3.02 * 10^{-1}$	1.485
C	$1.69 * 10^{-1}$	1.452
N	$1.19 * 10^{-1}$	1.397
O	$6.75 * 10^{-2}$	1.342
Au	$7.84 * 10^0$	1.772

A damping function is included to avoid singularities near the origin.

$$f_{dmp}(R_{ij}) = \frac{1}{1 + e^{-d(R_{ij}/R_r - 1)}} \quad (2.61)$$

Where s_6 is a global scaling factor based on the functional that is being used, C_6^{ij} and R_0 are empirically derived atomic parameters.

2.9.2 Solvent Model

Implementing liquids into first principles calculations can be done with two different approaches. Explicitly puts a realistic density of the solvent molecules into the simulations. The other way to implicitly simulate a solvent in the calculations is to model the solvent as a dielectric. The system of interest is placed in a cavity of the solvent.

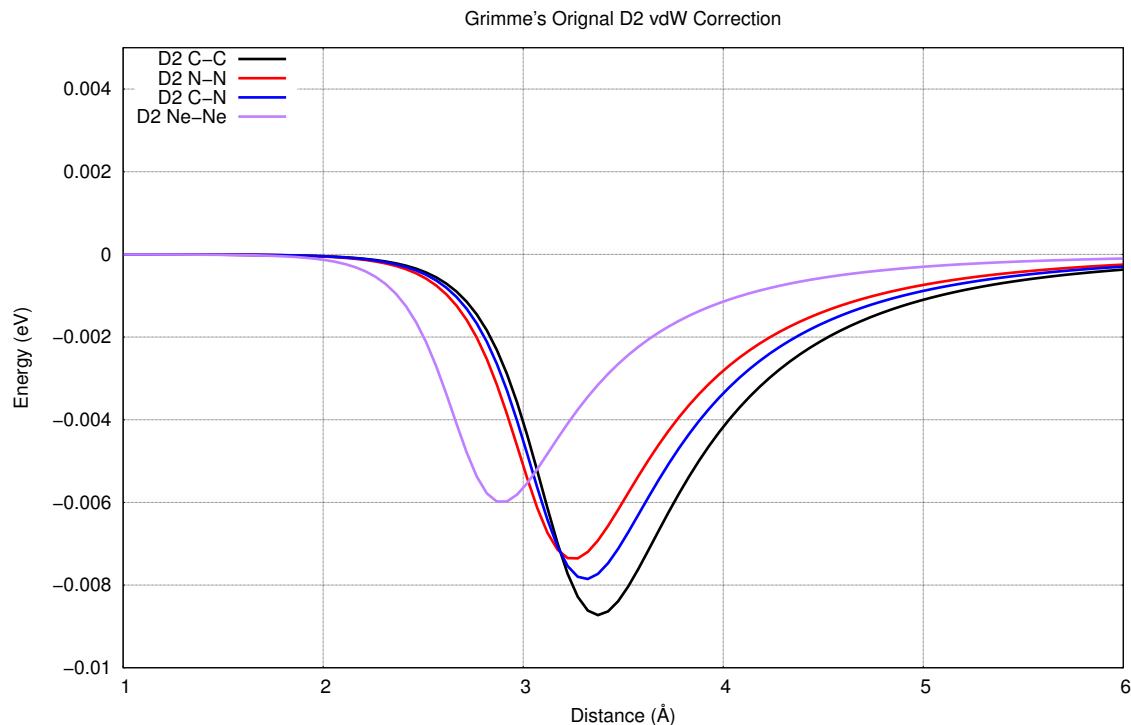


Figure 2.3: The long-ranged dispersion energy correction (Grimme-D2) vs distance for carbon-carbon, nitrogen-nitrogen, carbon-nitrogen and neon-neon interactions. Equation was used along with the values in reference [111]. The C_6 is traditionally given in units of Jnm/mol , but they were converted to give the final units in eV.

For the implicit model there are empirical parameters that first need to fit for each solvent. Polarizable Continuum Models (PCM) in Gaussian09 has been tested and many solvents that have been characterized [298]. The parameters for each solvent is prepackaged and specified only through its name.

Chapter 3

Boron Nitride

Boron nitride nanotubes were predicted in 1994 [289] and then synthesized in 1995 [50]. Its 2-D analogue, monolayer hexagonal boron-nitride, was first predicted in 2006[359] and then synthesized in 2009[154]. Boron-nitride is analogous to graphene and carbon nanotube in structure. All of the atoms are sp_2 bonded and they share the same number of electrons per atomic pair (C-C with four each and B-N with three and five electrons). Due to the difference in nuclei, the B-N bonds are more ionic, which leads to stronger interlayer properties, this may lead to difficulties in exfoliation. The difference in atoms types leads to a variation in the distributions of chiralities observed. Carbon nanotubes have an equal probability of forming all three variations of nanotubes (arm-chair, chiral and zig-zag) when grown. Boron-nitride,

however is predominately zig-zag.[101] Another artifact of the ionicity is that boron-nitride nanotubes tend to be multi-walled, resulting in the hybridization of the σ and π states of the inner and outer tubes.[151, 247]

Both boron-nitride nanotubes and monolayers are wide band gap semiconductors with a band gap around 5-6 eV.[16, 30] The properties of boron-nitride nanotubes are almost independent of chirality. There are two differences between the zig-zag and armchair nanotubes. First, that the zig-zag boron nitride nanotube's band gap decreases as the radius decreases and the arm-chair BNNTs have an indirect band gap. In Figure 3.2, the band gap for both zig-zag (n,0) and armchair (n,n) nanotubes are shown, chiral nanotube band gaps always fall in-between these two extremes.[117] A sheet of boron nitride has a direct band gap, at the K k-point, of 4.67 eV, as shown in Figure 3.4 and published previously by Guo and Lin in 2005.[117] Experiments have shown that the band gap of monolayer h-BN is around 6 eV, with recent findings narrowing the value to 6.17 eV. [16]

Boron-nitride is known for its excellent chemical inertness and thermal stability [47, 102]. However, these properties change when with smaller boron-nitride nanotubes.[117, 285, 349] It has been shown with small molecules, water, ammonia and formic acid, that chemical bonds will form with polar molecules. [285] All of the molecular interactions with these nanotubes show stronger interactions, except for aromatic molecules which bind through $\pi - \pi$ interactions.[283, 285, 349] Below

is an overview of the materials and the initial investigation into different models used for the studies.

3.0.1 Nanotube Chirality

The structures of nanotubes can be described in a quantitative manner in terms of the unit cell.[75] This term is called the chiral vector and it is given by the following formula

$$C_h = n\vec{a}_1 + m\vec{a}_2 \quad (3.1)$$

where a_1 and a_2 are the unit vectors and n and m are positive integers. n and m are typically written as (n,m) when describing the chirality of a nanotube. The circumference of the nanotube can be calculated using the chiral vector

$$|C_h| = a(n^2 + m^2 + nm)^{1/2} \quad (3.2)$$

where a is the length of the unit vector of the unit cell, 2.46 Å for graphene and 2.50 Å for h-BN boron-nitride. A "cut-out" from the unit cell is show in Figure 3.1. There are are three names to describe the chiralities; zig-zag $(n,0)$, arm-chair (n,n)

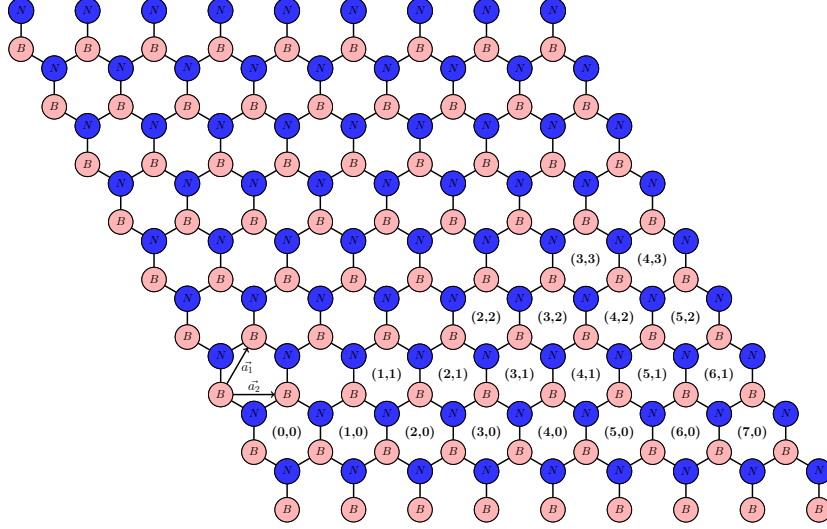


Figure 3.1: A sheet of h-BN with the lattice vectors of the unit cell, \vec{a}_1 and \vec{a}_2 , where both are equal to 2.50 Å. The sheet can be rolled up with the labeled hexagons to form the corresponding (n,m) nanotube. The zig-zag nanotube have a chiral angle of 0° , so for a (7,0) nanotube only the strip of (n,0) is needed. For an arm-chair nanotube a chiral angle of 30° is needed, for reference, the angle between \vec{a}_1 and \vec{a}_2 is 60° .

and chiral (n,m). These names correspond to the chiral angle q , zig-zag nanotubes have an angle of 0° , arm-chair 30° , and chiral have an angle between 0° and 30° . For chiral nanotubes n and m can take any integer value as long as they are not equal or zero, where the larger integer is always n. The names derive from the structure of the idealized termination of the end of the nanotube. For all nanotubes, the diameter is given by the following

$$d_{tube} = \frac{|C_h|}{\pi} = \frac{a(n^2 + m^2 + nm)^{1/2}}{\pi} \quad (3.3)$$

Table 3.1

Chirality and diameters of nanotubes that were considered in the initial investigation. The diameters were calculated using Equation 3.3 with a lattice vector magnitude of $a = 2.50 \text{ \AA}$.

Zig-zag ($m = 0$)		Arm-Chair ($m = n$)	
n	Diameter (\AA)	n	Diameter (\AA)
3	2.39		
4	3.18	4	5.52
5	3.98	5	6.90
6	4.78	6	8.27
7	5.57	7	9.65
8	6.37	8	11.03
9	7.17	9	12.41
10	7.96	10	13.79
11	8.76	11	15.17
12	9.55	12	16.55
13	10.35	13	17.93
14	11.15	14	19.31
15	11.94	15	20.69
16	12.74		
17	13.54		
18	14.33		
19	15.13		
20	15.92		
21	16.72		
22	17.52		
23	18.31		
24	19.11		
25	19.90		

and the chiral angle can be calculated.

$$\theta = \sin^{-1}\left(\frac{\sqrt{3}m}{2n+m}\right) \quad (3.4)$$

3.0.2 Computational Details

Two separate approaches were taken to model and benchmark the boron-nitride structures. Cluster calculations were performed using the Gaussian09[91] software using two different functionals. The first functional used was PBE [259], which was used to compare the electronic structure to the periodic plane-wave calculations. The second was the hybrid B3LYP[24, 187, 316, 340] functional, it was used to compare the electronic properties to experimental values. The 6-31G(d,p) [278] was used for all atoms. For the convergence criteria the following was used; 3×10^{-5} eV for the energy, 2×10^{-2} eV/Å for the force and 7×10^{-8} e/Å³ for the density matrix.

For the periodic plane-wave calculations the VASP 5.3.5 [179, 181, 182, 183] simulation package was used. The PBE[259] was used with projector-augmented-wave (PAW) pseudo-potentials[31, 180]. A plane-wave cutoff energy of 900 eV was used and for the convergence criteria; 1×10^{-5} eV was used for the energy and 3×10^{-2} eV/Å for the force. For the nanotube calculations a k-point grid of 1 x 1 x 25 was used, for the band structure calculations the Γ to Z k-points were sampled. At least 10 Å of vacuum space was placed between mirror images. The unit cells for the defective boron nitride monolayers have a hexagonal ($P6_3/mmc$) space group and the parameters were 10 Å x 10 Å x 23 Å for 3% and 8 Å x 8 Å x 23 Å for 6% and 5 Å x 5 Å x 23 Å for 12%, shown in Figure 3.7. All the unit cells had a γ value of 120°, same as the h-BN unit

cell. For the defective boron-nitride monolayers the following k-point schemes were used; 10x10x1 for 3%, 15x15x1 for 6% and 20x20x1 for 12%.

3.0.3 Pristine Boron-Nitride

The initial investigation was on pristine h-BN and boron nitride nanotubes. The properties of each materials needs to be understood, for the monolayer case this consisted of a few calculations. However, for the nanotube the variable of chirality needed to be taken into consideration. To reduce the computational demands of future investigations, it was necessary to see where the properties of large radii boron-nitride nanotubes and h-BN converged. This knowledge will reduce the atomic size of the structures that would be mimicking large nanotubes. Cluster models of h-BN would also be investigated, in one study, Chapter 5, an implicit solvent model was used and the tools required a molecular model.

3.0.3.1 Periodic Model

For the periodic structures the investigation was focused on the difference between the h-BN monolayer, the zig-zag nanotubes and the arm-chair nanotubes. In Figure 3.2, the band gaps are presented. The gray area of the plot indicates nanotube sizes that have not been yet been seen in an experimental setting, the smallest radius

measured had a radius of 7.5 Å[175]. The band gap of the monolayer is about 4.6 eV, it is smaller than experimental values due to level of theory. Theory models the structures of boron-nitride nanotubes well, but when it comes to predicting the band gap is it know that traditional functionals, LDA or GGA, underestimate the gap. This short coming is well know and is due to the weakness of the exchange terms in the LDA and GGA functionals. [262] As the curvature of the nanotube increases, the values diverge from the monolayer value around 15 Å diameter. The different chiralities diverge, with the zig-zag structure's band gap decreasing to almost 1 eV, where the arm-chair never becomes smaller than 4 eV. Another difference is that arm-chair nanotubes always have an indirect band gap. The monolayer, whose band structure is shown in Figure 3.4, and zig-zag nanotubes, except for the (3,0) and (4,0) structure have a direct band gap. This chiral dependent phenomena is present in carbon nanotubes, but due to the overlap in the p_z orbitals in carbon, the change is stronger which leads to nanotubes changing from semi-conducting to metallic.[288]

As the curvature increases for small radii nanotubes the strain energy increases.[385]

To quantify the strain, the following formula was used

$$E_{strain} = \frac{E_{BNNT}}{n} - \frac{E_{h-BN}}{m} \quad (3.5)$$

where E_{strain} is the strain energy of the system, E_{BNNT} is the total energy of the

nanotube, n and m are the number of atoms in the unit cell, E_{h-BN} is the total energy of a pristine monolayer and m is the total number of atoms in the monolayer. In the nanotubes the atoms are put into a coordination that elongates the bond and the bonds start to move toward a sp_3 hybridization, as shown by the elongation in Figure 3.3. The graph indicates that a smaller nanotube could allow for easier pathways for functionalization, this is shown in Chapter 5 and the work done by Rimola et. al[283, 285]. This ease of functionalization may not be optimal, it may lead to the degradation of the structure.

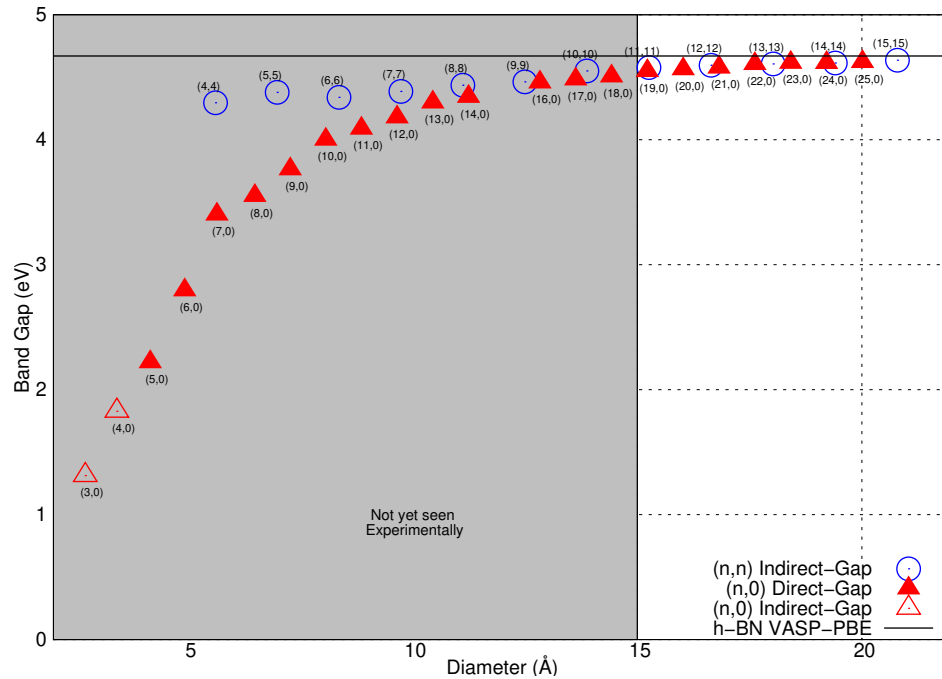


Figure 3.2: The band gap of selected zig-zag $(n,0)$ and armchair (n,n) nanotubes. The gray area covers nanotubes sizes that have not yet been observed. The smallest sized that has been observed has a radius of around 7.5\AA [175]. The arm-chair nanotubes all have indirect gaps and the most of zig-zag nanotubes and h-BN have a direct gap 3.4.

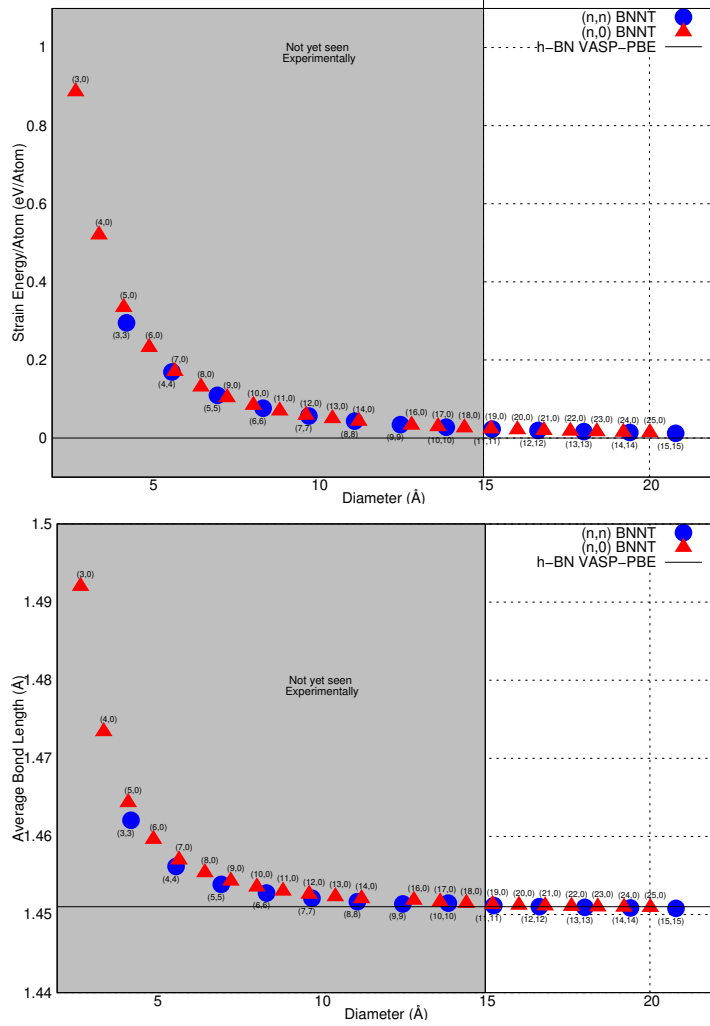


Figure 3.3: The strain energy (top) and average bond length (bottom) of selected zig-zag (n,0) and armchair (n,n) nanotubes. The gray area covers nanotubes sizes that have not yet been observed. The smallest sized that has been observed has a radius of around 7.5Å[175]. The strain energy is defined by the difference in energy from a pristine monolayer of h-BN (Equation 3.5). As the radius of the nanotube decreased the bond lengths increase and bonds tend toward a sp_3 configuration.

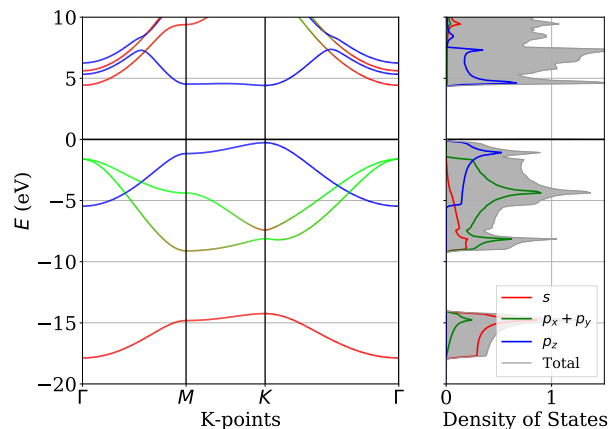


Figure 3.4: The band structures and projected density of states (PDOS) and total density of states (TDOS) of the unit cell of h-BN, where s (blue), in-plane p_x and p_y (green), out-of-plane p_z (blue) and total (grey) are shown.

3.0.3.2 Cluster Model

To model the 2-D BN systems pristine and defective structure, a finite structural model was considered and validated against a periodic material model, shown in the previous section. The structure started as simple ring ($B_6N_6H_6$) and it was expanded up to eight concentric rings containing 432 atoms ($B_{193}N_{193}H_{46}$). The hexagonal structure, in Figure 3.5, was selected to allow for a system with a negligible dipole moment, similar to that of a periodic structure.

As the concentric rings become larger, the HOMO-LUMO gaps approached the VBM and CBM periodic plane-wave values. In Figure 3.6 the HOMO-LUMO gap of the system is shown as the cluster increases in size. For the calculations using the PBE

functional the values overshoot the periodic value, this may be an artifact of the difference in basis set. For the B3LYP functional it appears to asymptotically approach the periodic value. For the calculations of defects, $n = 5$ was chosen, the choice was a balance of accuracy and simulation cost.

Table 3.2

Cluster models generated to model a periodic boron nitride monolayer. The clusters contain n concentric rings that create 2-D hexagonal flake shapes, an example is shown in Figure 3.5.

$n = \#$	Total Atoms	Composition
1	12	$B_6N_6H_6$
2	36	$B_{12}N_{12}H_{12}$
3	72	$B_{27}N_{27}H_{18}$
4	120	$B_{48}N_{48}H_{24}$
5	180	$B_{75}N_{75}H_{30}$
6	252	$B_{108}N_{108}H_{36}$
7	336	$B_{148}N_{148}H_{40}$
8	432	$B_{193}N_{193}H_{46}$

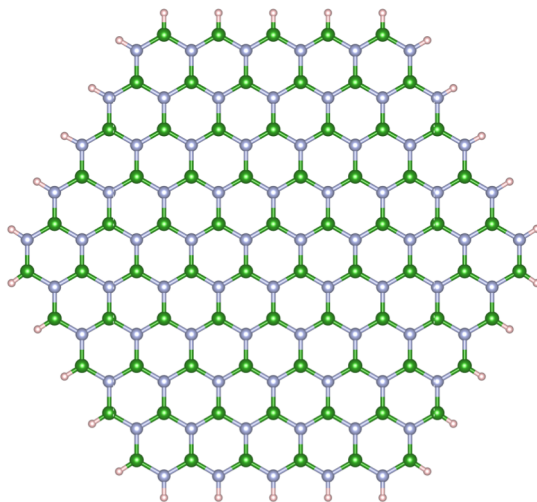


Figure 3.5: The boron nitride cluster (with 5 concentric rings), it contains 75 boron (green) atoms 75 nitrogen (white) atoms and 30 hydrogen (tan) atoms passivating the edges.

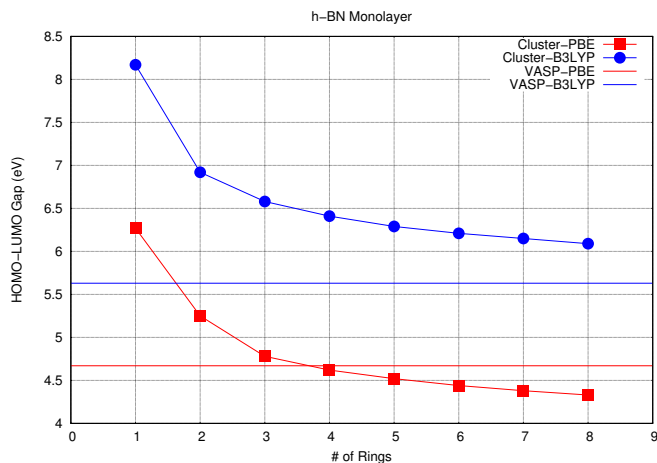


Figure 3.6: The HOMO-LUMO gap (eV) is given for the cluster approximations of boron-nitride monolayer. The smallest ring (borazine) with 12 atoms and the largest is constructed of eight rings consisting of 432 atoms. The corresponding periodic calculations are done with VASP and are given as solid lines.

3.0.4 Defects

To utilize the nanotube’s thermal stability, chemical inertness and insulating properties [101], the tubes can be functionalized to address specific applications. The method of functionalization depends on the desired application, they can be strongly bound through covalent bonds or weakly bound through non-covalent means. [391] Most methods require modification of the surface and these can alter critical properties of the nanotubes. Xie et. al.[371] and Li et. al.[202] have both experimentally shown the ability for hydrophobic BNNTs to exhibit hydrophilic properties with the attachment of polyethylene glycol and amine groups.

To generate defects during synthesis, some groups control the growing conditions other modify the surfaces after synthesis with ion beam irradiation, ball-milling or through chemical means. Experimental images for 2-D h-BN vacancies and dislocations have been published. [57, 99, 154, 224] Vacancies were generated with high-energy electron beams on monolayer h-BN[154, 177, 224]. This approach has also been used to generate defects in BNNTs[394]. These vacancies take the form of mono, tri, and penta vacancies that lead to triangular holes in the monolayers.[154] In 2013 the 5-7 dislocations at grains boundaries were observed[99] and then later in 2014, using temperatures of 1000K, 4-8 dislocations were seen.[57] The 5-7 defects are expected to be less favorable due to the homo-elemental bonds, but research suggests that they are the dominant dislocations seen so far. [377] Ball milling has also been used to generate defects, which lead to nanoparticle attachments. [310] Arc ammonia plasma treatment has been applied to BNNTs successfully in 2007[146]. This method has led to many other surface modifications by using the amine groups as pathways to add other molecules of interest, for instance a thiol containing compound.[293]

Defects that are boron and nitrogen vacancies (V_B and V_N) and a 5-7-7-5 Stone-Wales defect. The 5-7-7-5 Stone-Wales defect was selected over a 4-8-8-4 defect because Bettinger et. al. showed that the formation energy for the 5-7-7-5 was about half of that of a 4-8-8-4 defect for both a sheet (5.5 eV vs. 11.0 eV) and for a (5,5) (5.6 eV vs. 10.6 eV) nanotube using the PBE functional and a 6-31G* basis set.[29] Other than Stone-Wales defects there has been theoretical work on mono-vacancies[15, 300],

di-vacancies[386], dislocation lines[393] and substitutions[15, 300], including boron, nitrogen and carbon atoms with varying charges[270] for both monolayer h-BN and BNNTs. Adsorption studies have been conducted with defective BN to see the reactivity modifications created by the defects. [212, 220] Researchers in 2011 investigated the means to generate different vacancies that have been observed in experiments by modeling ion bombardment using molecular dynamics to produce statistics that match some experimental work. [194] They showed that by altering the beam angle and energies, they could control the distribution of defects that occurred in the monolayer of h-BN.

3.0.5 Defect Investigation

The formation energy for defects in BN was previously calculated using the following formula:

$$E_{Form.} = E_{Total} - n_B\mu_B - n_N\mu_N + q(\mu_e + \epsilon_v) \quad (3.6)$$

using the total energy of the system (E_{Total}), the chemical potential of boron and nitrogen (μ_B and μ_N), the number of atoms (n_B and n_N), the charge of the system q , the electronic chemical potential (μ_e) and the energy of the top valence band (ϵ_v).

The chemical potentials (μ_B and μ_N) are calculated using a simulated boron-rich and a nitrogen-rich environment. For a boron-rich environment, μ_B is calculated from a phase of bulk boron $\beta-R$ containing 315 atoms[97], for the nitrogen-rich environment the chemical potential is calculated from a N_2 gas molecule. The nitrogen chemical potential is then solved by using the following formula:

$$\mu_B + \mu_N = \mu_{BN}^{Structure} \quad (3.7)$$

where $\mu_{BN}^{Structure}$ is the chemical potential of a pair of boron and nitrogen atoms in the specified nanostructure (nanotube or sheet).

Table 3.3

Formation energies of a monolayer of h-BN and a (10,0) nanotube. The formation energies are calculated in a B-rich and N-rich environment as explained in the text.

Defect	Formation Energy (eV)			
	Monolayer [15]		(10,0) Nanotube [300]	
	B-Rich ¹	N-Rich	B-Rich ²	N-Rich
N_B	10.08	4.80	9.19	0.37
B_N	2.88	8.16	4.66	13.5
C_B	3.84	1.44	3.57	-0.84
C_N	1.92	4.80	1.18	5.59
V_B	10.08	7.20	8.84	4.43
V_N	5.28	7.69	4.56	8.96

¹ μ_B (" $\alpha - \beta$ " B), ² μ_B "hexagonal bulk B"

To see the effects of defects in boron nitride, three types of defects were investigated. The concentrations are 3% (1 of 32 total atoms is removed for a total of 31 atoms),

6% (1 of 16, with a total of 15), and 12% (1 of 8 with a total of 7). The boron vacancies are shown in Figure 3.7 with the unit cell shown with the black outline. Similar structures were used for the nitrogen defects, except that the atom colors in Figure 3.7, green (boron) and white (nitrogen), would be interchanged.

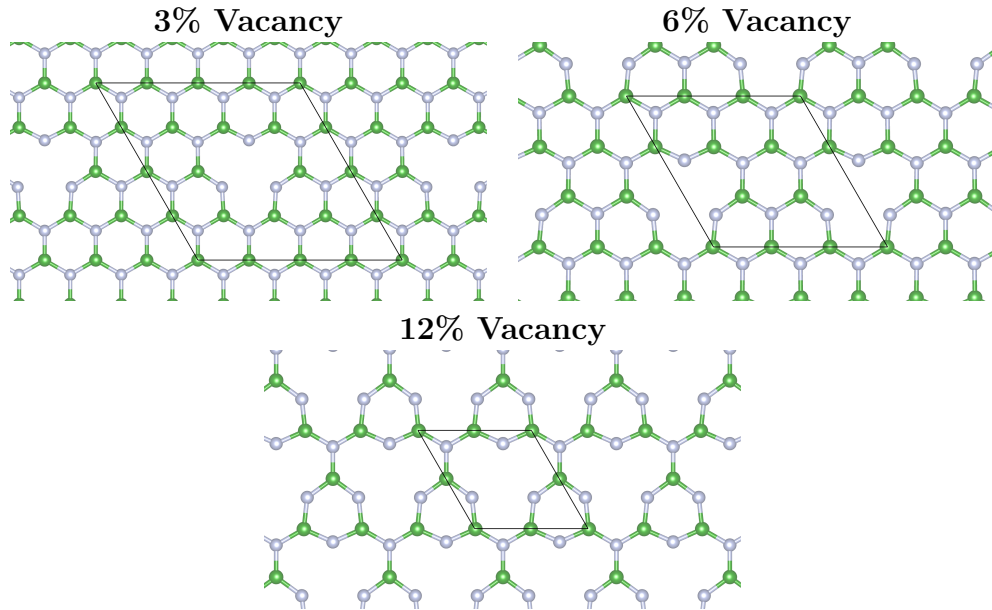


Figure 3.7: The unit cells used to calculate the formation energies for the vacancies for boron. A similar structure was used to calculate the nitrogen vacancies, but the boron (green) and nitrogen (white) atoms were switched. The concentrations are 3% (1 of 32 total atoms), 6% (1 of 16), and 12% (1 of 8). The black outline is the shape and size of the unit cell.

The formation energies (Table 3.4) for a nitrogen-rich environment show contrasting trends for the different vacancies. The energy for the boron vacancy decreases as the concentration increases, the formation energy for the nitrogen vacancy increases as the concentration of defects increases. The nitrogen structures show a constant magnetic moment (Table 3.5) of one. For boron vacancies the magnetic moment

decreases as the concentration of defects increases. At 3% the magnetic moment of the system is $3.0 \mu_B$, at 6% it is $1.53 \mu_B$ and then $0.30 \mu_B$ for a vacancy concentration of 12%. A net magnetic moment of one is expected for the nitrogen vacancies and a moment of three is expected for the boron vacancies.

Table 3.4

Formation energies for defects in a periodic sheet of boron nitride, where the following values were used $\mu_B = -6.65$ eV, $\mu_N = -8.32$ eV, and $\mu_{BN} = -17.58$ eV.

		Formation Energy (eV)					
Type	N-Rich			B-Rich			
5-7-7-5	6.21			6.21			
Type	N-Rich			B-Rich			
	3%	6%	12%	3%	6%	12%	
V_B	7.43	7.32	6.39	5.76	5.65	4.72	
V_N	7.61	7.64	7.69	9.28	9.31	9.36	

Table 3.5

The magnetic moment and band gap for the h-BN sheet with 3%, 6% and 12% vacancies of either boron (V_B) or nitrogen (V_N).

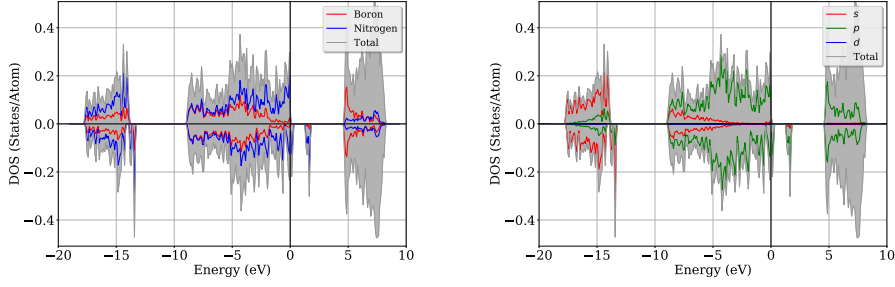
		V_B		
		3%	6%	12%
μ_B		3.00	1.53	0.30
Gap (eV)		0.00	0.00	0.00
		V_N		
		3%	6%	12%
μ_B		1.00	1.00	1.00
Gap (eV)		0.28	0.10	0.00

All the boron vacancy defect concentrations altered the material to be metallic, (Table 3.5). However, for the nitrogen vacancies, the gap decreased with an increase in vacancy concentration, with the highest density of vacancies (12%) becoming metallic. Each system's density of states can be seen in Figure 3.8 for the boron vacancies and

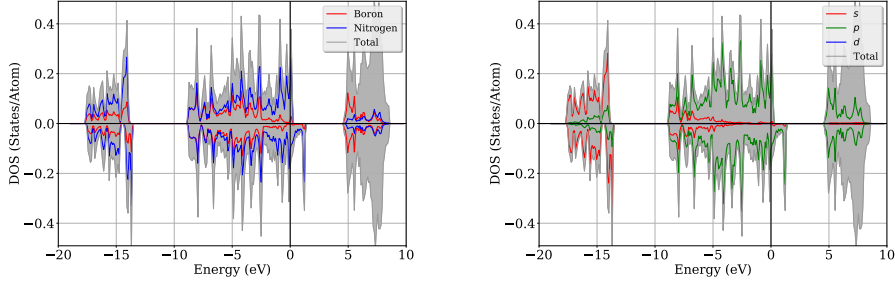
Figure 3.9 for the nitrogen vacancies. The density of states in the figures are projected onto both the atoms and the orbitals. The decreasing gap in the nitrogen structures is between spin-up and spin-down states, giving the 12% structure a semi-metallic property. For the 3% boron vacancy structure the Fermi level is only populated by spin-down states and for the 6% boron vacancies it is occupied by both spin-up and spin-down states. The 12% structure is almost spin unpolarized and the Fermi level is crossed by both by spin-up and spin-down states.

Defects for the cluster model of boron-nitride were also investigated. The $n = 5$ structure with 180 atoms, as shown in Figure 3.5, was used. The boron and nitrogen vacancies and the 5-7-7-5 were constructed with the cluster. The relaxed structures with the corresponding bond lengths, at the center of the cluster, for the pristine, 5-7-7-5 Stone-Wales defect, boron vacancy and nitrogen vacancy are shown in Figure 3.10 For the pristine structure the distances between the similar atoms (N-N, B-B) is 2.52 Å this number is also the lattice constant for a periodic structure. The B-N bond distance for the pristine structure is 1.45 Å the same seen in periodic structures. For the boron vacancy, the N-N bond increases to a range of 2.68 to 2.80 Å, this is due to the lone electron of the nitrogen atoms, that were previously bonded to the boron, repelling each other. The bond exterior to the defect also changed, with the nearest lengths decreasing to between 1.40 and 1.42 Å and the next nearest increasing to between 1.45 Å and 1.49 Å. The opposite is seen with the nitrogen vacancy, the distance between similar atoms decreases to 2.27 Å. The nearest bonds both increase

Boron Vacancy (3%)



Boron Vacancy (6%)



Boron Vacancy (12%)

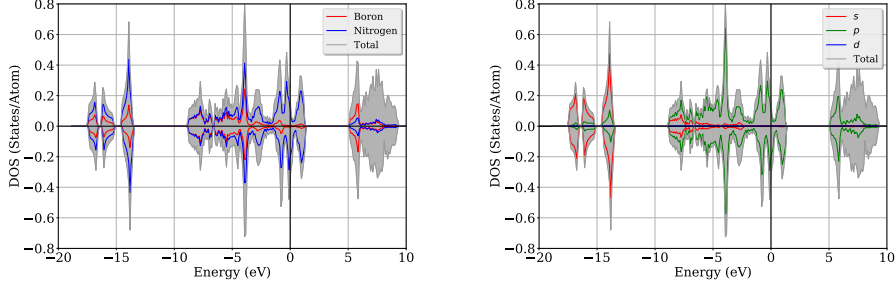
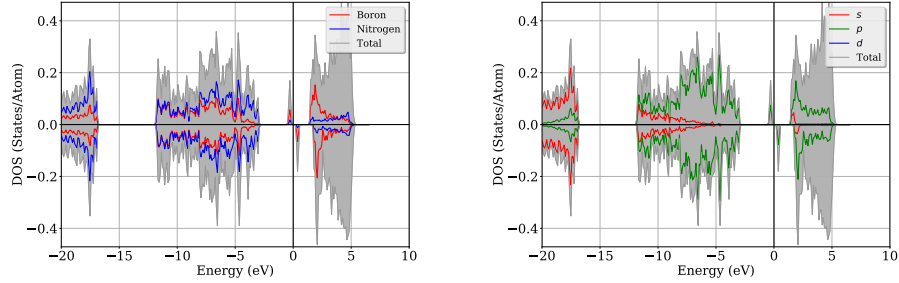


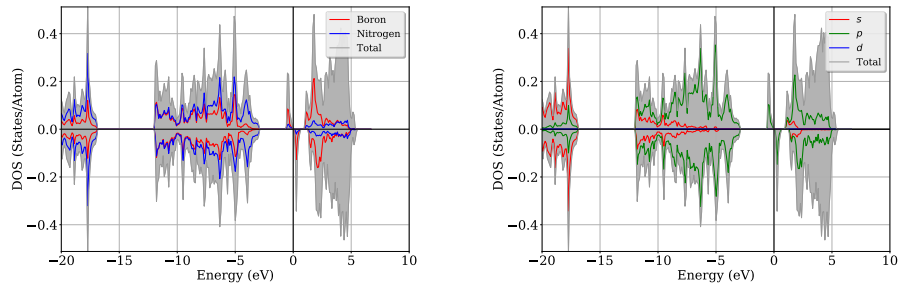
Figure 3.8: The projected density of states (PDOS) and total density of states (TDOS) of the different concentrations of boron vacancies of h-BN, top plots are the PDOS projected onto the atoms (boron (red), nitrogen (blue) and total(grey)), the bottom is the PDOS projected on the orbitals where s(blue), p(green), d(blue) (none in the system) and total(grey) are shown for both spin-up and down.

to 1.47 Å and decrease to 1.44 Å. The next nearest bonds increase to 1.47 Å, while the boron atoms remain the same at 1.45 Å.

Nitrogen Vacancy (3%)



Nitrogen Vacancy (6%)



Nitrogen Vacancy (12%)

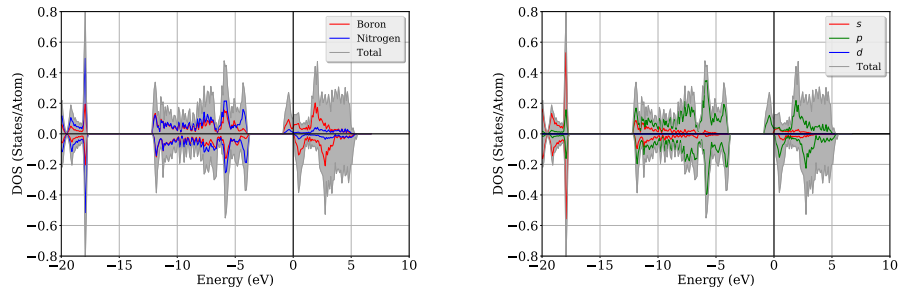


Figure 3.9: The projected density of states (PDOS) and total density of states (TDOS) of the different concentrations of nitrogen vacancies of h-BN, top plots are the PDOS projected onto the atoms (boron (red), nitrogen (blue) and total(grey)), the bottom is the PDOS projected on the orbitals where where s(blue), p(green), d(blue) (none in the system) and total(grey) are shown for both spin-up and down.

Cluster Model of Defects

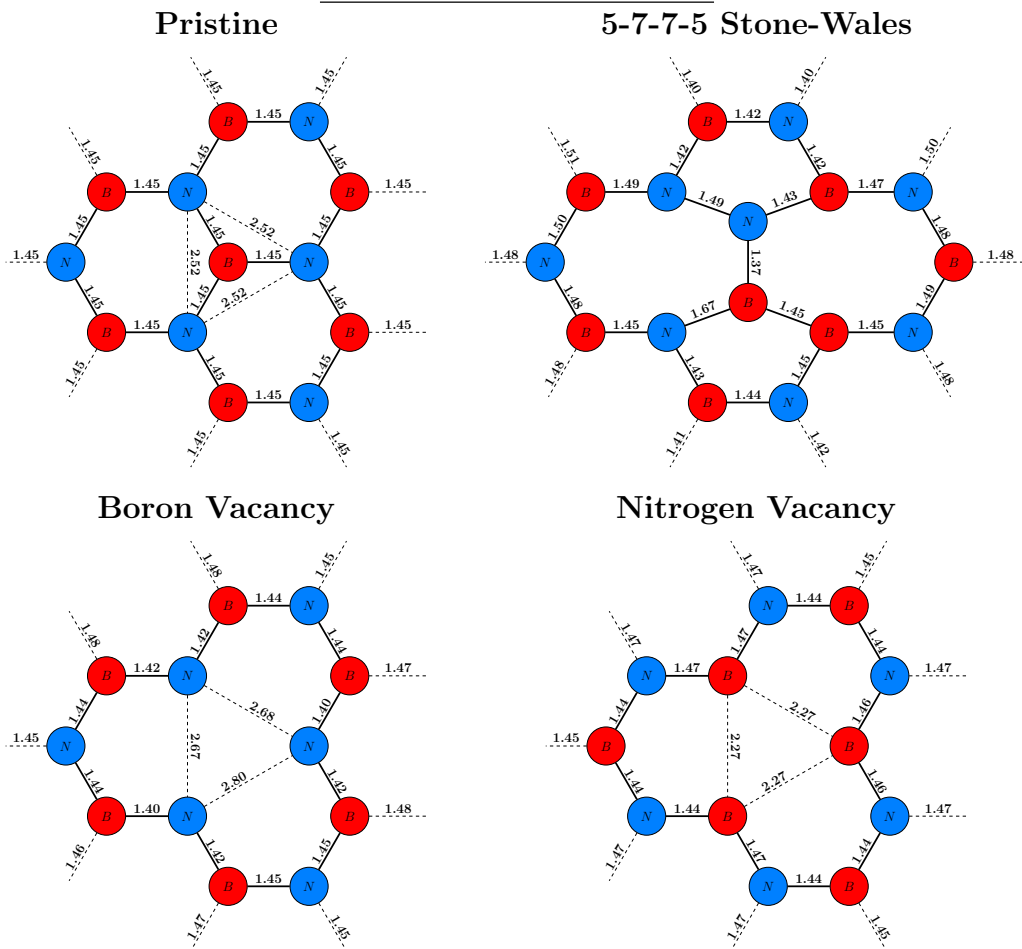


Figure 3.10: A series of cartoons given to present the cluster model structures and bond lengths of the localized effects of the defects, the boron atoms are red and nitrogen atoms are blue. All defects were generated in a pristine BN finite model with 180 atoms (75 boron, 75 nitrogen, 30 hydrogen) (top left) and the same cluster with a boron-nitrogen bond rotated by 90° (top right) in the center of the cluster created a 5-7-7-5 Stone-Wales defect and a defected BN cluster formerly of 180 atoms with a boron vacancy (bottom left) and a nitrogen vacancy (bottom right) representing possible defects.

Chapter 4

Stability and Electronic properties of of Gold Quantum Dots on Boron Nitride Nanotubes

4.1 Introduction

Since their initial prediction [30] and synthesis [50] in the early 90's boron nitride nanostructures including nanotubes (BNNTs) have gained significant attention from the scientific community [101, 207, 343]. BNNTs have a morphology similar to that of well-characterized carbon nanotubes (CNTs), however they exhibit distinct electronic and mechanical properties, thermal stability and chemical inertness[101]. To enhance or exploit BNNT's unique properties for nanoscale applications, functionalization of BNNTs has been recommended[355]. The functionalization can be achieved via covalent bonds forming strongly-bonded complexes or non-covalent bonds forming weakly-bonded complexes[391]. Both of these conditions have been realized with colloidal nanoparticles (PbSe, CdSe, and ZnO)[339], SnO₂[124, 390], Fe₃O₄[142], TiO₂ [319], and Au[188] nanoparticles. Specifically, it has been observed that Au can form nanoparticles of various sizes [9, 80, 188, 293, 310]. Furthermore, the role of substrate has been investigated considering the case of gold on BN monolayer deposited on a Rh substrate [173, 174, 255]. Note that a hexagonal-BN monolayer (h-BN) can be considered as a flattened BNNT which exhibits physical and chemical properties similar to those associated with large radii BNNTs[117, 284, 349].

4.2 Computational Details

Electronic structure calculations were performed in the framework of density functional theory. The generalized gradient approximation was used in the form of the Perdew-Burke-Ernzerhof (PBE) [259] functional with projector-augmented-wave (PAW) potentials [31, 180]. To take into account of the long-range dispersive interactions in the weakly-bonded complexes, the Grimme D2 semi-empirical approximation was included [111]. The plane wave cutoff energy was set to 400 eV and the Brillouin zone was sampled with a Γ -centered k-point grid of (5x5x1) [249]. The convergence criterion for the energy was set to 10^{-5} eV for the isolated clusters and 10^{-4} eV for the large conjugated structures ($\text{Au}_x/\text{h-BN}$). For all the calculations the force convergence criterion was set to $3 * 10^{-2}$ eV/Å and the Gaussian smearing was set to 0.05 eV.

Since the PBE-DFT level of theory is known to underestimate the band gap of a given material, we also performed Γ -point calculations on the pristine gold clusters using the hybrid HSE06 functional form [185]. The HSE06-DFT level of theory has been shown to provide an agreement between calculated and measured band gap of a given material.[96] Calculations were performed using the Vienna Ab initio Simulation Package (VASP) [179, 181, 182, 183].

Considering the fact that the observed Au clusters deposited on BNNT appears to mimic fragments of Au(111) surface, we considered Au_n clusters with $n=6$ [368], 10[368], 12[169, 367], 14[368] and 16[44, 368] and their 3D counterparts found in the literature. The Au_8 was excluded, the minimum energy structure in the literature[368] does not resemble a fragment of an Au(111) surface. The substrate was simulated in a 23 Å x 23 Å periodic supercell, the Au_6 substrate supercell is 15 Å x 15 Å. A separation of 10 Å between the clusters from their mirror images was used in the periodic supercell model. For the supported cluster-complex the binding energy is calculated with $E_{Complex} - E_{Cluster} - E_{Substrate}$, where $E_{Complex}$ is the total energy of the complex, $E_{Cluster}$ is the total energy of the isolated cluster and $E_{Substrate}$ is the total energy of the isolated substrate.

4.3 Results and Discussion

4.3.1 Au_n Clusters

Au_n clusters have been subject of several theoretical and experimental investigations over the past decade. There still exists ambiguity about the inflection point for 2D-to-3D structural transition [21, 36, 85, 169, 216, 367, 368, 381]. The inflection point associated with the structural transition from 2D to 3D was found to be dependent on

the level of theory employed for electronic structure calculations [21, 85, 216, 367, 381].

The initial cluster configurations for the calculations were taken from the previously reported results on Au₆ [368], Au₁₀ [368], Au₁₂ [169, 367], Au₁₄ [368] and Au₁₆ [44, 368]. Calculations were performed only for the 2D and 3D minimum structural configurations that were previously reported, without making an attempt to find the global minimum for either free Au clusters or Au clusters supported by the substrate. Figure 4.1 displays the equilibrium configurations of 2D and 3D structural configurations of Au_n clusters with n=6, 10, 12, 14 and 16.

Figure 4.2 displays the energy/Au atom, it suggests that the 2D-to-3D structural transition occurs between six and ten atoms in Au clusters, with the inflection point on the graph indicating a nine atom cluster. The difference in the energy between 2D and 3D structural configurations changes from -0.12 eV for n=6 to +0.16 for n=14 indicating that the 3D structural configurations are energetically preferred for larger isolated Au clusters at the PBE-DFT level of theory.

Table 4.2 lists the calculated bond lengths of equilibrium configurations of the 2D and 3D Au clusters. The calculated results show an excellent agreement with the previously reported results, except the case of the 3D-Au₁₀ cluster for which buckling at the edges was noticed. The buckling in 3D-Au₁₀ was not seen in the previously reported results [367, 368]. Note that the average bond length was calculated by taking the sum of the distances under 3.0 Å and then divided by the number of

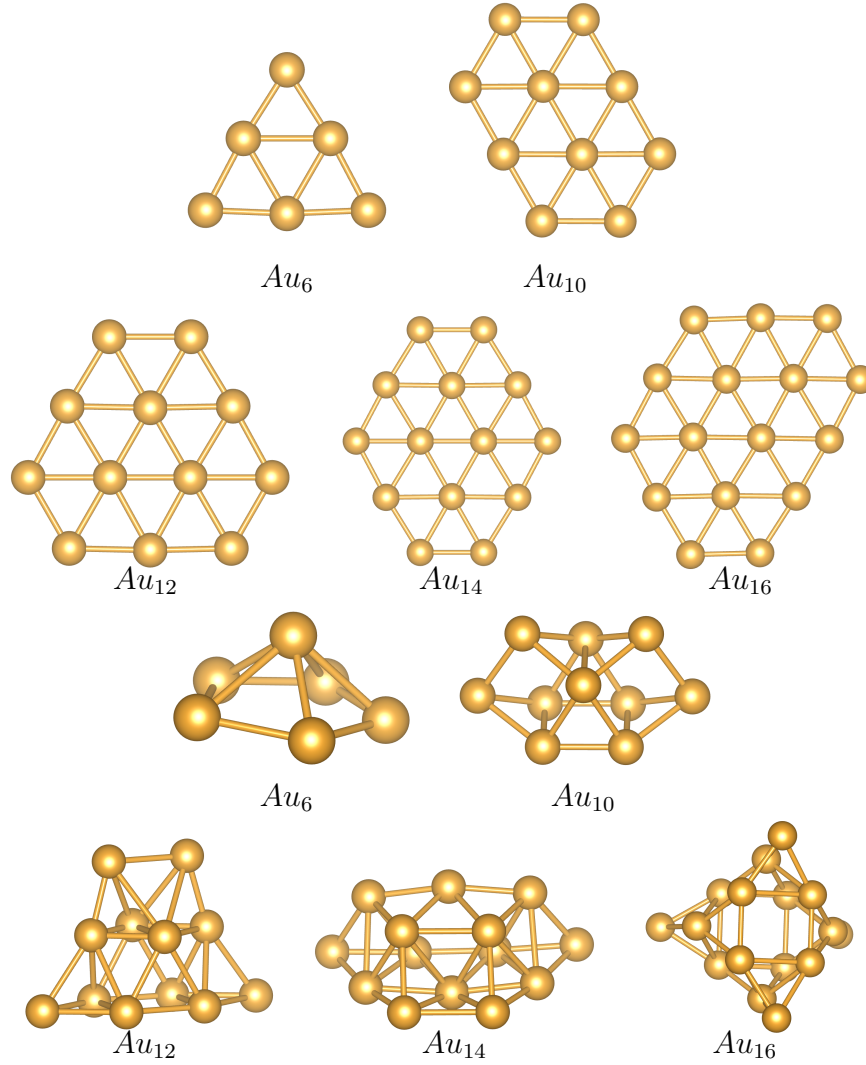


Figure 4.1: Calculated structural configurations of the isolated Au_6 , Au_{10} , Au_{12} , Au_{14} and Au_{16} clusters. The top 5 are the 2D structures and the bottom 5 are the 3D structures.

unique bonds in a given cluster.

The calculated density of states (DOS) find Au_n clusters to have non-zero band gaps except the case of 2D- Au_{14} which appears to be metallic at the PBE-DFT level of theory. Application of the HSE functional form yields the non-zero band gaps for

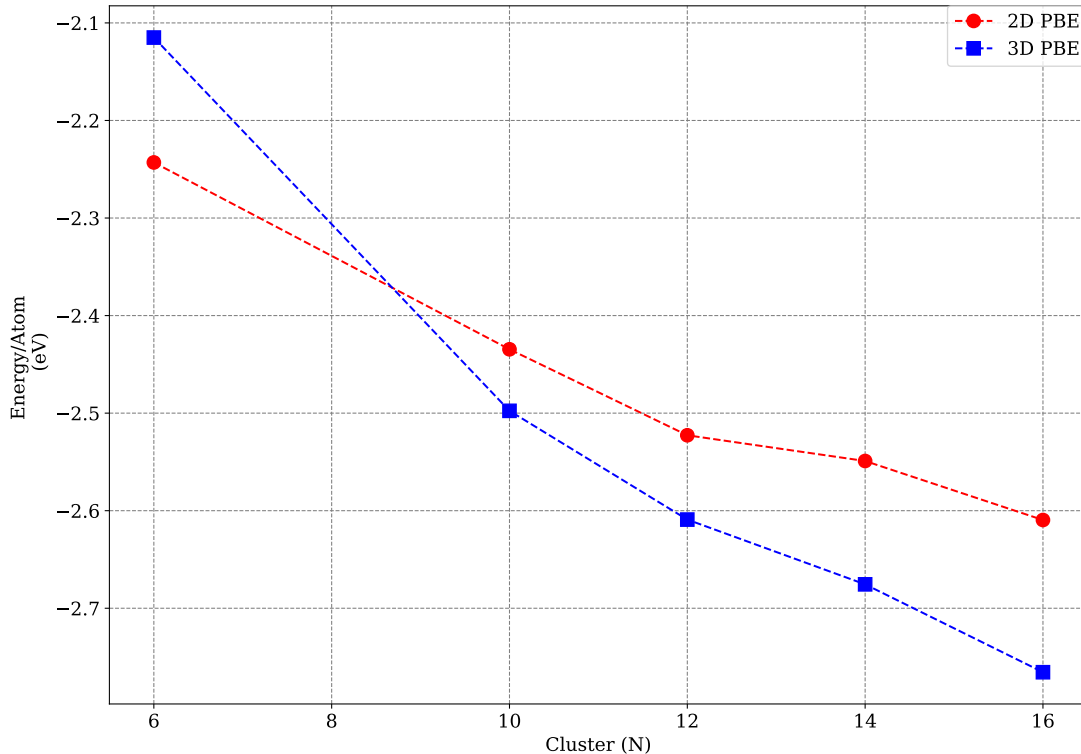


Figure 4.2: The total energy/atom as a function of cluster size (n). The plot indicates that after about nine atoms the 3D structures are more stable than the 2D structures when they are isolated. The 2D structures are given in red (squares) and the 3D structures are given in blue (circles).

all Au clusters considered, as expected. Note that a recent theoretical study which employed B3LYP, B3PW91, HSE, and PBE0 hybrid density functionals over a large benchmark data set of materials [96] reported no significant difference in their overall performance of the functional forms. The screened hybrid HSE was found to be relatively accurate for typical semiconductors. For a h-BN monolayer, the calculated PBE and HSE band gaps are 4.36 and 5.69 eV, respectively [379]. The measured gap of h-BN monolayer is reported to be 5.97 eV [348]. For the 2D-Au_{*n*} clusters, the HSE band gaps are 2.76, 1.47, 1.47, 0.35 and 0.95 for $n=6, 10, 12, 14,$ and 16,

Table 4.1

Calculated structural properties of the isolated and supported 2D Au_n clusters.

Structure	2D configurations		
	Symmetry	Avg. Bond (Å)	Bonds (#)
Au ₆	D _{3h}	2.69	9
Au ₆ /h-BN	D _{3h}	2.70	9
Au ₁₀	D _{2h}	2.71	19
Au ₁₀ /h-BN	D _{2h}	2.72	19
Au ₁₂	D _{3h}	2.71	24
Au ₁₂ /h-BN	D _{3h}	2.72	24
Au ₁₄	D _{2h}	2.71	29
Au ₁₄ /h-BN	D _{2h}	2.72	29
Au ₁₆	C _s	2.72	34
Au ₁₆ /h-BN	C _s	2.72	34

Table 4.2

Calculated structural properties of the isolated and supported 3D Au_n clusters.

Structure	3D configurations		
	Symmetry	Avg. Bond (Å)	Bonds (#)
Au ₆	C _s	2.73	10
Au ₆ /h-BN	C _s	2.74	10
Au ₁₀	C _{2v}	2.72	23
Au ₁₀ /h-BN	C _s	2.72	18
Au ₁₂	C _{2v}	2.75	26
Au ₁₂ /h-BN	C _{2v}	2.76	24
Au ₁₄	C _s	2.74	33
Au ₁₄ /h-BN	C ₁	2.74	29
Au ₁₆	T _d	2.73	36
Au ₁₆ /h-BN	C ₁	2.72	32

respectively. On the other hand, the HSE band gaps for 3D-Au_n clusters are 1.91, 0.72, 1.43, 0.53, and 1.65 eV, respectively. As n increases to larger values, both 2D- and 3D-Au_n clusters will exhibit metallic electronic properties[234].

4.3.2 Supported Au Clusters: 2D-Au_n and 3D-Au_n clusters on h-BN monolayer

Figures 4.3 and 4.1 display the equilibrium configurations of 2D-Au_n and 3D-Au_n clusters interacting with h-BN monolayer, respectively. Overall, the base of a cluster configuration and the monolayer are found to be in parallel to each-other with a distance of about 3 Å. All of the 2D-Au_n clusters retained their configurations with the same symmetry. However, lowering of the symmetry is predicted for some of the 3D-Au_n clusters with n=10, 14, and 16. Au₁₀ has a small deformation in the base, whereas Au₁₄ retains its overall shape, though structure has noticeable deformations. Au₁₆ is predicted to have significant deformation in its configuration reducing the symmetry from T_d to C₁, Table 4.2. Note that the average bond lengths in Au clusters has increased slightly (0.1 Å) when deposited on the h-BN monolayer.

Table 4.3

Supported Au clusters: the nearest distance between the cluster atom and h-BN monolayer (R_{Au-BN}) and the binding energy/Au atom (B.E/Au).

Cluster	2D configurations		3D configurations	
	R_{Au-BN} (Å)	B.E/Au (eV/Au)	R_{Au-BN} (Å)	B.E/Au (eV/Au)
Au ₆ /h-BN	2.91	-0.49	2.77	-0.48
Au ₁₀ /h-BN	2.98	-0.50	2.74	-0.34
Au ₁₂ /h-BN	2.92	-0.49	2.73	-0.34
Au ₁₄ /h-BN	2.95	-0.49	2.88	-0.35
Au ₁₆ /h-BN	2.97	-0.49	2.44	-0.31

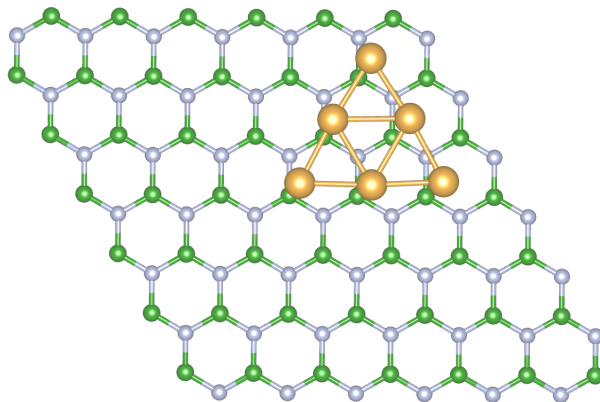


Figure 4.3: A top view of the equilibrium configuration of the supported 2D-Au₆ cluster.

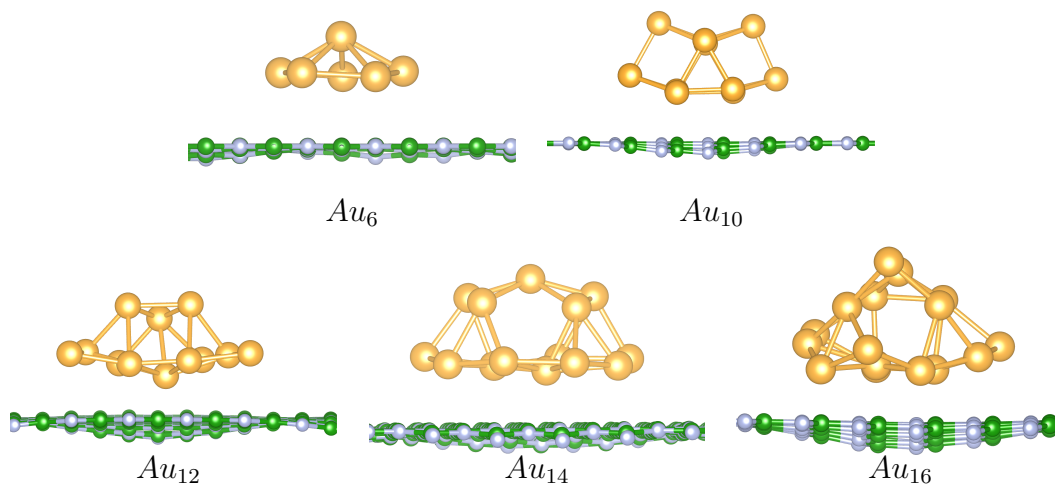


Figure 4.4: A side view of the equilibrium configurations of the supported 3D-Au_n clusters.

Interestingly, a preference for 2D-Au_n configurations over 3D-Au_n configurations on h-BN monolayer is clearly seen as the 2D structural configurations appear to substrate tend to maximize the interaction with the substrate, unlike their 3D counterparts. The binding energy per atom is nearly constant at about at 0.50 eV for all the 2D

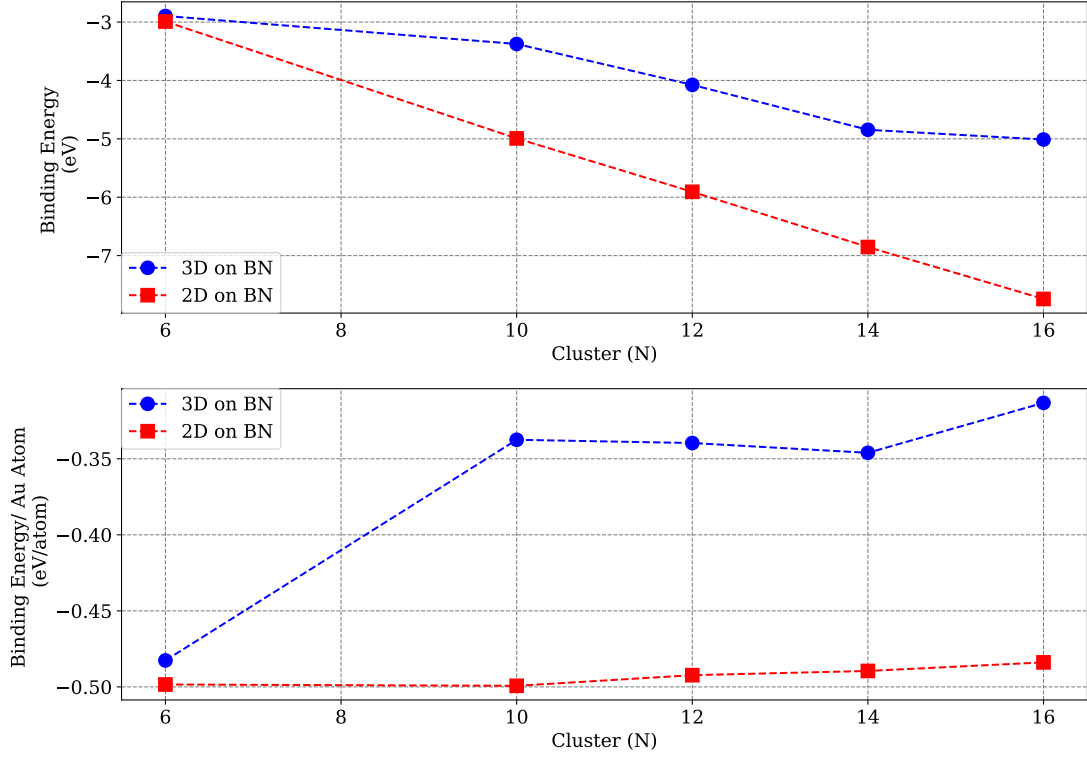


Figure 4.5: Supported Au_n clusters: Variation in the binding energy/Au atom as a function of cluster size, n . The 2D structures are given in red (squares) and the 3D structures are given in blue (circles).

configurations, whereas it varies from -0.48 eV for 3D- Au_6 to -0.31 eV for 3D- Au_{16} (Figure 4.5). Employing the limited data that has been aggregated, we now make an attempt to estimate the inflexion point where the 3D configurations becomes energetically preferred over the 2D configurations on h-BN monolayer. An extrapolation of a linear fit to the values of the binding energy/atom of 2D- Au_n and 3D- Au_n configurations suggests the inflexion point to be associated with Au_{100} cluster for which 3D configuration is preferred on h-BN clusters. This is in agreement with experiments which have shown stabilization of larger 3D- Au_n configurations (i.e. quantum dots) on the surface of a large-diameter BNNT [188]).

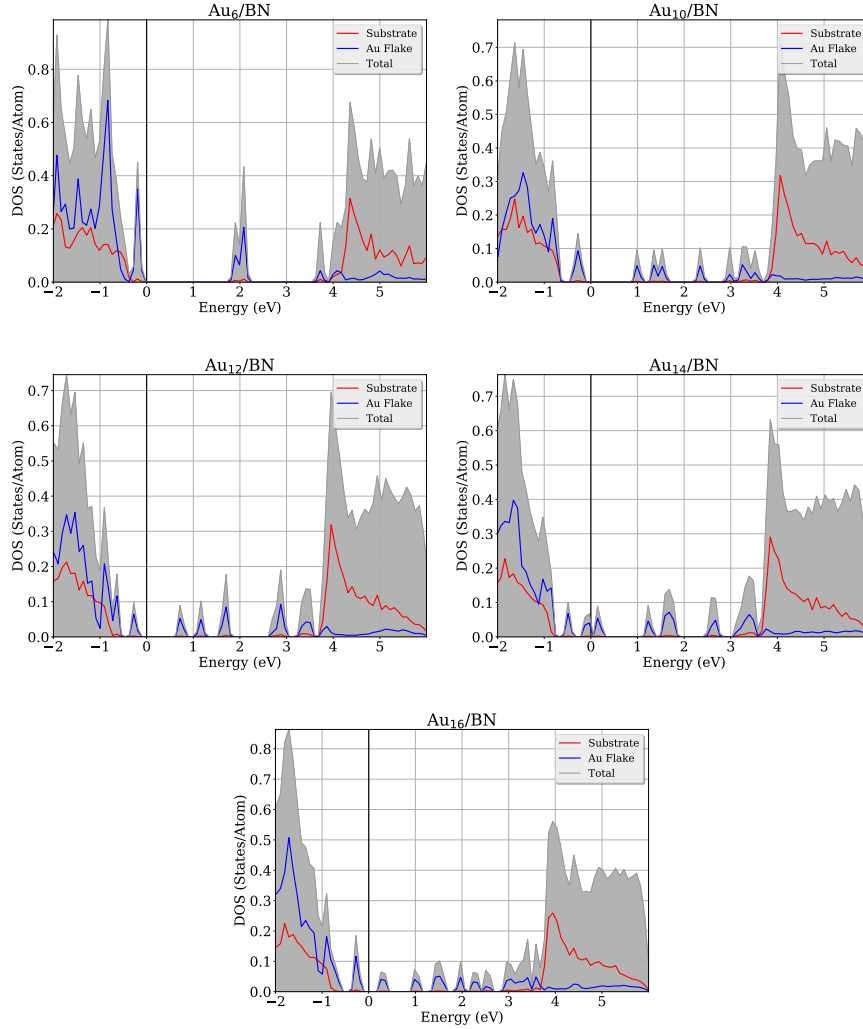


Figure 4.6: Projected density of states (PDOS) and total density of states (TDOS) of the supported 2D-Au_n clusters. Color code: grey-TDOS, red-PDOS of 2D-Au_n cluster, blue-PDOS of h-BN monolayer.

For the supported Au clusters, the band gap is defined by that of the pristine h-BN monolayer. All of the clusters induce mid-gap states in the band gap Figure 4.6. Note that the band gap of a pristine h-BN monolayer is calculated to be about 4.30 eV in agreement with the previously reported results obtained at the PBE-DFT level of theory [117, 349]. Interacting with h-BN monolayer, 2D-Au_n clusters retain their

band gaps, and vary only within about 0.1 eV of their respective values obtained for the isolated clusters. This is also the case with 3D-Au_n clusters where difference in the band gap of about 0.2 eV is predicted between the isolated and supported clusters.

4.4 Summary

2D and 3D Au₆, Au₁₀, Au₁₂, Au₁₄ and Au₁₆ clusters on h-BN substrates were investigated. It was shown that when the clusters are isolated, they prefer the 3D structures. However, when they are placed on a h-BN substrate the 2D structures become energetically favorable. The structures are bound to the substrate through long-ranged interactions. The gold cluster retain their semiconducting nature, while introducing mid-gaps states to the h-BN.

Chapter 5

Amino Acid Analogue-Conjugated BN Nanomaterials

Reprinted with permission from ACS. Copyright 2017 American Chemical Society.

More information is in Appendix D

5.1 Amino Acids and Proteins

During the investigation of this dissertation, a background in additional fields was necessary. If the interactions between biological molecules and nanomaterials were to be investigated, some fundamental concepts of biochemistry needed to be learned. In this section the fundamentals of amino acids and proteins will be discussed. To a chemist and biologist this section is elementary, but due to the absence of biochemistry in a traditional physics curriculum, it will be covered. There will be a build up from the structure of amino acids to the complex structure of a protein.

Amino acids are molecules that are made up of three distinct groups. The first two groups are the same for all amino acids, they each have an amine group ($-\text{NH}_2$) and a carboxyl group ($-\text{COOH}$). The third group is the side chain, called the R-group. This group makes each amino acid unique. There are over 500 types of amino acids, by the 22 proteinogenic amino acids are the ones used in the synthesis of proteins.[193] The three groups of these amino acids are connected by one carbon atom called the α carbon. This is where the name α amino acids comes from. The backbone of an amino acid contains the amine group, the α -carbon and the carboxyl group. Most amino acids found in a biological setting are L-stereoisomers ("left-handed"), opposed to the D-stereoisomers ("right-handed"). 20 of the 22 amino acids are directly coded into the DNA, and these are the ones that will be discussed. The two that will

not be not included are selenocysteine and pyrrolysine.[8] Selenocysteine[210] has the same structure as cysteine, but it has a selenium atom instead of a sulfur atom and pyrrolysine[127], which is not present in humans. The other 20 can be found in Figure 5.1, they are categorized into four distinct groups; acidic, basic, polar and non-polar.

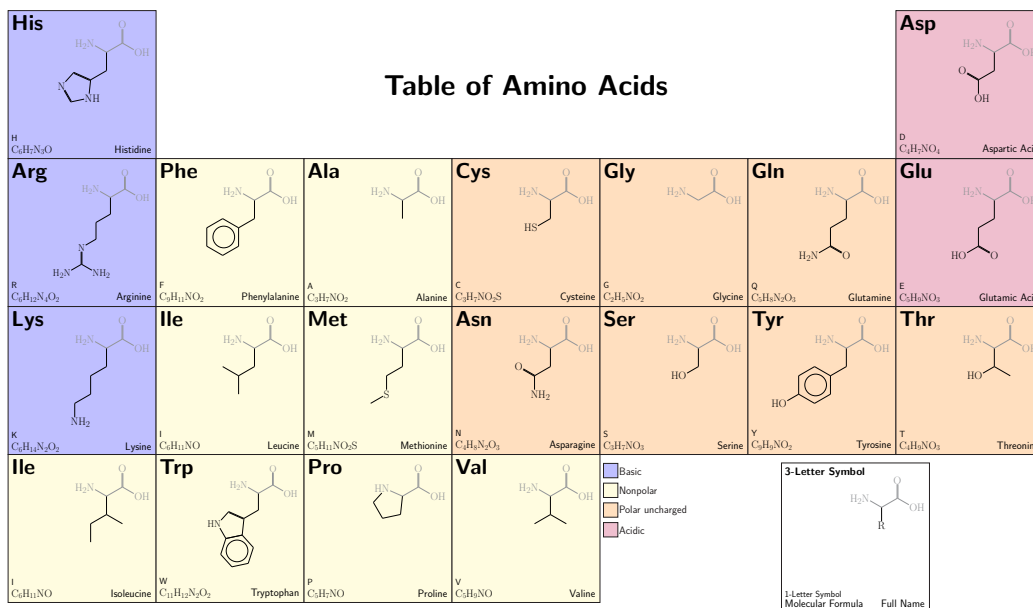


Figure 5.1: Amino acid table containing 20 proteinogenic α -amino acids with a legend in the bottom right hand corner. The common backbone is in faded gray and the unique R-groups are in black. Each amino acid is grouped, acidic, basic, aromatic, polar and non-polar, by color. The table concept was adapted from a table from bio-connect.nl [18]

The structures of amino acids have different states when introduced into different environments. Each group (amine, carboxyl and R-group) of each amino acids has its own unique pK_a (acid dissociation constant). This means that the structure changes depending on the local pH, two examples of aspartic acid and arginine are shown in Figure 5.2. Each group's pK_A value is given in Figure 5.2, pK_1 is for the carboxyl group, pK_2 is for the amine group and pK_R is for the R-group. The labels

are inserted between the tiles, because at the specific pH the states have an equal probability of existing. The distribution is described logarithmically, at a pH of ± 1 , the probability shifts to a 90%/10% distribution. Due to the interest in the interaction in physiological conditions, the structures used in this dissertation are the amino acids at a pH of 7.4. The zwitterionic structure of the backbone is shown in the middle two panels in Figure 5.2. The amine group is protonated (NH_3^+) and the carboxyl group is deprotonated (COO^-), giving the groups different charges, but the backbone, overall, is still neutral. At a pH of 7.4 all backbones are in a zwitterionic state. The only amino acid without a definitive state at this pH is histidine, with a pK_R of 6.04, the NH group in Figure 5.1 can be either protonated or deprotonated. The states of the amino acids can still change, the pK_a values are subject to change depending on their local environment.[378]

To form proteins, as shown in Figure 5.3, amino acids need to bind with each other to form chains. To combine two amino, their backbones bind to each other to form a peptide bond. Two amino acids create a dipeptide with an amine group at one end of the chain and a carboxyl group on the other. With three amino acids they form a tripeptide and it continues on to larger prefixes (tetra, penta, oligo(2 to 20),...polypeptide(n)), but typically they are generalized to peptide. These chain sizes range from a few hundred[178] up to 27,000 amino acids[93]. Once in the chain, amino acids are typically called amino acid residues, due to the loss of a H_2O molecule in the formation of a peptide bond. To mimic this phenomena in the calculations, the backbone

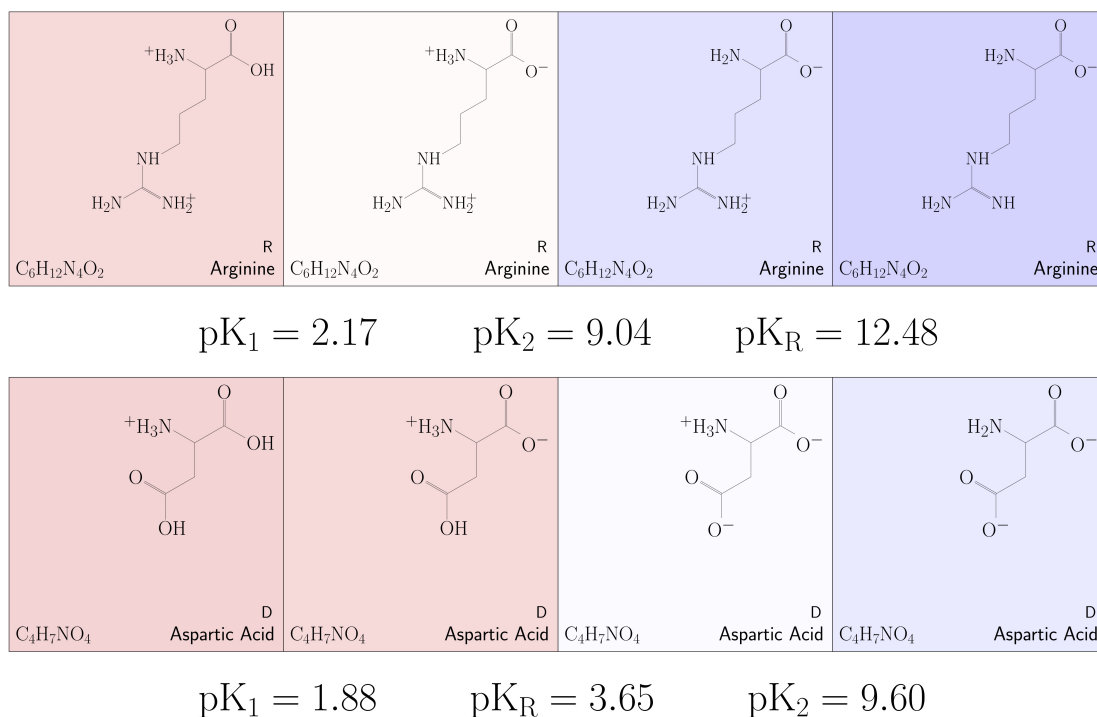


Figure 5.2: Each group in an amino acid has a pK_a associated with it, pK_1 is for the carboxyl group, pK_2 is for the amine group and pK_R is for the R-group. The tiles are colored to represent how acidic (red) or basic (blue) the environment is, with white representing a neutral pH. The labels are inserted between the tiles, because at the specific pH the structures have an equal probability of existing.

was replaced with a non-polar methyl (CH_3) group. The approximation serves two purposes, first it eliminates the potential interactions from the amine and carboxyl group that would otherwise be bonded to form the peptide bonds and it reduces the number of electrons in the simulation.[349] This approach has been successfully done by a few groups for both amino acids and nucleic acids.[109, 220]

There are four structural aspects to a protein; the primary, secondary, tertiary and the quaternary structure. The sequence of amino acids in the polypeptide chain, or

peptide chain, is the protein's primary structure. These chains are long and relatively flexible, allowing for hydrogen bonds to form between local amino acids, forming structures from the sequences of amino acids. These structures are the protein's secondary structure, and the most common are the α -helix, β -sheet and turns.

The next level up in the protein's structure is the tertiary structure. It is determined by non-local interactions of the peptide chains and the process is typically associated with protein folding. Interactions leading to the tertiary structure include disulfide bonds, salt bridges and hydrogen bonds. The last level of the protein structure is the quaternary structure, it is determined by the number and the interactions of peptide chains with each other. An example of the peptide chains in a bovine serum albumin (BSA) protein is shown in Figure 5.4.

The protein structure shown in Figures 5.3, 5.4 and 5.5 were generated using x-ray diffraction.[213] The protein contains 8784 atoms, excluding hydrogen atoms, which are not resolvable with x-ray diffraction. The structure contains 1166 amino acid residues, and each unique type (20 total) is shown in Figure 5.3. These figures convey the complexity of modeling proteins with either molecular dynamics or quantum mechanical calculations. Proteins lack symmetry and need to be in a solvated environment in hopes to obtain a realistic structure, which adds more variables and atoms to the simulations. With the limitations of the imaging technologies, some of the protonation states of the amino acids may also be incorrect. New advances in x-ray

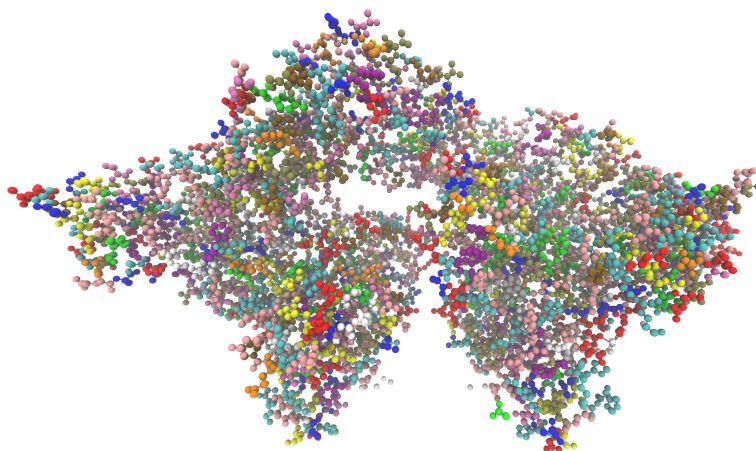


Figure 5.3: An atomic representation of a BSA protein based from experimental x-ray diffraction data.[213] The hydrogen atoms are omitted, missing due to the experimental technique with highlighted each type of amino acids having its own color.

crystallography may be able to bring more clarity to the hydrogen atoms for future structures.[360] Some of the amino acids on the inside of the protein may be in a local pH that changes the structure that is typically considered at a physiological pH.

The most challenging aspect of studying proteins is the number of atoms. For almost two decades, investigating proteins using force fields for molecular dynamics[22, 61] has been possible, but currently it is extremely difficult for quantum mechanical methods to simulate a full protein. Some ways to approach the problem is through a divide and conquer method, dividing the areas into molecular mechanics and quantum mechanical regions, called QMMM[335]. Care must be taken when constructing these

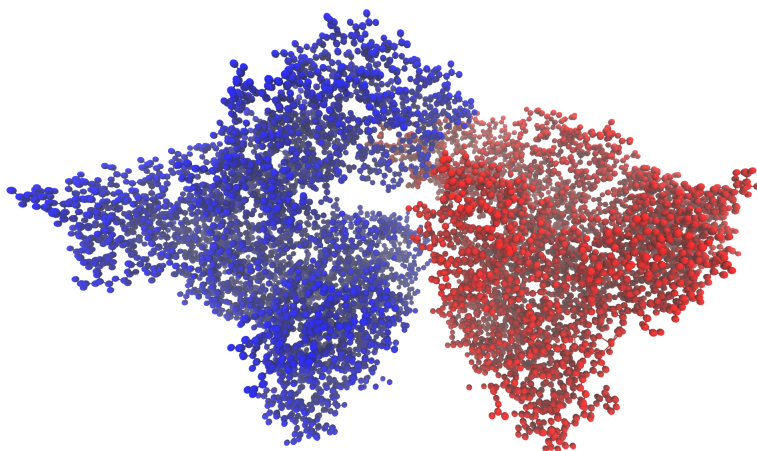


Figure 5.4: An atomic representation of a BSA protein based from experimental x-ray diffraction data. [213] Each peptide chain in the protein has a unique color, one red and the other blue.

simulations, correctly modeling the boundary region between the quantum mechanical and molecular mechanical is difficult.[113] The models will also have to use molecular mechanics, which has the potential to inaccurately model the atomic interactions.

5.2 Conjugated Systems

Introducing substrates and nanomaterials with proteins and protein sub-structures has been of great interest in the past decade, as discussed in Chapter Section 1.4. Groups have started to investigate small building blocks of amino acids with boron-nitride nanotubes in the gas-phase using first principle methods.[232] However to gain

a better understanding of these interactions, the physiological conditions need to be modeled. Water plays an important role in the reactions and stabilizes the zwitterionic structure of the amino acids.[1] To do this water needs to be introduced through implicit solvent models or through, preferably, explicit solvent. Another important consideration is introducing temperature into the simulations. In biology most of the systems are dominated by long-ranged forces and simulating these environments at 0K or 300K has a potential to change the structures and potentials chemistries.[114] However, to achieve these conditions, molecular dynamics must be used. In Chapter 5 an implicit solvent model is used and amino acids are used to investigate some basic properties with boron-nitride nanotubes. In Chapter 6 the next steps of introducing temperature and explicit solvent models using ab initio molecular dynamics (AIMD) is presented.

Groups in the past years have started to use various classical force fields and molecular dynamics methods to model physiological conditions. They have simulated amino acids interacting with a Pd(111) surface[118], a TiO₂ surface [35], a graphene surface[143] and nanoparticles [305] and Au(111) [134]. Some have moved past the amino acid stage and started to work with peptide chains with substrates.[37, 66] With large enough computation power and a crude enough model, it is possible to even simulate full proteins with carbon nanotubes[115] or boron-nitride nanosheets with cell membranes[133]

Force fields have been parameterized to replicate specific chemistries, if new structures or bonds form the force field may not replicate accurate interactions. A method to work around this issue is to use AIMD methods. With this increase in accuracy, the potential system size that can be simulated is drastically reduced when compared to classical molecular dynamics. The goal is to be able to simulate systems as shown in Figure 5.5, model the interactions accurately between the systems. Using this information derived from these results, experiments can be assisted leading to a more complete understanding.

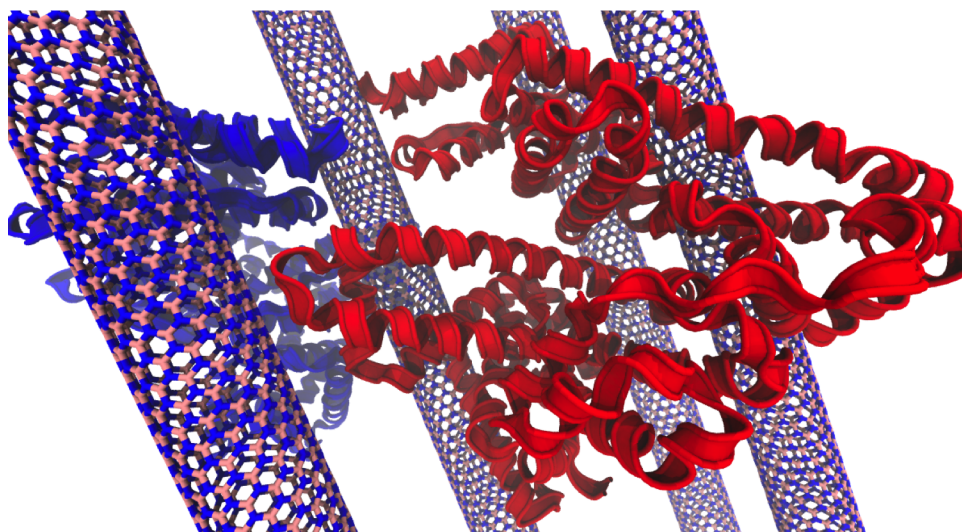


Figure 5.5: A ribbon representation of a BSA protein, with one peptide chain colored blue and the other red, interacting with several boron nitride nanotubes. For a complete simulation this would also need the additional a large amount of water molecules. This would drastically increase the cost of the simulation.

5.3 BNNT with Amino Acids

Nanomaterials with different topologies possess unique and distinct properties that can be exploited for biologically related applications, such as biosensing[46], drug delivery[290], and bioimaging[201]. Some of the topologies that have been investigated as substrates for these applications include nanotubes (NTs)[46, 48, 161, 251, 364] nanowires[58], nanoparticles[138], nanorods[38], and two-dimensional (2-D) sheets[309]. Boron nitride NTs[50] (BNNTs), one of the emerging nanomaterials, have a morphology similar to that of the well-established carbon NTs (CNTs). BNNTs are recognized as viable candidates for conjugation with biomolecules[101], showing a strong affinity toward proteins[389]. However, experiments show contrasting results in terms of the toxicity effects of BNNTs.[67, 86, 87, 373]

To provide a strong foundation for the biologically related applications of BN nanomaterials, the nature of the interface has been the focus of several theoretical investigations. For DNA and RNA nucleotides, physisorbed configurations were predicted.[231, 392] For amino acids interacting with BNNTs, the calculated results show that arginine (Arg) and aspartic acid (Asp) exhibit relatively strong bonds with the surface of the BNNTs relative to the case of tryptophan (Trp).[283, 284, 285] A recent theoretical study considering only the side chains of α -amino acids interacting with a (6,0) BNNT and a BN monolayer (ML) reported that the nature of the

interaction strongly depends on the side chain of the analogue molecules in the gas phase.[283] Interactions of the neutral configurations of the basic and acidic amino acids with both the ML and NT appeared to be weak and associated with the oxygen-containing side groups (e.g., serine, Asp, glutamic acid, asparagine, and glutamine). Stronger interactions with the BNNTs are predicted by the presence of nitrogen-containing groups (e.g., lysine, histidine, and Arg). The aromatic amino acids (e.g., Trp, tyrosine, and phenylalanine) weakly interact with the BNNTs. For the case of BNML, dispersive-type interactions follow the order of aromatic > N-containing groups > O-containing groups of amino acid analogues in the gas phase.

As physiological conditions include the presence of water, theoretical results obtained for the gas phase may not provide a direct correlation to experimental results. This is due to the occurrence of different protonated states within the amino acids in the solvated phase. This is addressed in this study by considering the interaction of the analogues of Arg, Asp, and Trp with a BNML and a (5,0) zigzag-type BNNT in a solvated phase. It is important to note that a small-diameter BNNT was chosen for its large curvature and BNML was chosen for the lack of curvature, facilitating the end points to examine the role of topology in defining the interface of the conjugated (by conjugated it is meant put together, not relating to the bonding) complexes in the solvated phase. Armchair and zigzag BNNTs may show different characteristics, with the latter found to be more reactive, thereby providing an end point for the investigation.[164] The role of curvature can be expressed in terms of induced

strain of the sp^2 bonds in defining the nature of the interface for the conjugated BN nanomaterials. The smaller zigzag NTs have greater strain as compared to that of the armchair configurations.[30] Both zigzag and armchair NTs converge to the same properties exhibited by larger NTs;[385] for this reason, armchair NTs were not considered in this study.

The amino acids considered are Arg and Asp, representing basic and acidic side-chain functional groups, respectively, and Trp for its aromatic properties. Asp is a polar amino acid with a side chain of carboxylic that can be protonated/deprotonated, resulting in a net neutral/negative charge, and Arg is a polar amino acid with a side chain of guanidyl that can be protonated/deprotonated, resulting in a net positive/neutral charge. Under the physiological condition of pH 7, both the amino acids are charged, with Arg being protonated and Asp being deprotonated. The equilibrium configurations of the conjugated complexes were analyzed in terms of binding energy, bond distances, and Mulliken charges to gain insight into the nature of the interface under solvated conditions. Specifically, the calculated results are expected to shed light on the topological and chemical conditions for “physisorption versus chemisorption” of amino acids interacting with BN nanomaterials under physiological conditions.

5.4 Computational Model

The BNML and BNNT configurations were represented by finite cluster models, as shown in Figure 5.7. The BNML (18 Å x 16 Å) was simulated using a $B_{49}N_{49}H_{22}$ cluster, and the (5,0) BNNT (4 Å x 20 Å) was simulated using a $B_{50}N_{50}H_{10}$ cluster. The cluster edge atoms were passivated by hydrogen atoms to ensure their appropriate coordination in both the ML and tubular configurations.[303] The cluster model has been successfully used to describe the properties and interactions that are localized in nature[291], such as the cases considered in the present study.

The DFT calculations were carried out using the Gaussian09 program package.[91] The exchange and correlation functional form was represented by the PBE functional form.[259] The 6-31g(d,p) basis set[278] was used for the constituent atoms of the amino acids and BN nanomaterials. Grimme's D2 semi-empirical approximation was included within DFT via a posteriori term to the total energy of the system.[111] The importance of the inclusion of the dispersive term has been emphasized in previous calculations of interfaces consisting of BN nanomaterials.[283, 284, 285, 311]

Initially, constraint-free geometry optimizations of the complexes were performed to determine the preferred orientation and optimum height of amino acid relative to the surface of nanomaterial with the exception of BNML, where sheet was frozen

to mimic its periodic nature. This step was then followed by further calculations, including (i) height scan of the molecule perpendicular to the surface in incremental steps of 0.1 Å and (ii) surface grid scan in steps of 0.25 Å at the height obtained in step (i). These calculations were performed at each level of theory, including PBE (gas phase), PBE-D2 (gas phase), and PBE-D2 (solvated). It is worth noting that a similar procedure has been successfully employed to obtain the equilibrium configurations of the complexes consisting of organic molecules interacting with graphene, CNT, and BNNTs.[108, 109, 232]

To test the reliability of the cluster model, a comparison is made with the properties calculated using the periodic supercell model[284] (Chapter 3 S1). For BNNT, the bond lengths (R_{BN}) along the tube axis and the zigzag direction are 1.45 and 1.47 Å, respectively; periodic DFT calculations also showed the same values of (R_{BN}).[284] For BNML, the calculated (R_{BN}) is 1.45 Å, which is in agreement with the previously reported value of 1.45 Å.[284] The semi-ionic nature of bonding displayed in the cluster model is similar to that predicted by the periodic model, with N having negative charge in the 2-D lattice.[303] Both the ML and tubular configurations are predicted to be semiconducting.[284] For the ML, the calculated energy gap between the highest occupied molecular orbital (HOMO) and the lowest unoccupied molecular orbital (LUMO) is 4.1 eV, which compares well with the previously reported value of 4.6 eV obtained using DFT (B3LYP).[284] The calculated HOMO-LUMO gap in (5,0) BNNT is 1.7 eV at the DFT (PBE) level of theory. BNNTs show band gap properties

similar to those of their analogue CNT for tubes smaller than (15,0) or (15,15).[289]

In general, the inner electronic states interact with tubes having smaller diameter, thereby reducing the band gap, as was calculated for zigzag-type (n,0) BNNTs.[385]

The α -amino acids contain amine ($-NH_2$) and carboxylic acid ($-COOH$) groups, which are connected with the α -C, forming the backbone of amino acids. Each amino acid is characterized by its side chain attached to the α -C. The side chains range from one hydrogen atom to an indole group, giving each a unique functionality. The backbones form polypeptide chains, which then fold to form a complex protein structure. In a recent calculation, a methyl group (CH_3) is used to represent a termination of the backbone, mimicking the protein configuration in a computationally efficient way.[283] Amino acid analogues are then defined as $[CH_3 - R]$ molecules consisting of the side chain (R) and the α -C terminated by three H atoms (5.6). This approximation is similar to the one employed previously with the exception that the α -C atom is also excluded from the configurations.[283, 286]

Each amino acid has specific pKa (i.e., logarithmic acid dissociation constant) values for the dissociation of each proton. The pKa of the Asp side chain is 3.65, indicating that the side chain can be protonated or deprotonated. The calculated results find small differences between the protonated and deprotonated structures at the PBE-D2 level of theory (e.g., R_{O-C} is 1.21 (1.26) Å and the R_{C-C} is 1.53 (1.59) Å in the protonated (deprotonated) Asp). This is also the case with Arg, where R_{NH_2-C} is

1.35 (1.40) Å and the R_{C-N} is 1.33 (1.40) Å in the protonated (deprotonated) Arg.

As biological processes occur in a solvated environment, inclusion of the effect of such environment in a theoretical model is necessary for accurate calculations. This fact has also been brought out by calculations on glycine-conjugated BNNT.[285] In this study, the implicit solvation was modeled using a PCM.[226] This model simulates the solvent by representing it as a homogenous continuum medium with a dielectric constant of 78.36 (for water). The adsorption energy of amino acids interacting with the BN nanomaterials is then calculated using the following equation

$$E_{adsorption} = E_{complex} - (E_{nanomaterial} + E_{molecule}) - E_{BSSE} \quad (5.1)$$

where $E_{complex}$ is the total energy of a bioconjugated complex, $E_{nanomaterial}$ is the total energy of BNML or BNNT, $E_{molecule}$ is the total energy of the amino acids considered, and E_{BSSE} is the BSSE, which was calculated using the counterpoise method.[34] The BSSE can only be calculated for the gas phase. NBO analysis was also conducted on the conjugated NT to characterize the nature of bonding of the chemisorbed states in the conjugated BNNT complexes.[100]

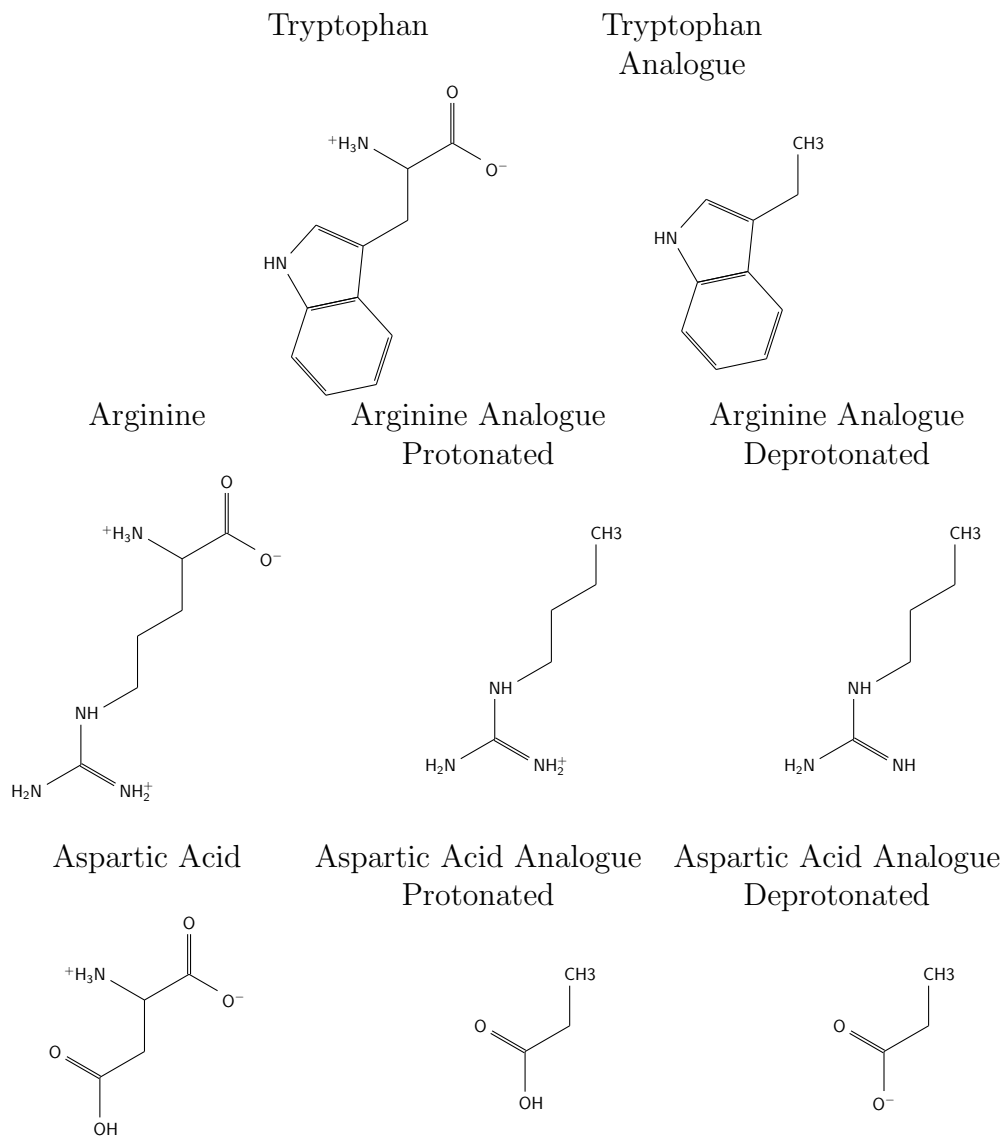


Figure 5.6: Chemical structures of the amino acids considered. The first column is the amino acid in its zwitterionic form, followed by the analogues in different protonated states. In the analogues, the backbone is replaced by a $-CH_3$ group.

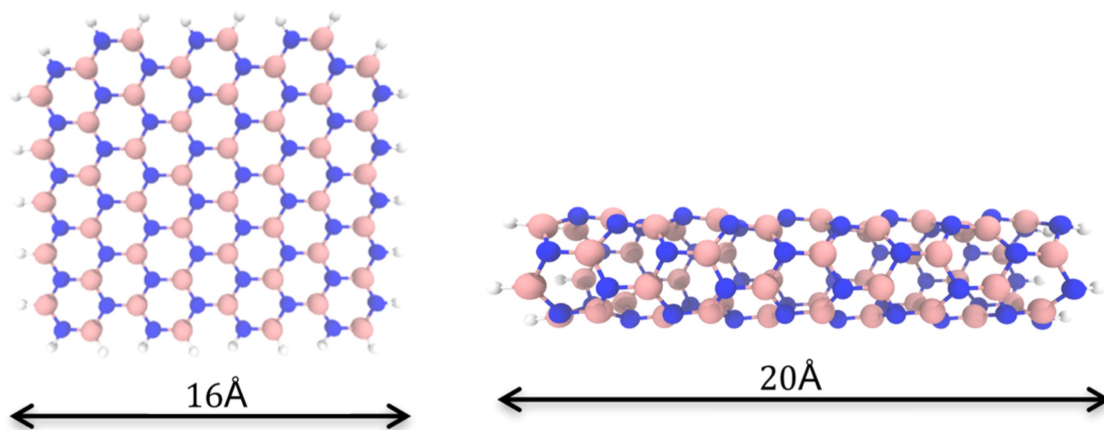


Figure 5.7: Cluster models of BN nanomaterials: (left) BNML represented by the $(B_{49}N_{49}H_{22})$ cluster and (right) $(5,0)$ BNNT represented by the $(B_{50}N_{50}H_{10})$ cluster. The cluster edge atoms are passivated with H atoms (atomic symbols: N (blue), B (pink), and H (white)).

5.5 Results & Discussion

To benchmark the calculated results, we first report the gas-phase results of Trp-, Arg-, and Asp-conjugated BN nanomaterials. Later, results of the solvated-phase calculations considering the different protonated states of Arg and Asp interacting with BN nanomaterials are presented.

In gas phase, the calculated results are in qualitative agreement (Table S1 of the Supporting Information) with those obtained using the periodic supercell models.[232, 283] For all cases, the D2 term shows its importance in capturing contributions from dispersive interactions, which are generally dominant in the conjugated complexes

considered.

It is known that the interaction of Trp with nanomaterials is governed by long-range dispersive interactions, with a capability of forming weak ionic bonds in a conjugated system. Calculations at the density functional theory (DFT) (Perdew, Becke, and Ernzerhof (PBE)) level of theory find the adsorption energy to be +0.02 eV for Trp-conjugated BNML. Inclusion of the D2 term yields the value of -0.74 eV for BNML. This is not the case with Trp-conjugated BNNT, where the increase in adsorption energy is small after including the D2 term. The calculated adsorption energies are -0.74 and -0.29 eV for BNML and BNNT, respectively, at the DFT (PBE-D2) level of theory. The reduced surface area of the BNNT decreases the interaction with Trp relative to that available for BNML. This is what has also been seen for the cases of organic molecules interacting with the BN nanomaterials in the gas phase.[7, 232, 284]

Inclusion of the basis set superposition error (BSSE) correction term lowers the adsorption energy while maintaining the hierarchy of the interaction strength: protonated Asp < deprotonated Arg < Trp < deprotonated Asp < protonated Arg toward BNML and Trp < protonated Asp < protonated Arg < deprotonated Arg < deprotonated Asp toward BNNT (Table S2). The calculations involving the interaction of BNML with amino acids were performed with the ML frozen; relaxing the ML configuration only slightly lowered the adsorption energy. The calculated difference in the adsorption energy of Asp interacting with the frozen and relaxed MLs was about 0.01

Table 5.1

Amino Acid-Conjugated BN Nanomaterials in the Solvated Phase: Adsorption Energy ($E_{ads.}$), Nearest-Neighbor (N.N.) Distance, Mulliken Charge Transfer (ΔQ), and Dipole Moment (D.M.) Obtained Using the Polarizable Continuum Model (PCM) at the DFT (PBE-D2) Level of Theory

BNML					
Amino Acid	$E_{ads.}$ (eV)	N.N. (Å)	R (Å)	ΔQ (e)	D.M. (D)
Arg (p (+))	-0.92	R($N_{ML} - H$)	2.61	-0.1	15.0
Asp (d (-))	-0.57	R($B_{ML} - H$)	2.61	+0.1	11.6
Arg (d)	-0.96	R($B_{ML} - H$)	2.61	≈ 0.0	5.9
Asp (p)	-0.67	R($N_{ML} - H$)	2.79	≈ 0.0	7.4
Trp	-1.04	R($B_{ML} - H$)	2.55	≈ 0.0	1.2
(5,0) BNNT					
Amino Acid	$E_{ads.}$ (eV)	N.N. (Å)	R (Å)	ΔQ (e)	D.M. (D)
Arg (p)	-0.85	R($B_{NT} - N$)	1.86	+0.1	27.9
Asp (d)	-2.17	R($B_{NT} - O$)	1.51	+0.6	13.4
Arg (d)	-2.12	R($B_{NT} - N$)	1.58	+0.4	14.8
Asp (p)	-1.23	R($B_{NT} - O$)	1.59	+0.3	12.8
Trp	-0.71	R($N_{NT} - H$)	2.88	+0.1	7.3

eV at the DFT (PBE-D2) level of theory. The results for the tubular configurations were obtained by constraint-free optimization of BNNT interacting with amino acids.

In the solvated phase, the calculated adsorption energies of Arg, Asp, and Trp interacting with the BNML and the (5,0) BNNT obtained at the DFT (PBE-D2) level of theory are listed in Table 1. The calculated nearest-neighbor distances between the amino acids and BN nanomaterials, Mulliken charge transfer, and dipole moments associated with the equilibrium configurations are also given in Table 1. The calculated equilibrium configurations of amino acids interacting with BNML and BNNT are displayed in Figures 5.8, 5.9, and S1.

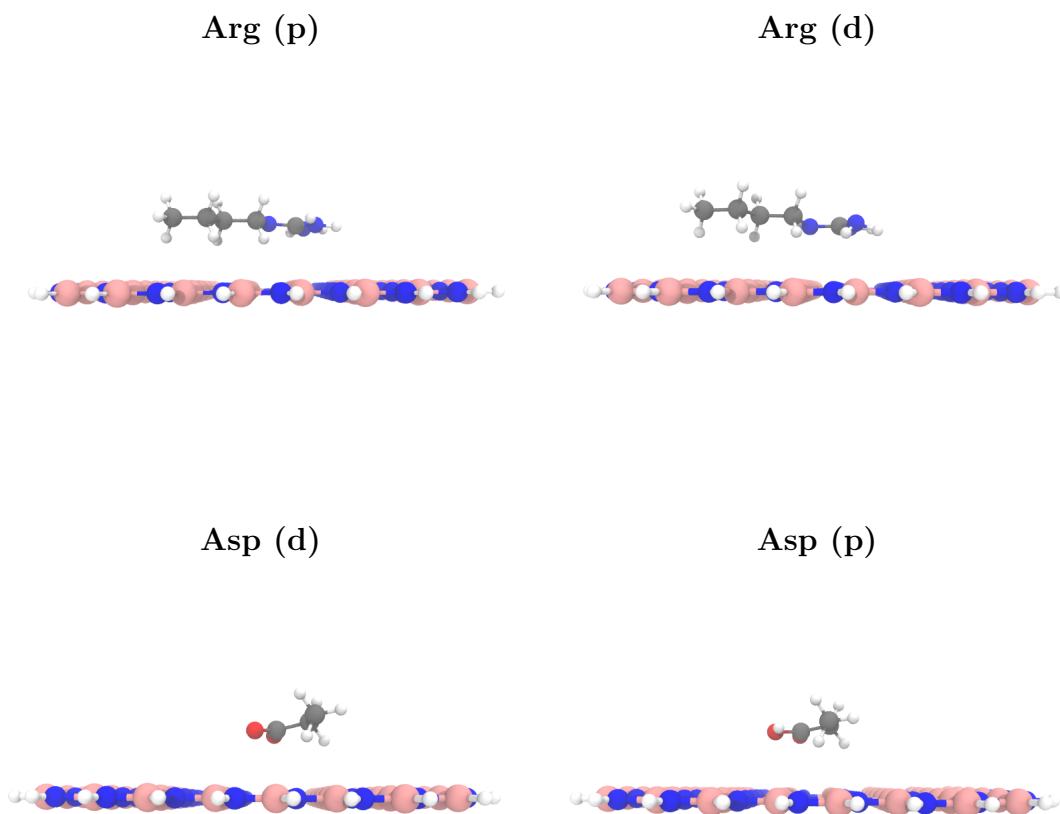


Figure 5.8: Calculated equilibrium configurations of Arg- and Asp-conjugated BNML (atomic symbols: N (blue), B (pink), C (black), and H (white)).

When conjugated with the BNML, the interactions are dominated by the long-range dispersive interactions, yielding physisorbed configurations (Figure 5.8). This is affirmed by the noticeable increase in the adsorption energies after the inclusion of the D2 correction term in calculations; the BNML-conjugated complexes show an

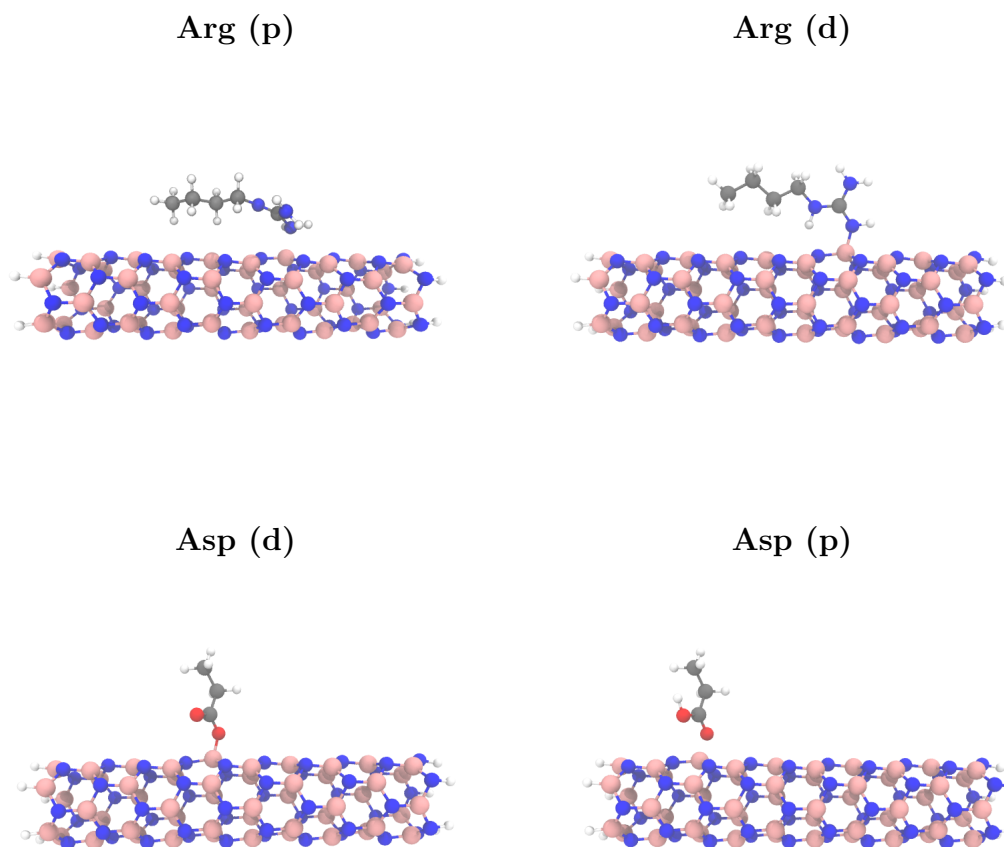


Figure 5.9: Calculated equilibrium configurations of Arg- and Asp-conjugated BNNT (atomic symbols: N (blue), B (pink), C (black), and H (white)).

order of magnitude increase in the adsorption energies relative to that of the BNNT-conjugated complexes (Table S2). In the solvated phase, the protonated or deprotonated Arg and Asp interacting with BN nanomaterials have similar adsorption energies (-0.57 to -0.96 eV) and near-neighbor distances (2.61-2.79 Å). A negligible charge transfer occurs in BNML complexes, and the charged BNML complexes have

a higher dipole moment relative to that of neutral BNML complexes as expected.

For BNNT, the calculated results show a difference between the chemisorbed configurations of the protonated and deprotonated complexes (Figure 5.9). The protonated Arg (i.e., Arg(+)) forms a bond between N (amino group) and B (tubular surface) atoms, with the near-neighbor distance and adsorption energy of 1.86 Å and -0.85 eV, respectively. Mulliken charge analysis shows a small charge transfer between Arg(+) and BNNT. The protonated Asp prefers to interact with the O (carboxyl group) in the equilibrium configuration, with the near-neighbor distance and adsorption energy of 1.59 Å and -1.23 eV, respectively; a larger charge transfer from the BNNT to Asp also accompanies it. The increased electro- negativity of oxygen in Asp yields a stronger interaction of the protonated Asp with BNNT. The interaction energies and distances are summarized in Figure 5.10. The deprotonated Arg and Asp interact with the BNNT to form stable complexes, where Asp and Arg are chemisorbed on the NT surface with a higher adsorption energy of about -2.1 eV and a smaller near-neighbor distance of 1.5-1.6 Å. The nearest-neighbor distance of Arg-conjugated BNNT (i.e., R(BNNT-N)) is similar to that of the cubic BN[266], suggesting a sp_3 -type bond at the tubular surface. A higher charge transfer from BN nanomaterials to the deprotonated Arg and Asp suggests the interaction to be partially ionic in the conjugated complexes. It should be noted that the deprotonated Arg and Asp exist together only at a basic pH. The low pKa value (3.86) of Asp does not facilitate its coexistence with Arg at a neutral pH.

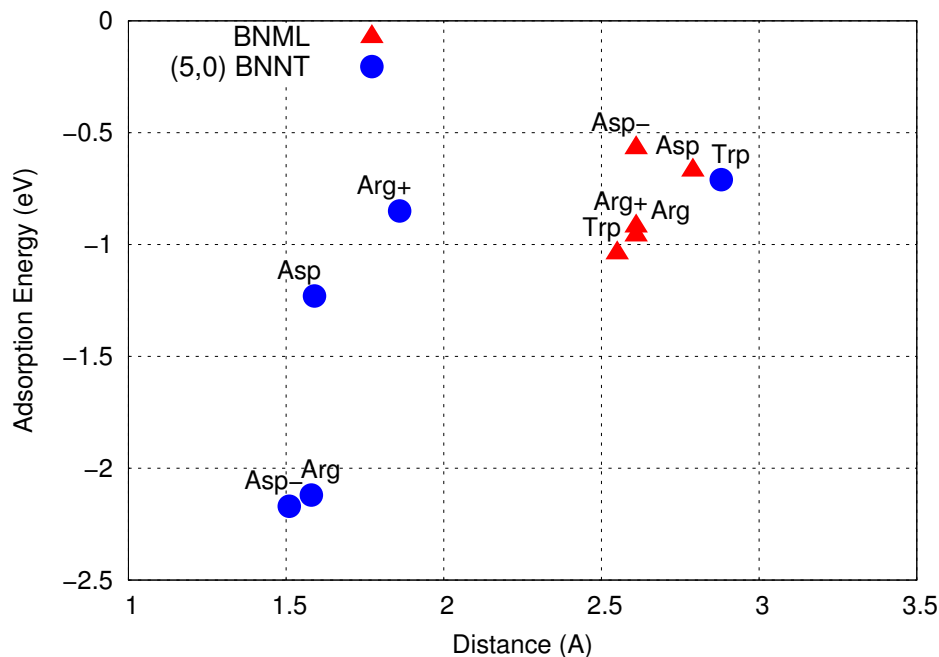


Figure 5.10: Physisorbed vs chemisorbed configurations in the solvated phase: adsorption energy vs near-neighbor distance of amino acid- conjugated BN complexes. The red triangles are the BNML systems and the blue circles are the (5,0) nanotube.

To ascertain the nature of bonding in chemisorbed configurations, natural bond orbital (NBO) analysis is performed for the BNNT complexes. For deprotonated amino acids, B_{BNNT} atom on the tubular surface changes its local environment; originally, its characteristic is a strained sp 1.9-2.2 bond. When conjugated, the B atom accommodates the newly formed bonds with the neighboring N-BNNT atoms. The bond characteristics are sp 2.83 (sp 2.71), sp 2.92 (sp 3.02), and sp 2.86 (sp 2.71) for the deprotonated Arg (Asp(-))-conjugated complexes, whereas the bond characteristic of the $B_{BNNT} - N_{AA} (O_{AA})$ bond is predicted to be sp 3.42 (sp 3.66) for the deprotonated Arg (Asp-) conjugated complexes. The tubular surface atoms, therefore, form

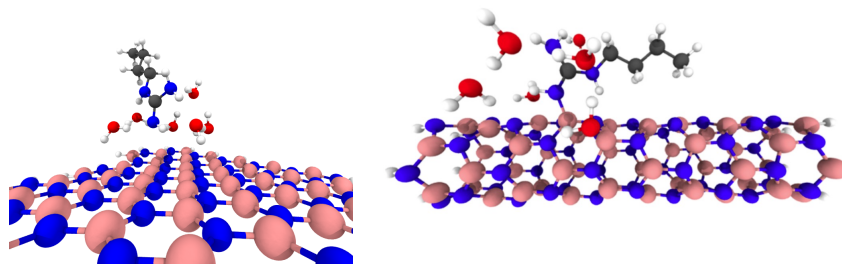


Figure 5.11: Deprotonated Arg interacting with BNML (left) and (5,0) BNNT (right) in the presence of several water molecules (atoms: H (white), B (pink), C (gray), N (blue), and O (red)).

sp³-like bonds in the deprotonated complexes. Interestingly, the protonated amino acids show sp²-like characteristics with a larger p-orbital contribution from B-BNNT atom in the conjugated complexes. The B-BNNT bonds are predicted to have characteristics of sp 2.28 (sp 2.56), sp 2.41 (sp 2.57), and sp 2.43 (sp 2.63) for Arg(+) (Asp)- conjugated complexes. The bond characteristic of the $B_{BNNT}-N_{AA}$ (O_{AA}) bond is sp 7.99 (sp 5.06) for the Arg+ (Asp) complexes.

The calculated adsorption energies are in a stark contrast with the results of a recent DFT (B3LYP-D2) study[311] employing a finite cluster model. For the cases of Arg and Asp interacting with BNML, the reported energy values²⁰ are -172.21 kcal/mol (-7.46 eV) and -156.96 kcal/mol (-6.81 eV), respectively. These values seem inconsistent as they are significantly higher relative to the PBE-D2 results together with the results of the periodic supercell model employing the B3LYP-D2 functional form.[283]

Considering that Trp is a nonpolar aromatic amino acid, investigation of an interaction of Trp with BN nanomaterials in the solvated phase can quantify the effect of solvated phase with reference to gas-phase results. In the solvated phase, Trp stabilizes in the physisorbed configurations with π -stacking interactions with the indole ring of Trp and BN nanomaterials, as was the case in the gas phase (Figure S2). The calculated results agree with recent experimental results, suggesting physisorption of Trp on BNML.[215] In the solvated phase, the calculated results show that the interaction strength with BNML follows the order of deprotonated Arg > protonated Arg(+) > protonated Asp > deprotonated Asp(-). This is slightly different for BNNT, with the hierarchy being deprotonated Asp(-) > deprotonated Arg > protonated Asp > protonated Arg(+). The interaction strength in terms of the adsorption energy shows a contrasting behavior for BNML and BNNT complexes; BNMLs prefer to form physisorbed complexes irrespective of the charge states of amino acids, and BNNTs prefer to form chemisorbed complexes via the formation of a covalent bond dictated by either dominant p-type (e.g., protonated Arg) or s-type (e.g., deprotonated Asp) electronic states.

We are aware of the fact that the PCM may not accurately represent the interaction of amino acids with water molecules. In general, the presence of H-bond networks between the amino acid-conjugated complexes in the solvated phase is likely to modify the equilibrium geometries. This fact was examined for the case of deprotonated Arg interacting with both the BNML and BNNT using explicit solvation by including six

water molecules. The calculated results shown in Figure 5.11 reflect the configurations obtained using the implicit solvation model. The conclusion is that the topological variation determines the physisorbed versus chemisorbed state for amino acids interacting with BN nanomaterials. Furthermore, it is found that water molecules do not dominate the interface between the amino acids and the BN nanomaterials. Interestingly, both theoretical and experimental studies revealed the hydrophobic nature of pristine BNNT.[202, 283]

It should be noted here that capturing of the the physics and chemistry of the solvation effect by the PCM was demonstrated in a theoretical study of the zwitterionic forms of glycine and alanine.[51] Our recent study of the interaction of DNA with chalcogenide quantum dots also shows an effective screening of the electrostatic interaction between QD and DNA by the solvation model.[346] Considering that Figure 5.11 represents the results of limited DFT calculations, we plan to use the molecular dynamics method to obtain a detailed atomistic view of the interface of amino acid-conjugated BN nanomaterials in the solvated phase.

5.6 Summary

The interactions of neutral and charged amino acid analogues with BN nanomaterials are investigated in a solvated environment using the implicit solvation model. The

calculated results based on DFT show that the deprotonated states of the polar amino acids facilitate the formation of chemically bound states between the donor electron moieties (i.e., O(Asp) and N(Arg)) and the NT surface of B_{BNNT} . In the absence of curvature for the BNML, the amino acids form physisorbed complexes, which are governed by dispersive interactions. The calculated results show that BNNTs would have the ability to immobilize proteins through strong interactions with the acidic and basic amino acids and therefore can be used in health-related applications.

Chapter 6

AIMD Investigation of Boron

Nitride Nanotubes

6.1 Introduction

To gain an understanding of the bio-nano interface, explicit solvent models need to be taken into account. Traditional density functional theory calculations have a limited scope. With AIMD methods, dynamics and temperature can be added to the model to uncover the dynamic nature at the interface. Most groups approach the simulations using traditional force fields to model the interface behavior. In 2008, the density and behavior of water molecules inside and outside of four different sized carbon nanotubes were simulated using Lennard-Jones potentials.[326]

Work on boron nitride nanotubes and water have been investigated by various groups over the past decade. Until recently the groups used classical molecular dynamics to investigate the water boron-nitride interaction. Most of the investigations [105, 191, 362, 363] trace their Lennard-Jones parameters from the DREIDING generic force field.[222] In the force field the LJ potentials for boron were found through interpolation and nitrogen was taken from a study of azahydrocarbons.[358]

Wu et. al. investigated the water contact angle after deriving bulk h-BN force field parameters from quantum Monte Carlo simulations.[365] Some groups like, Hilder et.al, performed CPMD simulations to calculate the interactions energies of water and nanotubes using the BLYP functional to fit new LJ parameters for (5,5) nanotubes.

[132] Born-Oppenheimer molecular dynamics simulations on a monolayer of h-BN, where the peak density of about 4 g/cm³ was observed about 3.1 Å.[165] AIMD graphene and h-BN using the optB88-vdW functional.[330]

6.2 Computational Details

Car-Parrinello molecular dynamics (CPMD)[39] simulations in canonical ensemble at 300K were performed for the interface between boron nitride nanomaterials and Amino Acids. The pseudopotential plane-wave density functional theory (DFT) [176] module within the NWChem package[334] was used. The PBE [259] form of the GGA was used for the exchange-correlation functional. The core-valence interactions of the B, C, N, and O atoms were approximated using norm-conserving Hamann type pseudopotentials[122, 123], in the separable form of Kleinman and Bylander.[170] The Kohn-Sham wave functions and charge density were expanded using plane waves basis up to a kinetic energy cutoffs of 100 and 200 Ry. The $\Gamma(\vec{k} = 0)$ point was used to sample the Brillouin zone for all simulations.

A fictitious electron mass of 750 au and simulation times step of 5 au (0.121 fs) was used. The temperature was controlled by the Nose-Hoover thermostat.[139, 242] The intermolecular water interaction was modeled by the rigid body SPC/E potential.[26] For the C, O, H the derived QM/MM potentials from Cauët et.al were used[41] and

the for boron and nitrogen the boron-nitride nanotube potentials from Hilder et.al were utilized[132].

With the cells being periodic in two directions and needing at least 10 Å of space to mitigate image contributions, the cell volumes were dictated by the distances between the mirror images of the amino acids. The density of water in the cells was approximately 1 g/cm³. The QM/MM models were run for 13.30 ps and the AIMD models were run for 6.65 ps

For the simulations a monolayer and two boron-nitride nanotube were used. The sheet was 15.1 Å x 15.1 Å containing 85 atoms, The (5,0) boron-nitride nanotube has a length of 12.8 Å with containing 78 atoms and the (8,0) boron-nitride nanotube has a length of 4.3 Å with containing 40 atoms. Each system had at least 10 Å of vacuum space between mirror images.

6.3 Results and Discussion

The first step for the simulations using an explicit solvent is to find the most cost efficient parameters for each system. If possible, a QM/MM model would drastically reduce the cost of the simulations and allow for longer and more complex simulations. Previous studies (See Chapter 5) have shown that smaller nanotubes tend to be more

chemical active, this includes water [284]. Finding which boron-nitride structures will work for each model is the first step. In Figure 6.4 and Figure 6.5 the density of water is calculated from six different simulations. There are two simulations for each structure, (5,0) nanotube, (8,0) nanotube, and monolayer h-BN, a QM/MM simulations and an AIMD simulation.

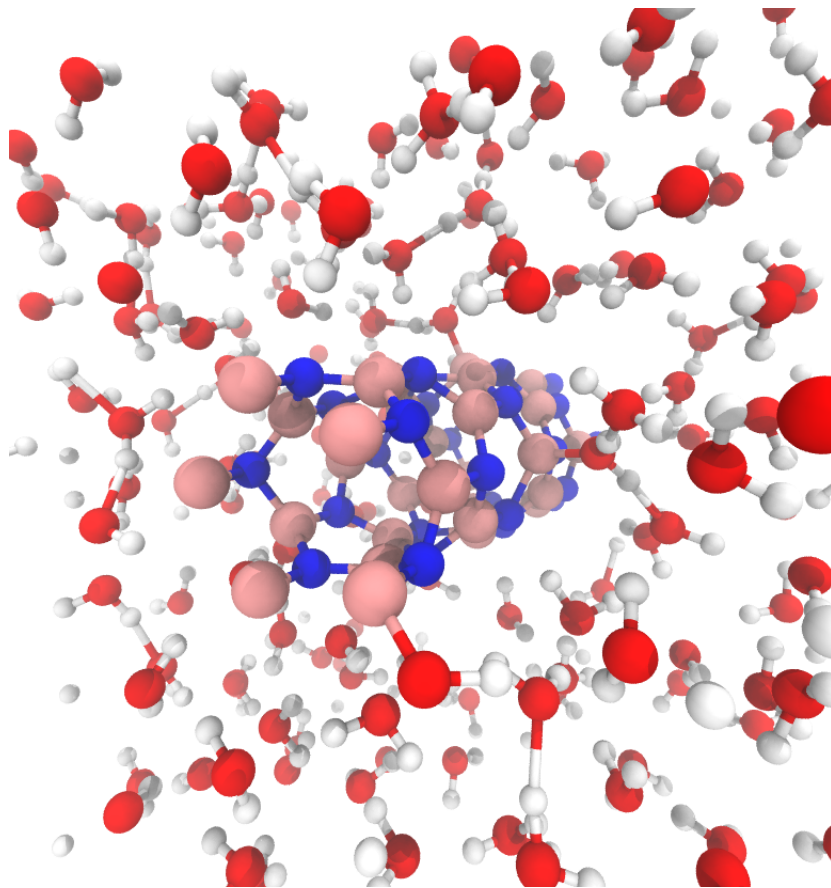


Figure 6.1: The last snapshot of the AIMD simulation containing a (5,0) boron nitride nanotube with water molecules surrounding it. The simulation cell has periodic boundary conditions implemented, leading to an infinite tube. The small radius tube has large amount of strain leading to the hydrolyzation of the nanotube as seen by formation of chemical bonds with water.

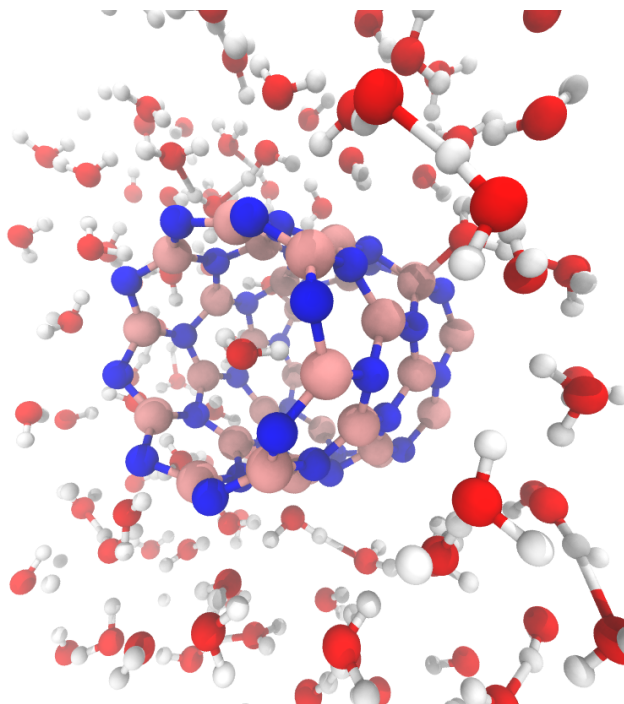


Figure 6.2: The last snapshot of the AIMD simulation containing a (8,0) boron nitride nanotube with water molecules surrounding it. The simulation cell has periodic boundary conditions implemented, leading to an infinite tube. Due to the solvation conditions some water molecules are present on the inside of the nanotube for the large size nanotube. The small radius tube has large amount of strain leading to the hydrolyzation of the nanotube as seen by formation of chemical bonds with water.

This effect is smaller than the (5,0) nanotube as shown by Figure 6.5

To calculate the density profiles of water histograms were generated that binned the water for each time-step as a function of distance from the nanomaterial surface and averaged them. For the monolayer bins were rectangles with the dimensions of the sheet (15.1 Å x 15.1 Å) and a depth of 0.250 Å. The nanotubes water density were calculated in a similar fashion, but the bins were hollow cylinders that were centered

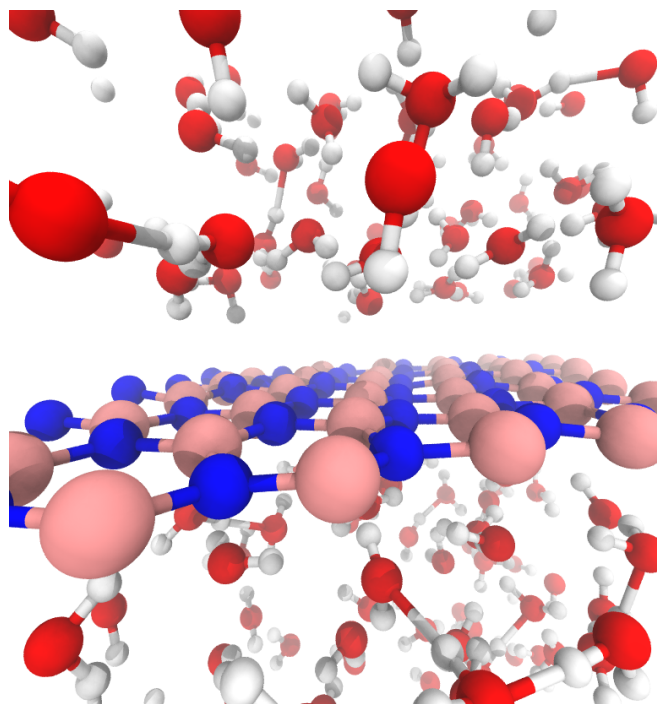


Figure 6.3: The last snapshot of the AIMD simulation containing a monolayer h-BN sheet with water molecules surrounding it. The simulation cell has periodic boundary conditions implemented, leading to an infinite sheet. The flat surface reduces any strain to zero and the hydrolyzation of the sheet nanotube does not occur, all of the water interactions are long-ranged.

around the middle of the nanotube. The height is equal to the length of the tube and a thickness of δr , the volume of each bin increased as the distance from the tube increased. Where δr is the bin size of 0.250 \AA .

The parameters governing the water molecules purely mechanical for the QM/MM model. Using the same force fields parameters leads to the identical density curves in Figure 6.4. It is known that the smaller radii nanotubes will have a more reactive

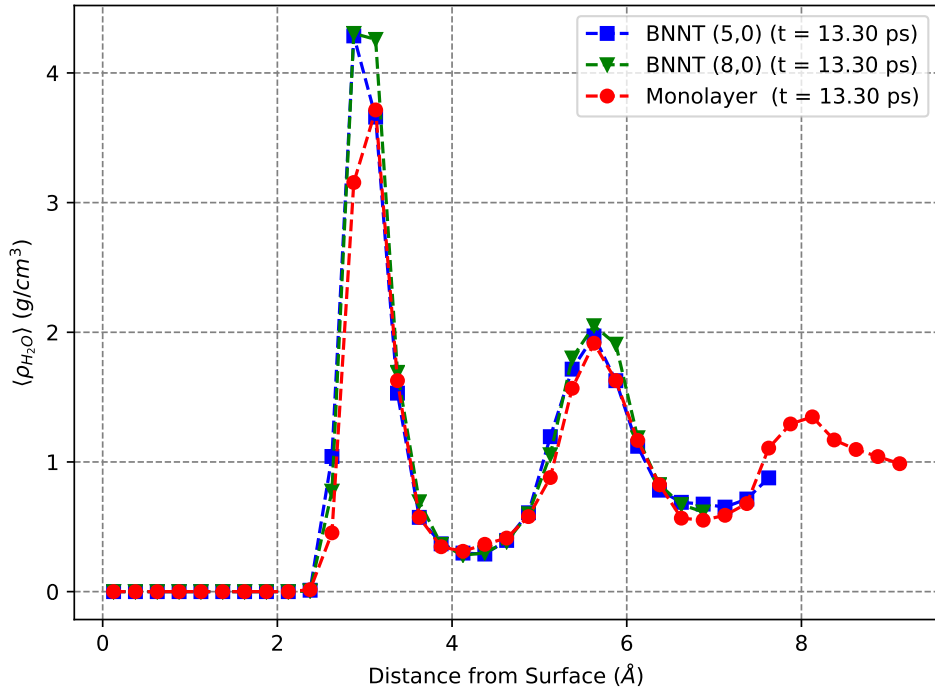


Figure 6.4: The density of water for a QM/MM model where the substrate, boron-nitride, is treated with DFT and the water molecules are simulated using the SPC/E potentials.

surface leading to the formation of chemical bonds. It is not known when the shift from reactive nanotubes to inert boron-nitride nanotubes occurs. The force field that has been selected was parameterized for a (5,5) nanotube by Hilder et. al.[132] This did not allow for the electronic structure of the water to be modeled and react to the surface of the nanotube. As shown in the Figure 6.4 and Figure 6.5 the monolayer had similar features, with the first peaks occurring around 3\AA . The monolayer did not undergo hydrolyzation, this is also seen in other simulations [165, 349]. The monolayer is known to be chemically inert[101] as are most experimental nanotubes. For the more reactive nanotubes[284], (5,0) and (8,0), the nanotubes start to undergo

hydrolysis as shown by the initial peaks in Figure 6.5 at 2 Å. The (5,0) nanotube is more reactive leading to the a larger density near the surface of the nanotube. The bonds forming on the nanotube surface can be seen in the following Figures 6.1 and 6.2.

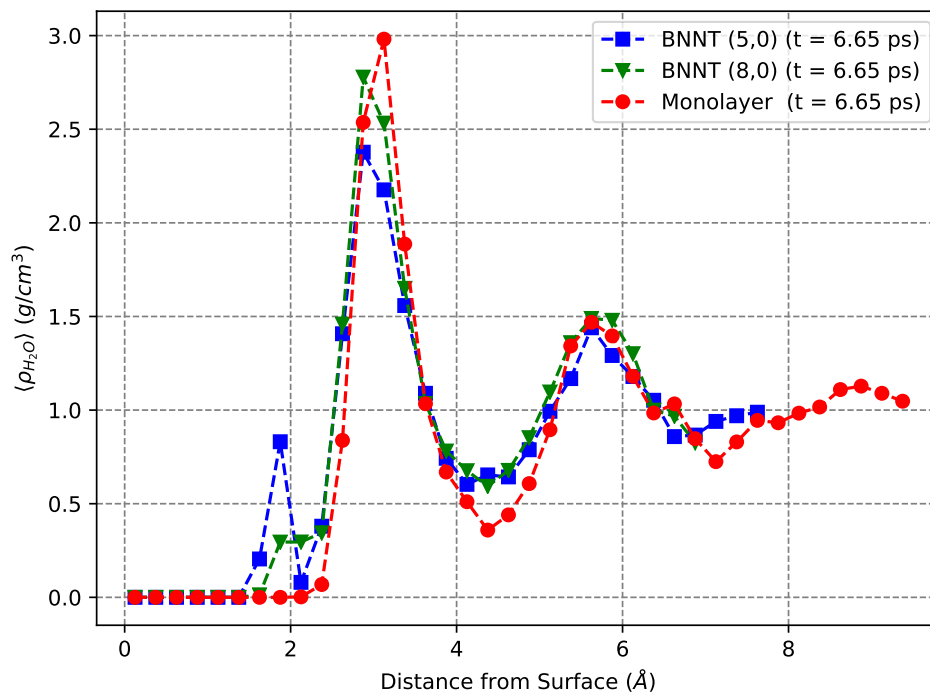


Figure 6.5: The density of water for AIMD calculations, the peaks around two Å are water molecules bonding to the surface of the (5,0) and (8,0) nanotube.

6.4 Summary

A brief report is given for the work that will lead to the future direction of this research. To accurately simulate the bio-nanomaterial interface AIMD methods will

need to be utilized in cases where the force fields fail. It has been shown that QM/MM methods do not accurately predict the surface behavior when it comes to interactions with "simple" water molecules. In this research, along with the the work presented in Chapter 5, it has been shown that additional care needs to be taken when considering boron-nitride nanotubtes for biological applications.

Chapter 7

Stability, Elastic and Electronic

Properties of a novel BN₂ sheet

with extended hexagons with N-N

bonds

See Appendix E for reproduction permission.

7.1 Introduction

The 'materials by design' approach using state-of-art computational tools has led to new experimental discoveries that have pushed the forefronts of materials science. In recent years, this approach has generated deeper insight into the physics and chemistry of the next generation materials with the help of tools and resources which allow for high-throughput calculations with utilities such as genetic and particle-swarm algorithms [269, 345]. Furthermore, there exists a wealth of knowledge on the structures of known materials which subsequently has led to suggest new combinations of atoms to create new materials that are stable and can then be synthesized.

Theory has anticipated many new materials which were synthesized in the scientific laboratories. An example of this is the academic discussion of Dirac cones in monolayer graphite [74]. Thirty years later the discovery of what we know now as graphene was announced [243]. White graphene referred to as a h-BN monolayer, soon followed with theoretical predictions [359] and then it's synthesis [104, 154]. More recently this tradition has continued with Borophene, first predicted in 2014 [267] and then synthesized in 2015 [217]. Materials, outside of the B-C-N group, have also been predicted and synthesized, e.g. silicene [89, 119, 338].

The foundation for the 2-D family of the B-C-N materials was set with the discovery

of both graphene and the h-BN monolayer. Since then numerous materials in the B-N family have been predicted using first-principles methods based on density functional theory. Some of the carbon-based 2-D materials include α Graphyne/BNyne [248], 6-6-12 Graphyne hetero-structures [214], and Graphdiyne [204]. Due to the similar chemistry, between C atoms and B/N atoms, many of the carbon-based materials also have B-N analogues [200]. Following the prediction of penta-graphene [384], the stability of BN sheets with similar structures, penta-BN and penta-BN₂, have been reported [200]. These structures form pentagons with penta-BN having B-N, B-B and N-N bonds with semiconducting properties. On the other hand, penta-BN₂ shares a similar morphology as penta-BN, but with N-N bonds with metallic properties.

Following the pentagonal and hexagonal structures of B-C-N materials, we now consider a network of extended hexagons with N-N bonds forming a BN₂ monolayer. The material proposed, BN₂, has a similar structure to both graphene and h-BN. BN₂ contains the same constituent atoms as the insulating monolayer of h-BN, while possessing metallic properties. There is, however, a reduction in symmetry that allows for the anisotropic nature of the material's mechanical properties. Calculations based on density functional theory (DFT) find this BN₂ structure to be stable. This material has similar structural motifs that would enable it to be present at boundaries between graphene/graphene, h-BN/h-BN monolayers and graphene/h-BN monolayer hybrid sheets. Note that these extended hexagons are not regular hexagons typically associated with graphene, and the bonded nitrogen atoms (N-N) modify the hexagon

structure of the h-BN monolayer. If synthesized or discovered this materials will not replace graphene or h-BN in applications or systems. It would, however, provide a novel material that can be exploited to solve current inefficiencies or develop new devices.

7.2 Computational Model

Electronic structure calculations were performed using the generalized gradient approximation to DFT. The Perdew-Burke-Ernzerhof (PBE) functional with projector-augmented-wave (PAW) pseudo-potentials [31, 180] as implemented in the Vienna Ab initio Simulation Package (VASP) [179, 181, 182, 183] were used. The plane wave cutoff energy was set to 900 eV. The convergence criteria for the energy was set to 10^{-5} eV, while the force was to set to 10^{-4} eV/Å. The Brillouin zone was sampled with (7 x 21 x 1) and (7 x 21 x 3) Monkhorst-Pack grids [249] for the monolayer and bilayer calculations. For the density of states calculations Gaussian smearing was set to 0.05 eV, and the k-point grids were increased by a factor of four in all directions. Bader's charge analysis was performed using the code and methods given by [130]. Note that the semi-empirical vdW correction terms (D3) [112] were added for the bilayer BN₂ calculations.

To investigate the stability of the BN₂ monolayer, a larger supercell (2x2x1) was generated for calculations of the force constants, which was then used by the Phonopy software [331]. The energy convergence criterion in the VASP calculations were increased to 10⁻⁸ eV to obtain the Hessian matrix for the Phonopy calculations. For structure symmetry identification and high symmetry points, the Bilbao Crystallographic Server [10, 11, 12, 13, 321] and utilities within the Pymatgen library [269] were used.

The cohesive energy of a monolayer was calculated using the following formula:

$$E_{cohesive} = \frac{E_{struc.} - nE_B - mE_N}{n + m} \quad (7.1)$$

The interlayer binding energy for the bilayer was calculated using the following:

$$E_{Binding} = E_{Bilayer} - 2E_{Monolayer} \quad (7.2)$$

To calculate the elastic constants the Pymatgen library [269] was utilized to apply the strain to the structures yielding stress-strain data for both the monolayer and bilayer. For the monolayer, the calculation of the in-plane Young's modulus involved steps in which the stresses were multiplied by the cell thickness (*c*), following the procedures of [353] and [258]. The lattice parameter varied with a strain (ϵ) of -2.0%

to 2.0% with a mesh of 0.2% and -1.0% to 1.0% with a mesh of 0.1% for the off-diagonal components. This approach resulted in 20 calculations for each direction of deformation in the lattice. Larger strains were considered, but 2.0% was chosen to limit the stress-strain relationship to a linear regime, as was done in previous studies [217, 350].

To calculate the elastic constants the following formula was used:

$$\boldsymbol{\sigma}_{ij} = \mathbf{C}_{ijkl}\boldsymbol{\eta}_{kl} \quad (7.3)$$

where $\boldsymbol{\sigma}_{ij}$ is the 3x3 stress matrix (Cauchy in this case), \mathbf{C}_{ijkl} is the stiffness tensor, and $\boldsymbol{\eta}_{kl}$ is a 3x3 strain matrix. Using Voigt notation the indices can be reduced to [244]:

$$\boldsymbol{\sigma}_I = \mathbf{C}_{IJ}\boldsymbol{\eta}_J \quad (7.4)$$

Where $\boldsymbol{\eta}$ is calculated using the following:

$$\boldsymbol{\eta} = \frac{1}{2}(\mathbf{F}^T\mathbf{F} - \mathbf{I}) \quad (7.5)$$

where \mathbf{F} is the deformation gradient tensor and \mathbf{I} is the identity matrix. Solving for

the elastic constants C_{IJ} we get:

$$[\boldsymbol{\sigma}_I \boldsymbol{\eta}_J^+]^T \approx \mathbf{C}_{IJ} \quad (7.6)$$

where $\boldsymbol{\eta}_J^+$ is calculated using the Moore-Penrose pseudo-inverse as implemented in the NumPy library [336]. Due to the least square fitting, \approx is used to imply that an exact solution is not found.

The deformation gradient tensors for the orthorhombic case are [230]:

$$\begin{aligned} \mathbf{F}_{11} &= \begin{bmatrix} \lambda_{11} & 0 & 0 \\ 0 & 1 & 0 \\ 0 & 0 & 1 \end{bmatrix} & \mathbf{F}_{22} &= \begin{bmatrix} 1 & 0 & 0 \\ 0 & \lambda_{22} & 0 \\ 0 & 0 & 1 \end{bmatrix} \\ \mathbf{F}_{33} &= \begin{bmatrix} 1 & 0 & 0 \\ 0 & \lambda_{33} & 0 \\ 0 & 0 & 1 \end{bmatrix} & \mathbf{F}_{44} &= \begin{bmatrix} 1 & 0 & 0 \\ 0 & \lambda_{44} & 0 \\ 0 & 0 & \lambda_{44} \end{bmatrix} \\ \mathbf{F}_{55} &= \begin{bmatrix} \lambda_{55} & 0 & 0 \\ 0 & 1 & 0 \\ 0 & 0 & \lambda_{55} \end{bmatrix} & \mathbf{F}_{66} &= \begin{bmatrix} \lambda_{66} & 0 & 0 \\ 0 & \lambda_{66} & 0 \\ 0 & 0 & 1 \end{bmatrix} \end{aligned} \quad (7.7)$$

$$\mathbf{F}_{12} = \begin{bmatrix} 1 & \epsilon_{12} & 0 \\ 0 & 1 & 0 \\ 0 & 0 & 1 \end{bmatrix} \quad \mathbf{F}_{13} = \begin{bmatrix} 1 & 0 & \epsilon_{13} \\ 0 & 1 & 0 \\ 0 & 0 & 1 \end{bmatrix}$$

$$\mathbf{F}_{23} = \begin{bmatrix} 1 & 0 & 0 \\ 0 & 1 & \epsilon_{23} \\ 0 & 0 & 1 \end{bmatrix}$$

where $\lambda_{11} = 1 + \epsilon_{11}$, $\lambda_{22} = 1 + \epsilon_{22}$, etc.

Using symmetry the stiffness tensor can be reduced to reflect the unique elements needed to describe an orthorhombic system. The matrix is symmetric across the diagonal and only the unique elements are given in Equation 7.8.

$$C_{IJ} = \begin{bmatrix} C_{11} & C_{12} & C_{13} & 0 & 0 & 0 \\ & C_{22} & C_{23} & 0 & 0 & 0 \\ & & C_{33} & 0 & 0 & 0 \\ & & & C_{44} & 0 & 0 \\ & & & & C_{55} & 0 \\ & & & & & C_{66} \end{bmatrix} \quad (7.8)$$

For the monolayer case the matrix in Equation 7.8 is reduced from nine (C_{IJ}) constants to four (C_{IJ}) constants. The deformation gradient tensor \mathbf{F}_{11} , \mathbf{F}_{22} , \mathbf{F}_{12} and \mathbf{F}_{66} are used to apply uniaxial ($\mathbf{F}_{11}, \mathbf{F}_{22}$), shear strain (\mathbf{F}_{12}) and biaxial (\mathbf{F}_{66}) strain to the monolayer. With the reduction of elements due to symmetry and dimensionality, the following are the stiffness tensor for the isotropic (Left) graphene and h-BN monolayer systems and the anisotropic (Right) BN_2 systems [244] :

$$C_{iso.} = \begin{bmatrix} C_{11} & C_{12} & 0 \\ & C_{11} & 0 \\ & & \frac{C_{11}-C_{12}}{2} \end{bmatrix} \quad C_{ani.} = \begin{bmatrix} C_{11} & C_{12} & 0 \\ & C_{22} & 0 \\ & & C_{66} \end{bmatrix} \quad (7.9)$$

where the anisotropic in-plane Young's Modulus can be calculated using:

$$E_{arm} = \frac{C_{11}C_{22} - C_{12}C_{12}}{C_{11}}, \quad E_{zig} = \frac{C_{11}C_{22} - C_{12}C_{12}}{C_{22}} \quad (7.10)$$

For the isotropic materials (graphene and h-BN monolayer), where $C_{11} = C_{22}$, the in-plane Young's Modulus can be reduced down to the following:

$$E = \frac{C_{11}^2 - C_{12}^2}{C_{11}} \quad (7.11)$$

The Poisson ratios are given as:

$$\nu_{xy} = \frac{C_{12}}{C_{22}}, \quad \nu_{yx} = \frac{C_{12}}{C_{11}} \quad (7.12)$$

7.3 Results and Discussion

7.3.1 Monolayer

To establish the reliability and accuracy of the modeling elements, we have first performed calculations on the well-characterized monolayers of graphene and h-BN. The structural, elastic and electronic properties of graphene and h-BN monolayer were well reproduced (Table 7.1) suggesting the reliability of the modeling elements for calculations on BN₂.

Figure 7.1 displays the equilibrium configuration of the BN₂ monolayer. It consists of a network of hexagons with *Amm2* (38) symmetry. These hexagons are distinctly different from the regular hexagon shapes associated with the graphene and h-BN monolayers. The unit cell contains two formula units with the lattice parameters of $a = 6.84 \text{ \AA}$ and $b = 2.55 \text{ \AA}$. Note that a large value of c ($\approx 19 \text{ \AA}$) was used to provide an adequate vacuum distance between the mirror images in the periodic DFT

calculations for the BN_2 monolayer. In the equilibrium configuration, the sp^2 bond lengths ($R_{B_1N_2}$) are 1.50 Å which is larger than that of a h-BN monolayer (1.45 Å). The bond extending to N_1/N_3 from B_2/B_1 has contracted to a more sp-like character with a distance of 1.34 Å. The shortest bond, 1.29 Å, is between the neighboring nitrogen atoms (N_1/N_2 and N_3/N_4) as shown in Figure 7.1. In the molecular BN_2 with the (B-N-N) configuration, *ab initio* calculations report that the B-N and N-N distances to be 1.51 and 1.15 Å [218]. Similarly, the N-N distance is reported to be 1.16, 1.14 and 1.13 Å in AlN_2 , GaN_2 and InN_2 molecules [160].

To gain a better understanding of the nature of the bonding in this 2-D material, calculations of the Bader charges were performed. Figure 7.1 (Right panel) shows a charge of 0.9e (i.e. loss of 2.1e) associated with the B atoms. The N atoms with lower coordination (N_1, N_3) have a charge of 6.0e (i.e. gain of 1.0e), whereas the other nitrogen atoms (N_2, N_4) have a slightly higher charge of 6.1e (i.e. gain of 1.1e). Note that the bonds are more ionic in a h-BN monolayer with the boron and nitrogen having charges of 0.8e (loss of 2.2e) and 7.2e (i.e. gain of 2.2). This bond between N_3 and N_4 atoms will yield the materials high in-plane Young's modulus as shown in the Section 7.3.3.

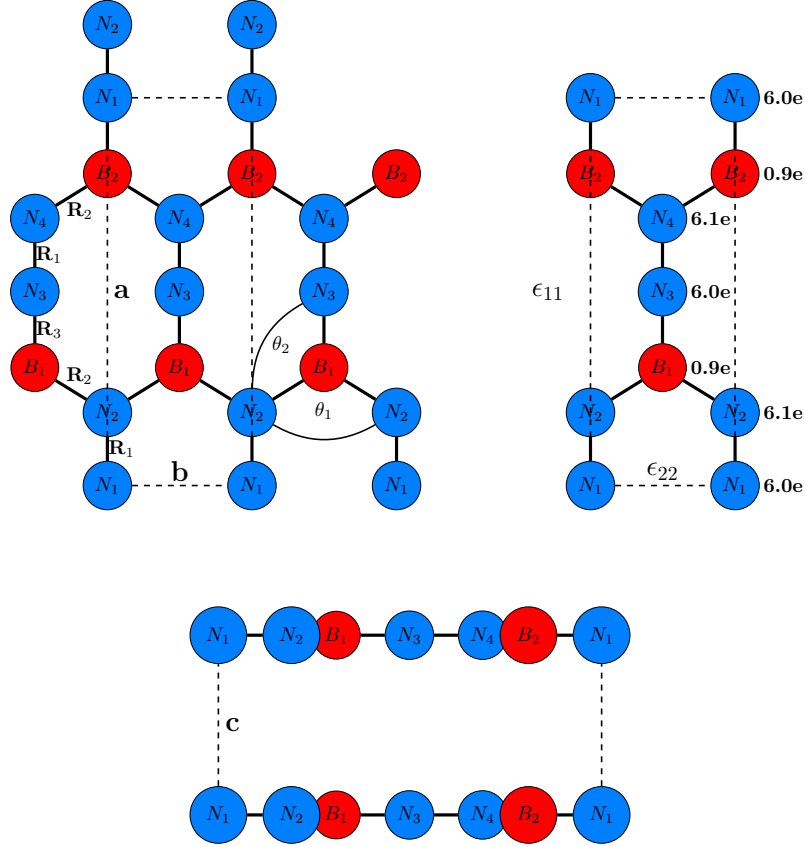


Figure 7.1: The structure of BN_2 (Top left). The unit cell consisting of two B atoms (red) and four N atoms (blue) is outlined with the dashed (–) lines. The lattice parameters, bond lengths and bond angles together with Bader charges on each atom are also listed (Table 7.1). Directions for the applied strain ϵ_{11} and ϵ_{22} are shown. The AA stacked bilayer structure (Bottom) is shown with the interlayer distance (c) of 3.17 Å.

7.3.2 Stability

Following Equation 7.1, the calculated cohesive energy (E_{cohesive}) for the BN_2 monolayer is found to be -7.64 eV/unit cell. In comparison, the calculated E_{cohesive} values of graphene and h-BN monolayers are -9.26 and -8.79 eV/unit cell. The BN_2 monolayer with the N-N bond appears to be stable at the PBE-DFT level of theory. Note that

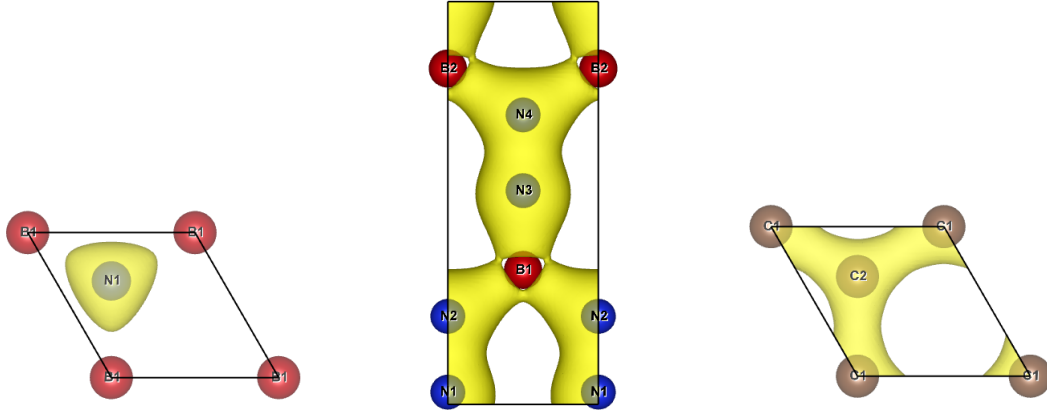


Figure 7.2: Charge density of BN (left), BN_2 (middle), graphene (right) with an isovalue = $0.2e$. The metallic, graphene and BN_2 structures show a delocalized electronic cloud as opposed the localized electronic cloud of the semiconducting h-BN

ab initio calculations suggest the kinetic factors to determine the stability of BN_2 as a molecule with the (B-N-N) configuration [218].

To further establish the stability of the BN_2 monolayer, phonon calculations are performed. The calculated phonon dispersion relationship is shown in Figure 7.3. Accordingly, the BN_2 monolayer is dynamically stable considering that small imaginary frequencies ($\omega < 5\text{cm}^{-1}$) near Γ are likely to be due to numerical artifacts that would dissipate if a larger super cell was taken into account or an increase in K-points was considered in calculations. The maximum frequency associated with the optical phonons is about 1700cm^{-1} , which may be associated with the stretching of the N-N bond. The N-N bond stretching mode in AlN_2 , GaN_2 and InN_2 molecules is 1887, 2036, and 2094cm^{-1} [160]. In contrast, the maximum frequency in the h-BN monolayer is about 1400cm^{-1} associated with the stretching of the B-N bond [225]. For the case of the BN_2 molecule, the highest frequency mode is predicted to be about 1900

Table 7.1

The calculated lattice parameters of graphene, h-BN, BN₂ and bilayer BN₂. Due to symmetry graphene and h-BN have reduced unique parameters. The Atom/Bond/Angle numbers correspond to Figure 7.1. The interlayer distance for the bilayer is 3.17 Å.

	Graphene	BN	BN ₂	BN ₂ Bilayer
Symmetry (#)	<i>P6/mmm</i> (191)	<i>P6m2</i> (187)	<i>Amm2</i> (38)	<i>Amm2</i> (38)
Lattice Parameters (Å)	a = 2.47	a = 2.51	a = 6.84 b = 2.55	a = 6.84 b = 2.55
Bond length (Å)	<i>C - C</i> 1.42	<i>B - N</i> 1.45	<i>N₁ - N₂(R₁)</i> 1.29	<i>N₁ - N₂(R₁)</i> 1.29
Bond length (Å)			<i>B₁ - N₁(R₂)</i> 1.50	<i>B₁ - N₁(R₂)</i> 1.50
Bond length (Å)			<i>B₁ - N₂(R₃)</i> 1.34	<i>B₁ - N₂(R₃)</i> 1.34
Bond angle (°)	<i>CCC</i> 120	<i>BNB</i> 120	<i>N₂B₁N₂(θ₁)</i> 116	<i>N₂B₁N₂(θ₁)</i> 116
Bond angle (°)			<i>N₂B₁N₃(θ₂)</i> 122	<i>N₂B₁N₃(θ₂)</i> 122

cm^{-1} at ab initio level of theory [218]. The carbon analogue of the BN₂ monolayer was also investigated, but the presence of large imaginary frequencies ($\omega > 500cm^{-1}$) suggesting the instability of the carbon analogue.

7.3.3 Electronic Properties

The calculated band structure and density of states find the BN₂ electronic properties to be metallic with the states around the Fermi level are dominated by the in-plane p-orbitals as shown in Figure 7.4. These in-plane orbitals are mainly associated with N₁ and N₃ atoms with smaller contributions from N₂, N₄ and B atoms (Figure 7.1)

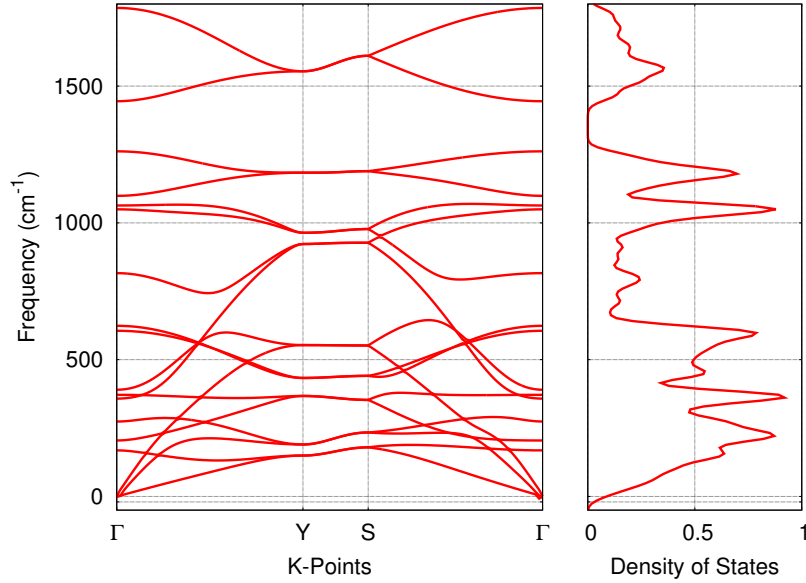


Figure 7.3: Calculated phonon dispersion (Left) and the associated phonon density of states (Right) of BN_2

. Note that the nitrogen atoms (N_1 and N_3) do not show a sp^2 coordination in the lattice. This is in contrast to the case of the h-BN monolayer for which all atoms are all sp^2 coordinated with network of alternating occupied out-of-plane p_z orbitals that do not overlap. In graphene, however, the out-of-plane p_z orbitals give its conducting properties. This can be shown in Figure 7.2 with the electron clouds of graphene and BN_2 being delocalized and h-BN is localized on the nitrogen atom. We find that the metallic properties exhibited by BN_2 can be attributed to the bonded nitrogen atoms (N-N) in the lattice. This metallic behavior is similar to what has been reported for penta- BN_2 [200].

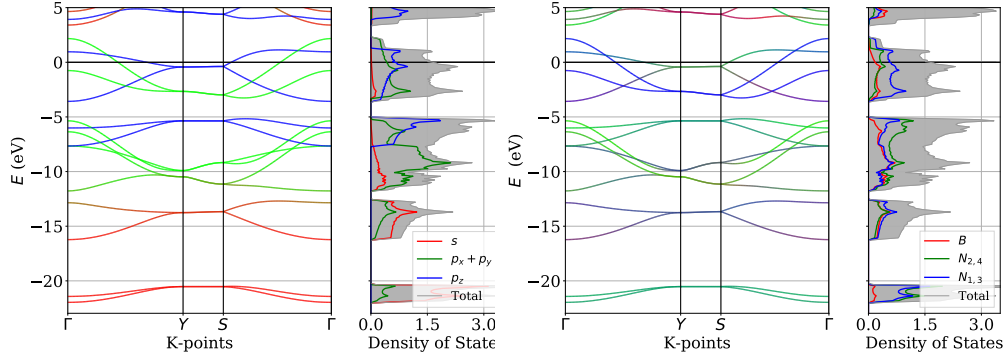


Figure 7.4: Calculated band structure and density of states of the BN_2 monolayer. (Left) orbital projected Color code: blue- s states, green -in-plane p_x and p_y states, blue - out-of-plane p_z states, grey- total density of states. (Right) atomic projected Color code: blue - $N_{1,3}$ states, green - $N_{2,4}$ states, red-B states, and grey- total density of states.

7.3.4 Elastic Properties

Table 7.2 lists the calculated values of the elastic constants and Poisson's ratios for BN_2 , together with those of graphene and the h-BN monolayer. First, we find a noticeable feature associated with BN_2 which shows the anisotropic behavior with the elastic constants being $C_{11} = 368.8$ N/m, $C_{12} = 47.2$ N/m, and $C_{22} = 153.3$ N/m. In the armchair direction, a Young's modulus of 354.3 N/m is predicted suggesting BN_2 to be stiffer than graphene (343 N/m) and the h-BN monolayer (276.2 N/m). In the zig-zag direction, a smaller modulus of 147.3 N/m is predicted. The same trend is exhibited for the Poisson's ratio in the zigzag and armchair directions of the BN_2 monolayer. The calculated elastic constants for graphene and the h-BN monolayer are in agreement with the previously reported theoretical results as show in Table

7.2 [258, 353]. For graphene, our calculated values of the elastic constants agree when compared to experimental work of graphene on metal substrates [272]. For example, the in-plane Young's modulus of graphene on Pt(111), Ru(0001), Ir(111), BC₃/NbB₂(0001) substrates is 342 N/m.

When compared to other similar 2-D materials such as Penta-Graphene [384], Penta-BN [200] and Penta-BN₂ [200], the BN₂ monolayer appears to be stiffer with a larger Poisson's ratio. The Young's modulus for penta-Graphene [384], penta-BN [200], and penta-BN₂ [200] are reported to be 263.8, 133, and 224 N/m.

Table 7.2

Calculated elastic constants (C_{xx}), in-plane Young's modulus defined in Equation 7.10 ($E_{arm/zig}$), and Poisson's ratio (ν) defined in Equation 7.12 for graphene and monolayers of h-BN and BN₂. C_{66} is computed using strain and stress data. Units are in N/m, except for ν which is unitless. 1) [353] 2) [258]

	Graphene ¹	This Work	BN ²	This Work	BN ₂	Bilayer
C_{11}	358.1	353.7	293.2	290.5	368.8	357.7
C_{12}	60.4	61.7	66.1	64.4	47.2	45.5
C_{13}						-5.2
C_{22}					153.3	107.3
C_{23}						-22.7
C_{33}						5.0
C_{44}						0.4
C_{55}						0.4
C_{66}		144.9		113.1	58.7	50.2
E_{Arm}	348	343.0	278.3	276.2	354.3	
E_{Zig}					147.3	
ν_{xy}	0.169	0.17	0.2176	0.22	0.31	0.42
ν_{yx}					0.13	0.13

All previously reported structures are isotropic which leads to $C_{11} = C_{22}$, the directions then have identical Young's Modulus and Poisson ratio for the 11 and 22 directions. For the symmetric values, e.g $C_{11} = C_{22}$, the values are identical, but due to numerical procedures there are slight variations. To address this discrepancy the average of each of these values are presented in Table 7.2. A similar procedure was done for the off-diagonal terms, due to the mirrored terms in the \mathbf{C}_{IJ} tensor.

7.3.5 Bilayer

Next, we considered the case of the bilayer BN_2 stacked in either AA or AB configuration. The AB stacked bilayer configuration was generated by rotating the second layer by 180° with respect to the first layer. The AA stacked bilayer configuration consists of atoms of the first layer are on top of the atoms of the second layer (Figure 7.1). In the equilibrium configuration obtained at the PBE+D3-DFT level of theory, the interlayer distance is calculated to be 3.17 \AA for both stacking configurations. The calculated binding energy (Equation 7.2) of the AA and AB- stacked configuration is found to be -0.28 eV and -0.22 eV suggesting the AA-stacked bilayer to be energetically preferred. The calculated band structure and density of states predict the bilayer to be metallic displaying features similar to those obtained for the monolayer (Figure 7.5).

The bilayer mechanical properties has similar in-plane properties when compared to the monolayer. C_{11} has a difference of about 10 N/m , C_{12} by about 2 N/m , C_{66} by about 9 N/m . The largest difference is in the C_{22} term with a difference of about 45 N/m . The extra dimension added by the layer requires more elastic constants, which are expected to be small due to the long-ranged interactions (C_{x3} , C_{44} , C_{55}). C_{13} has a value of -5.2 N/m , C_{23} -22.7 N/m , C_{33} 5.0 N/m , C_{44} and C_{55} 0.4 N/m . The change in C_{22} resulted in a greater value of ν_{xy} , 0.42 .

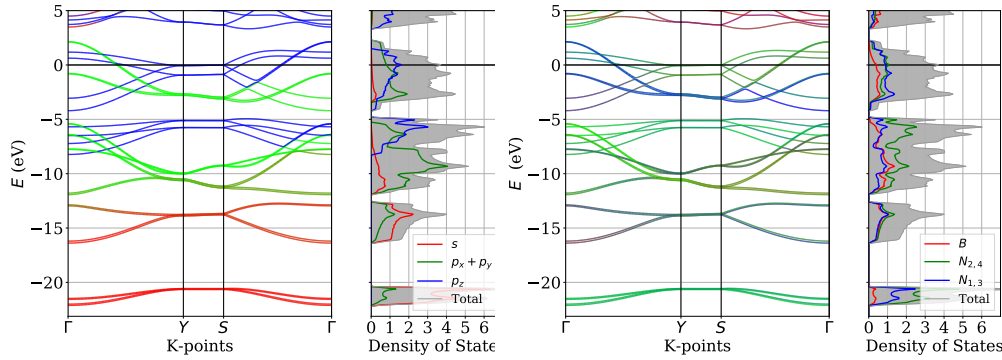


Figure 7.5: Calculated band structures and density of states of the AA BN_2 bilayer. (Left) orbital projected Color code: blue- s states, green- in-plane p_x and p_y states, blue: out-of-plane p_z states, grey-total density of states. (Right) atomic projected Color code: blue - $N_{1,3}$ states, green- $N_{2,4}$ states, red- B states, grey - total density of states.

7.4 Summary

A new B-N monolayer material (BN_2) consisting of a network of extended hexagons was predicted to be stable with a comparable value of the cohesive energy relative to that of the h-BN monolayer. The distinguishable nature of this 2-D material was found to be the presence of the bonded N atoms (N-N) in the lattice. The highest phonon frequency carries the signature of the N-N bond in the 2-D lattice. The monolayer is predicted to be metallic with in-plane p states dominating the Fermi level. We find that the monolayer exhibits anisotropic mechanical properties that surpass graphene in the armchair direction. This anisotropy may lead to novel applications in the future if some challenges are overcome in the synthesis of this material.

Chapter 8

Conclusion

For electronic structure calculations, the optimization problem needs to be taken to a grander scale. In the past modeling elements, e.g cutoff energies and k-point meshes, were optimized to make problems tractable, now this a trivial aspect of simulations. While these series and meshes cannot be set to infinity, they can be set to default values that capture the relevant physics associated with the given problem. The difficulties now lay in the determining the parameter space, how many permutations of a structure should be investigated and what rules can we apply to limit this space. Previously researchers only had the capabilities to look at a few select materials at a time. State-of-the-art calculations are oriented around discovery a material for a problem instead by searching hundreds if not thousands of potential candidates.[60, 304] We must integrate each computational tool that we have at our disposal to

solve problems on a multi-scale level, from all electron calculations to continuum mechanics to the laboratory bench. Researchers are building work flows that allow for high-throughput calculations. This requires a substantial amount of automation that must be done with care and thought.

In this dissertation, the ground work for a general understanding of the chemistry and physics for boron-nitride was gained. A few data points were filled in and disseminated to the public. We have only looked in to a handful of vectors for amino acids and gold to interact with pristine boron-nitride. The potential chemistry that can occur that have not been included are limitless. For the physiological setting there are countless other molecules that can interact and potentially degrade the desired properties of the structures. The inclusion of water can potentially change the chemistry that are possible.

Molecular dynamics simulations have the ability to simulate large number of atoms, but their limitation is that it can only simulate atoms and not electrons. The force fields can only simulate the chemistry that has been fitted. This issue can be eliminated by using first principles molecular dynamics. The trade of with the increased accuracy is the cost of the simulation, the size of the system is greatly reduced.

This is a challenging task with no clear solution, but to move to greater scientific horizons, it must be tackled. Now the scale of investigation needs to be expanded, large programs need to be built to generate and utilize large amount of data. The

last work that was conducted in this work, Chapter 6, the work transitioned from traditional DFT calculations to ab initio simulations. Explicit water, temperature and time were introduced into the model. The need to model the changing electronic structure due to the complexity of the morphologies of the surfaces has been shown. To continue the work free-energy methods will be used to quantify the interactions in the complex environment.

References

- [1] M. H. Abdalmoneam, K. Waters, N. Saikia, and R. Pandey. Amino-Acid-Conjugated Gold Clusters: Interaction of Alanine and Tryptophan with Au₈ and Au₂₀. *Journal of Physical Chemistry C*, 121(45):25585–25593, 2017.
- [2] J. Abrahamson, P. G. Wiles, and B. L. Rhoades. Structure of carbon fibres found on carbon arc anodes. *Carbon*, 37(11):1873–1874, 1999.
- [3] S. F. A. Acquah, A. V. Penkova, D. A. Markelov, A. S. Semisalova, B. E. Leonhardt, and J. M. Magi. Review—The Beautiful Molecule: 30 Years of C₆₀ and Its Derivatives. *ECS Journal of Solid State Science and Technology*, 6(6):M3155–M3162, 2017.
- [4] C. Adamo and V. Barone. Toward reliable density functional methods without adjustable parameters: The PBE0 model. *The Journal of Chemical Physics*, 110(13):6158–6170, 1999.

- [5] P. P. Adisheshaiah, J. B. Hall, and S. E. McNeil. Nanomaterial standards for efficacy and toxicity assessment. *Wiley Interdisciplinary Reviews: Nanomedicine and Nanobiotechnology*, 2(1):99–112, 2010.
- [6] K. L. Aillon, Y. Xie, N. El-Gendy, C. J. Berkland, and M. L. Forrest. Effects of nanomaterial physicochemical properties on in vivo toxicity. *Advanced Drug Delivery Reviews*, 61(6):457–466, 2009.
- [7] B. Akdim, S. N. Kim, R. R. Naik, B. Maruyama, M. J. Pender, and R. Pachter. Understanding effects of molecular adsorption at a single-wall boron nitride nanotube interface from density functional theory calculations. *Nanotechnology*, 20(35):355705, 2009.
- [8] A. Ambrogelly, S. Palioura, and D. Söll. Natural expansion of the genetic code. *Nature Chemical Biology*, 3:29, 2006.
- [9] C. André and Y. Claude. Boron nitride nanotubes and their functionalization via quinuclidine-3-thiol with gold nanoparticles for the development and enhancement of the HPLC performance of HPLC monolithic columns. *Talanta*, 93:274–278, 2012.
- [10] M. Aroyo, D. Orobengoa, G. de la Flor, E. S. Tasci, J. M. Perez-Matosa, and H. Wondratschek. Brillouin-zone database on the Bilbao Crystallographic Server. *Acta crystallographica. Section A, Foundations and Advances*, 70(2):126–137, 2014.

- [11] M. I. Aroyo, A. Kirov, C. Capillas, J. M. Perez-Mato, and H. Wondratschek. Bilbao Crystallographic Server. II. Representations of crystallographic point groups and space groups. *Acta crystallographica. Section A, Foundations and Advances*, 62:115–128, 2006.
- [12] M. I. Aroyo, J. M. Perez-Mato, D. Orobengoa, G. E. Tasci, de la Flor, and A. Kirov. Crystallography online: Bilbao Crystallographic Server. *Bulgarian Chemical Communications*, 43(2):183–197, 2011.
- [13] M. I. Aroyo, J. M. Perez-Mato, C. Capillas, E. Kroumova, S. Ivantchev, G. Madariaga, A. Kirov, and H. Wondratschek. Bilbao crystallographic server: I. Databases and crystallographic computing programs. *Zeitschrift für Kristallographie*, 221(1):15–27, 2006.
- [14] N. W. Ashcroft and N. D. Mermin. *Solid State Physics*. Saunders College, Philadelphia, 1976.
- [15] S. Azevedo, J. R. Kaschny, C. M. C. de Castilho, and F. d. B. Mota. Theoretical investigation of native defects in a boron nitride monolayer. *Nanotechnology*, 23, 2012.
- [16] K. Ba, W. Jiang, J. Cheng, J. Bao, N. Xuan, and Y. Sun. Chemical and Bandgap Engineering in Monolayer Hexagonal Boron Nitride. *Scientific Reports*, 7:45584, 2017.

- [17] G. B. Bachelet, D. R. Hamann, and M. Schlüter. Pseudopotentials that work: From H to Pu. *Phys. Rev. B*, 26(8):4199–4228, 1982.
- [18] BaChem. Bio-Connect Life Sciences, 2018.
- [19] J. Baggot. *The Quantum Story*. 2011.
- [20] J. Bardeen, L. N. Cooper, and J. R. Schrieffer. Theory of Superconductivity. *Phys. Rev.*, 108(5):1175–1204, dec 1957.
- [21] D. Bas, M. J. Ford, M. B. Cortie, and B. Soule. Low energy structures of gold nanoclusters in the size range 3 – 38 atoms. *Journal of Molecular Structure*, 686:193–205, 2004.
- [22] D. A. C. Beck and V. Daggett. Methods for molecular dynamics simulations of protein folding/unfolding in solution. *Methods*, 34(1):112–120, 2004.
- [23] A. D. Becke. Density-functional exchange-energy approximation with correct asymptotic behavior. *Phys. Rev. A*, 38(6):3098–3100, 1988.
- [24] A. D. Becke. Density-functional thermochemistry.III. The role of exact exchange. *The Journal of Chemical Physics*, 98(7):5648, 1993.
- [25] A. D. Becke. Perspective: Fifty years of density-functional theory in chemical physics. *The Journal of Chemical Physics*, 140:18A301, 2014.

- [26] H. J. C. Berendsen, J. R. Grigera, and T. P. Straatsma. The missing term in effective pair potentials. *The Journal of Physical Chemistry*, 91(24):6269–6271, 1987.
- [27] K. Bergman, S. Borkar, D. Campbell, W. Carlson, W. Dally, M. Denneau, P. Franzon, W. Harrod, J. Hiller, S. Karp, S. Keckler, D. Klein, R. Lucas, M. Richards, A. Scarpelli, S. Scott, A. Snavely, T. Sterling, R. S. Williams, K. Yelick, K. Bergman, S. Borkar, D. Campbell, W. Carlson, W. Dally, M. Denneau, P. Franzon, W. Harrod, J. Hiller, S. Keckler, D. Klein, P. Kogge, R. S. Williams, and K. Yelick. ExaScale Computing Study: Technology Challenges in Achieving Exascale Systems Peter Kogge, Editor & Study Lead, 2008.
- [28] E. Besalú and R. Carbó-Dorca. The general Gaussian product theorem. *Journal of Mathematical Chemistry*, 49(8):1769, 2011.
- [29] H. F. Bettinger, T. Dumitrica, G. E. Scuseria, and B. I. Yakobson. Mechanically induced defects and strength of BN nanotubes. *Physical Review B*, 65:2–5, 2002.
- [30] X. Blase, A. Rubio, S. G. Louie, and M. L. Cohen. Stability and Band Gap Constancy of Boron Nitride Nanotubes. *Europhysics Letters (EPL)*, 28(5):335–340, 1994.
- [31] P. E. Blöchl. Projector augmented-wave method. *Physical Review B*, 50(24):17953–17979, 1994.

- [32] W. Bollmann and J. Spreadborough. Action of Graphite as a Lubricant. *Nature*, 186:29, 1960.
- [33] M. Born and R. Oppenheimer. Zur quantentheorie der molekeln. *Annalen der Physik*, 20(84):457–484, 1927.
- [34] S. F. Boys and F. Bernardi. The calculation of small molecular interactions by the differences of separate total energies. Some procedures with reduced errors. *Molecular Physics*, pages 65–73, 2002.
- [35] E. G. Brandt and A. P. Lyubartsev. Molecular Dynamics Simulations of Adsorption of Amino Acid Side Chain Analogues and a Titanium Binding Peptide on the TiO₂ (100) Surface. *The Journal of Physical Chemistry C*, 119(32):18126–18139, 2015.
- [36] S. Bulusu and X. C. Zeng. Structures and relative stability of neutral gold clusters : Au_n (n = 15 – 19). *The Journal of Chemical Physics*, 154303:154303, 2006.
- [37] A. N. Camden, S. A. Barr, and R. J. Berry. Simulations of peptide-graphene interactions in explicit water. *Journal of Physical Chemistry B*, 117(37):10691–10697, 2013.
- [38] J. Cao, T. Sun, and K. T. V. Grattan. Sensors and Actuators B : Chemical Gold nanorod-based localized surface plasmon resonance biosensors : A review. *Sensors & Actuators: B. Chemical*, 195:332–351, 2014.

- [39] R. Car and M. Parrinello. Unified Approach for Molecular Dynamics and Density-Functional Theory. *Phys. Rev. Lett.*, 55(22):2471–2474, 1985.
- [40] J. a. Carr, H. Wang, A. Abraham, T. Gullion, and J. P. Lewis. l -Cysteine Interaction with Au 55 Nanoparticle. *The Journal of Physical Chemistry C*, 116:25816–25823, 2012.
- [41] E. Cauët, S. Bogatko, J. H. Weare, J. L. Fulton, G. K. Schenter, and E. J. Bylaska. Structure and dynamics of the hydration shells of the Zn²⁺ ion from ab initio molecular dynamics and combined ab initio and classical molecular dynamics simulations. *The Journal of Chemical Physics*, 132(19):194502, 2010.
- [42] C. A. Charitidis, P. Georgiou, M. A. Koklioti, A.-F. Trompeta, and V. Markakis. Manufacturing nanomaterials: from research to industry. *Manufacturing Rev.*, 1:11, 2014.
- [43] K. Chaudhari, P. L. Xavier, and T. Pradeep. Understanding the evolution of luminescent gold quantum clusters in protein templates. *ACS Nano*, 5(11):8816–8827, 2011.
- [44] G. Chen, Q. Wang, Q. Sun, Y. Kawazoe, P. Jena, G. Chen, Q. Wang, Q. Sun, Y. Kawazoe, and P. Jena. Structures of neutral and anionic clusters revisited Structures of neutral and anionic Au 16 clusters revisited. *The Journal of Chemical Physics*, 194306, 2010.

- [45] N. Chen, Y. He, Y. Su, X. Li, Q. Huang, H. Wang, X. Zhang, R. Tai, and C. Fan. The cytotoxicity of cadmium-based quantum dots. *Biomaterials*, 33(5):1238–1244, 2012.
- [46] R. J. Chen, S. Bangsaruntip, K. A. Drouvalakis, N. W. S. Kam, M. Shim, Y. Li, W. Kim, P. J. Utz, and H. Dai. Noncovalent functionalization of carbon nanotubes for highly specific electronic biosensors. *Proceedings of the National Academy of Sciences of the United States of America*, 100(9):4984–4989, 2003.
- [47] Y. Chen, J. Zou, S. J. Campbell, and G. L. Caer. Boron nitride nanotubes: Pronounced resistance to oxidation. *Applied Physics Letters*, 84(13):2430–2432, 2004.
- [48] Chen. Robert L., Y. Zhang, D. Wang, and H. Dai. Noncovalent side-wall functionalization of single-walled carbon nanotubes. *Journal of the American Chemical Society*, 123:3838–3839, 2001.
- [49] S. Choi, R. M. Dickson, and J. Yu. Developing luminescent silver nanodots for biological applications. *Chemical Society Reviews*, 41(5):1867–1891, 2012.
- [50] N. G. Chopra, R. J. Luyken, K. Cherrey, V. H. Crespi, M. L. Cohen, S. G. Louie, and A. Zettl. Boron nitride nanotubes. *Science*, 269:966–967, 1995.
- [51] B. Z. Chowdhry, T. J. Dines, S. Jabeen, and R. Withnall. Vibrational Spectra of α -Amino Acids in the Zwitterionic State in Aqueous Solution and the Solid

State : DFT Calculations and the Influence of Hydrogen Bonding. pages 10333–10347, 2008.

- [52] G. M. Church, Y. Gao, and S. Kosuri. Next-Generation Digital Information Storage in DNA. *Science*, 2012.
- [53] A. J. Cohen, P. Mori-Sanchez, W. Yang, P. Mori-s, W. Yang, P. Mori-Sánchez, and W. Yang. Challenges for Density Functional Theory. *Chemical Reviews*, 112(1):289–320, 2012.
- [54] J. N. Coleman, M. Lotya, A. O\textquoterightNeill, S. D. Bergin, P. J. King, U. Khan, K. Young, A. Gaucher, S. De, R. J. Smith, I. V. Shvets, S. K. Arora, G. Stanton, H.-Y. Kim, K. Lee, G. T. Kim, G. S. Duesberg, T. Hallam, J. J. Boland, J. J. Wang, J. F. Donegan, J. C. Grunlan, G. Moriarty, A. Shmeliov, R. J. Nicholls, J. M. Perkins, E. M. Grieveson, K. Theuwissen, D. W. McComb, P. D. Nellist, and V. Nicolosi. Two-Dimensional Nanosheets Produced by Liquid Exfoliation of Layered Materials. *Science*, 331(6017):568–571, 2011.
- [55] C. J. Cramer. *Computational Chemistry*. Wiley, 1st edition, 2002.
- [56] M. D. Crescenzi, P. Castrucci, M. Scarselli, M. Diociaiuti, P. S. Chaudhari, C. Balasubramanian, T. M. Bhave, and S. V. Bhoraskar. Experimental imaging of silicon nanotubes. *Applied Physics Letters*, 86(23):231901, 2005.
- [57] O. Cretu, Y.-c. Lin, and K. Suenaga. Evidence for Active Atomic Defects in

- Monolayer Hexagonal Boron Nitride: A New Mechanism of Plasticity in Two-Dimensional Materials. *Nano Letters*, 14:1064–1068, 2014.
- [58] Y. Cui, Q. Wei, H. Park, and C. M. Lieber. Nanowire nanosensors for highly sensitive and selective detection of biological and chemical species. *Science*, 293(5533):1289–1292, 2001.
- [59] Z. Cui, A. J. Oyer, A. J. Glover, H. C. Schniepp, and D. H. Adamson. Large scale thermal exfoliation and functionalization of boron nitride. *Small*, 10(12):2352–2355, 2014.
- [60] S. Curtarolo, G. L. Hart, M. B. Nardelli, N. Mingo, S. Sanvito, and O. Levy. The high-throughput highway to computational materials design. *Nature Materials*, 12(3):191–201, 2013.
- [61] V. Daggett. Molecular Dynamics Simulations of the Protein Unfolding/Folding Reaction. *Accounts of Chemical Research*, 35(6):422–429, 2002.
- [62] M. E. Dávila, L. Xian, S. Cahangirov, A. Rubio, and G. L. Lay. Germanene: a novel two-dimensional germanium allotrope akin to graphene and silicene. *New Journal of Physics*, 16(9):95002, 2014.
- [63] L. de Broglie. Recherches sur la théorie des quanta. *Ann. De Physique*, 3:22, 1925.

- [64] W. H. De Jong and P. J. A. Borm. Drug delivery and nanoparticles: Applications and hazards. *International Journal of Nanomedicine*, 3(2):133–149, 2008.
- [65] F. De Leo, A. Magistrato, and D. Bonifazi. Interfacing proteins with graphitic nanomaterials: from spontaneous attraction to tailored assemblies. *Chem. Soc. Rev.*, 44(19):6916–6953, 2015.
- [66] M. Deighan and J. Pfaendtner. Exhaustively sampling peptide adsorption with metadynamics. *Langmuir*, 29(25):7999–8009, 2013.
- [67] S. Del Turco, G. Ciofani, V. Cappello, M. Gemmi, T. Cervelli, C. Saponaro, S. Nitti, B. Mazzolai, G. Basta, and V. Mattoli. Cytocompatibility evaluation of glycol-chitosan coated boron nitride nanotubes in human endothelial cells. *Colloids and Surfaces B: Biointerfaces*, 111:142–149, 2013.
- [68] A. Dhawan and V. Sharma. Toxicity assessment of nanomaterials: Methods and challenges. *Analytical and Bioanalytical Chemistry*, 398(2):589–605, 2010.
- [69] I. Diez and R. H. A. Ras. Fluorescent silver nanoclusters. *Nanoscale*, 3(5):1963–1970, 2011.
- [70] P. A. M. Dirac. Quantum Mechanics of Many-Electron Systems. *Proceedings of the Royal Society of London. Series A*, 123(792):714–733, 1929.

- [71] P. A. M. Dirac. Note on Exchange Phenomena in the Thomas Atom. *Mathematical Proceedings of the Cambridge Philosophical Society*, 23(May):376–385, 1930.
- [72] P. A. M. Dirac. A new notation for quantum mechanics. *Mathematical Proceedings of the Cambridge Philosophical Society*, 35(3):416–418, 1939.
- [73] R. Ditchfield, W. J. Hehre, and J. A. Pople. Self-Consistent Molecular-Orbital Methods. IX. An Extended Gaussian-Type Basis for Molecular-Orbital Studies of Organic Molecules. *The Journal of Chemical Physics*, 54(2):724–728, 1971.
- [74] D. P. DiVincenz and E. J. Mele. Self-consistent effective-mass theory. *Physical Review B*, 29(4):1685, 1984.
- [75] M. S. Dresselhaus, G. Dresselhaus, and R. Saito. Carbon fibers based on C60 and their symmetry. *Phys. Rev. B*, 45(11):6234–6242, 1992.
- [76] S. Dutta and S. K. Pati. Novel properties of graphene nanoribbons: a review. *Journal of Materials Chemistry*, 20(38):8207, 2010.
- [77] S. L. Edwards, J. A. Werkmeister, and J. A. M. Ramshaw. Carbon nanotubes in scaffolds for tissue engineering. *Expert Review of Medical Devices*, 6(5):499–505, 2009.
- [78] W. Ekardt. Dynamical Polarizability of Small Metal Particles: Self-Consistent

- Spherical Jellium Background Model. *Physical Review Letters*, 52(21):1925–1928, 1984.
- [79] W. Ekardt. Work function of small metal particles: Self-consistent spherical jellium-background model. *Physical Review B*, 29(4):1558–1564, 1984.
- [80] G. Elumalai, H. Noguchi, A. Lyalin, T. Taketsugu, and K. Uosaki. Electrochemistry Communications Gold nanoparticle decoration of insulating boron nitride nanosheet on inert gold electrode toward an efficient electrocatalyst for the reduction of oxygen to water. *Electrochemistry Communications*, 66:53–57, 2016.
- [81] H. Erdogan, O. Metin, and S. Ozkar. In situ-generated PVP-stabilized palladium(0) nanocluster catalyst in hydrogen generation from the methanolysis of ammonia-borane. *Physical Chemistry Chemical Physics*, 11(44):10519–10525, 2009.
- [82] F. Erogbogbo, K.-T. Yong, I. Roy, G. Xu, P. N. Prasad, and M. T. Swihart. Biocompatible Luminescent Silicon Quantum Dots for Imaging of Cancer Cells. *ACS Nano*, 2(5):873–878, 2008.
- [83] D. Farmanzadeh and S. Ghazanfary. BNNTs under the influence of external electric field as potential new drug delivery vehicle of Glu, Lys, Gly and Ser amino acids: A first-principles study. *Applied Surface Science*, 320:391–399, 2014.

- [84] E. Fermi. Eine statistische Methode zur Bestimmung einiger Eigenschaften des Atoms und ihre Anwendung auf die Theorie des periodischen Systems der Elemente. *Zeitschrift für Physik*, 48(1):73–79, 1928.
- [85] E. M. Fernández and L. C. Balbás. Planar and cage-like structures of gold clusters : Density-functional pseudopotential calculations. *Physical Review B*, 73:235433, 2006.
- [86] M. A. Fernandez-Yague, A. Larrañaga, O. Gladkovskaya, A. Stanley, G. Tadayon, Y. Guo, J.-R. Sarasua, S. A. M. Tofail, D. I. Zeugolis, A. Pandit, and M. J. Biggs. Effects of Polydopamine Functionalization on Boron Nitride Nanotube Dispersion and Cytocompatibility. *Bioconjugate Chemistry*, 26(10):2025–2037, 2015.
- [87] T. H. Ferreira, D. C. F. Soares, L. M. C. Moreira, P. R. O. da Silva, R. G. dos Santos, and E. M. B. de Sousa. Boron nitride nanotubes coated with organic hydrophilic agents: Stability and cytocompatibility studies. *Materials Science and Engineering: C*, 33(8):4616–4623, 2013.
- [88] R. P. Feynman. There’s plenty of room at the bottom. *Journal of Microelectromechanical Systems*, 1(1):60–66, 1992.
- [89] A. Fleurence, R. Friedlein, T. Ozaki, H. Kawai, Y. Wang, and Y. Yamada-Takamura. Experimental Evidence for Epitaxial Silicene on Diboride Thin Films. *Physical Review Letters*, 108(June):245501, 2012.

- [90] A. D. Franklin. Nanomaterials in transistors: From high-performance to thin-film applications. *Science*, 349(6249), 2015.
- [91] M. J. Frisch, G. W. Trucks, H. B. Schlegel, G. E. Scuseria, M. A. Robb, J. R. Cheeseman, G. Scalmani, V. Barone, B. Mennucci, G. A. Petersson, H. Nakatsuji, M. Caricato, X. Li, H. P. Hratchian, A. F. Izmaylov, J. Bloino, G. Zheng, J. L. Sonnenberg, M. Hada, M. Ehara, K. Toyota, R. Fukuda, J. Hasegawa, M. Ishida, T. Nakajima, Y. Honda, O. Kitao, H. Nakai, T. Vreven, J. A. Montgomery Jr., J. E. Peralta, F. Ogliaro, M. Bearpark, J. J. Heyd, E. Brothers, K. N. Kudin, V. N. Staroverov, R. Kobayashi, J. Normand, K. Raghavachari, A. Rendell, J. C. Burant, S. S. Iyengar, J. Tomasi, M. Cossi, N. Rega, J. M. Millam, M. Klene, J. E. Knox, J. B. Cross, V. Bakken, C. Adamo, J. Jaramillo, R. Gomperts, R. E. Stratmann, O. Yazyev, A. J. Austin, R. Cammi, C. Pomelli, J. W. Ochterski, R. L. Martin, K. Morokuma, V. G. Zakrzewski, G. A. Voth, P. Salvador, J. J. Dannenberg, S. Dapprich, A. D. Daniels, Ö. Farkas, J. B. Foresman, J. V. Ortiz, J. Cioslowski, and D. J. Fox. Gaussian09 Revision D.01.
- [92] P. Fulde. *Electron correlations in molecules and solids*. Springer-Verlag, Berlin, 1991.
- [93] A. B. Fulton and W. B. Isaacs. Titin, a huge, elastic sarcomeric protein with a probable role in morphogenesis. *BioEssays*, 13(4):157–161, 1991.

- [94] J. D. Gale and A. L. Rohl. The General Utility Lattice Program (GULP). *Molecular Simulation*, 29(5):291–341, 2003.
- [95] Z. Gao, C. Zhi, Y. Bando, D. Golberg, and T. Serizawa. Functionalization of boron nitride nanotubes for applications in nanobiomedicine. In *Boron Nitride Nanotubes in Nanomedicine*, pages 17–40. 2016.
- [96] A. J. Garza and G. E. Scuseria. Predicting Band Gaps with Hybrid Density Functionals. *The Journal of Physical Chemistry Letters*, 7:5–10, 2016.
- [97] V. D. Geist, R. Kloss, and H. Follner. Verfeinerung des II-rhomboedrischen Bors*. *Acta Cryst.*, B26:1800, 1970.
- [98] J. M. Gernand and E. A. Casman. Machine learning for nanomaterial toxicity risk assessment. *IEEE Intelligent Systems*, 29(3):84–88, 2014.
- [99] A. L. Gibb, N. Alem, J.-h. Chen, K. J. Erickson, J. Ciston, A. Gautam, M. Linck, and A. Zettl. Atomic Resolution Imaging of Grain Boundary Defects in Monolayer. *Journal of Chemical Physics*, 135:6758–6761, 2013.
- [100] E. D. Glendening, A. E. Reed, J. E. Carpenter, and F. Weinhold. NBO.
- [101] D. Golberg, Y. Bando, Y. Huang, and T. Terao. Boron Nitride Nanotubes and Nanosheets. *ACS Nano*, 4(6):2979–2993, 2010.

- [102] D. Golberg, Y. Bando, K. Kurashima, and T. Sato. Synthesis and characterization of ropes made of BN multiwalled nanotubes. *Scripta Materialia*, 44(8):1561–1565, 2001.
- [103] J. Goldberger, R. He, Y. Zhang, S. Lee, H. Yan, H.-J. Choi, and P. Yang. Single-crystal gallium nitride nanotubes. *Nature*, 422:599, 2003.
- [104] R. V. Gorbachev, I. Riaz, R. R. Nair, R. Jalil, L. Britnell, B. D. Belle, E. W. Hill, K. S. Novoselov, K. Watanabe, T. Taniguchi, A. K. Geim, and P. Blake. Hunting for Monolayer Boron Nitride : Optical and Raman Signatures. *Small*, 7(4):465–468, 2011.
- [105] M. C. Gordillo and J. Martí. Wetting and prewetting of water on top of a single sheet of hexagonal boron nitride. *Physical Review E - Statistical, Nonlinear, and Soft Matter Physics*, 84(1):1–5, 2011.
- [106] N. Goswami, A. Giri, M. S. Bootharaju, P. L. Xavier, T. Pradeep, and S. K. Pal. Copper Quantum Clusters in Protein Matrix: Potential Sensor of Pb²⁺ Ion. *Analytical Chemistry*, 83(24):9676–9680, 2011.
- [107] U. S. Government. Materials Genome Initiative, 2013.
- [108] S. Gowtham, R. H. Scheicher, R. Ahuja, R. Pandey, and S. P. Karna. Physisorption of nucleobases on graphene: Density-functional calculations. *Physical Review B*, 76:2–5, 2007.

- [109] S. Gowtham, R. H. Scheicher, R. Pandey, S. P. Karna, and R. Ahuja. First-principles study of physisorption of nucleic acid bases on small-diameter carbon nanotubes. *Nanotechnology*, 19:125701, 2008.
- [110] S. Grimme. Accurate description of van der Waals complexes by density functional theory including empirical corrections. *Journal of Computational Chemistry*, 25(12):1463–1473, 2004.
- [111] S. Grimme. Semiempirical GGA-type density functional constructed with a long-range dispersion correction. *Journal of Computational Chemistry*, 27(15):1787–1799, 2006.
- [112] S. Grimme, J. Antony, S. Ehrlich, H. Krieg, S. Grimme, J. Antony, S. Ehrlich, and H. Krieg. A consistent and accurate ab initio parametrization of density functional dispersion correction (DFT-D) for the 94 elements H-Pu. *The Journal of Chemical Physics*, 132(154104), 2010.
- [113] G. Groenhof. Introduction to QM/MM Simulations. In *Biomolecular Simulations : Methods and Protocols*, pages 43–53. Humana Press, 1st edition, 2013.
- [114] M. Gromiha and S. Selvaraj. Importance of long-range interactions in protein folding1This article is dedicated to our teacher, Professor P.K. Ponnuswamy on the occasion of his 60th birthday.1. *Biophysical Chemistry*, 77(1):49–68, 1999.
- [115] Z. Gu, Z. Yang, Y. Chong, C. Ge, J. K. Weber, D. R. Bell, and R. Zhou. Surface

- Curvature Relation to Protein Adsorption for Carbon-based Nanomaterials. *Scientific Reports*, 5:10886, 2015.
- [116] Z. Guanghong, K. Seung-gu, X. Peng, Z. Yuliang, and Z. Ruhong. Interactions Between Proteins and Carbon-Based Nanoparticles: Exploring the Origin of Nanotoxicity at the Molecular Level. *Small*, 9(9-10):1546–1556, 2012.
- [117] G. Y. Guo and J. C. Lin. Systematic ab initio study of the optical properties of BN nanotubes. *Physical Review B*, 71:165402, 2005.
- [118] M. Gupta, T. S. Khan, M. Agarwal, and M. A. Haider. Understanding the Nature of Amino Acid Interactions with Pd(111) or Pd-Au Bimetallic Catalysts in the Aqueous Phase. *Langmuir*, 34(4):1300–1310, 2018.
- [119] G. G. Guzmán-Verri and L. C. L. Y. Voon. Electronic structure of silicon-based nanostructures. *Physical Review B*, 76:075113, 2007.
- [120] E. H. N. F. Mott Metal-insulator transition. Taylor & Francis, London 1990, × + 286 pages, 166 figures, ISBN 0-85066-783-6. *Crystal Research and Technology*, 26(6):788, 1991.
- [121] H. Häkkinen. The gold–sulfur interface at the nanoscale. *Nature Chemistry*, 4(6):443–455, 2012.
- [122] D. R. Hamann. Generalized norm-conserving pseudopotentials. *Phys. Rev. B*, 40(5):2980–2987, 1989.

- [123] D. R. Hamann, M. Schlüter, and C. Chiang. Norm-Conserving Pseudopotentials. *Phys. Rev. Lett.*, 43(20):1494–1497, 1979.
- [124] W. Q. Han and A. Zettl. Functionalized Boron Nitride Nanotubes with a Stan-
nic Oxide Coating : A Novel Chemical Route to Full Coverage. *Journal of the
American Chemical Society*, 2003:2062–2063, 2003.
- [125] R. D. Handy and B. J. Shaw. Toxic effects of nanoparticles and nanomaterials:
Implications for public health, risk assessment and the public perception of
nanotechnology. *Health, Risk & Society*, 9(2):125–144, 2007.
- [126] A. Hanene, K. T. Al-Jamal, K. H. Müller, S. Li, A. E. Porter, A. Eddaoudi,
M. Prato, A. Bianco, and K. Kostarelos. Cellular Uptake and Cytotoxic Impact
of Chemically Functionalized and Polymer-Coated Carbon Nanotubes. *Small*,
7(22):3230–3238, 2011.
- [127] B. Hao, W. Gong, T. K. Ferguson, C. M. James, J. A. Krzycki, and M. K. Chan.
A New UAG-Encoded Residue in the Structure of a Methanogen Methyltrans-
ferase. *Science*, 296(5572):1462–1466, 2002.
- [128] R. Haunschild, A. Barth, and W. Marx. Evolution of DFT studies in view of a
scientometric perspective. *Journal of Cheminformatics*, 8(1):1–12, 2016.
- [129] W. A. D. Heer. The physics of simple metal clusters : experimental aspects
and simple models. *Reviews of Modern Physics*, 65(3), 1993.

- [130] G. Henkelman, A. Arnaldsson, and H. Jonsson. A fast and robust algorithm for Bader decomposition of charge density. *Computational Materials Science*, 36:354–360, 2006.
- [131] J. Heyd, G. E. Scuseria, and M. Ernzerhof. Hybrid functionals based on a screened Coulomb potential. *The Journal of Chemical Physics*, 118(18):8207–8215, 2003.
- [132] T. Hilder, R. Yang, V. Ganesh, D. Gordon, A. Bliznyuk, A. Rendell, and S.-H. Chung. Validity of current force fields for simulations on boron nitride nanotubes. *Micro & Nano Letters*, 5(2):150, 2010.
- [133] T. A. Hilder and N. Gaston. Interaction of Boron Nitride Nanosheets with Model Cell Membranes. *ChemPhysChem*, 17(11):1573–1578, 2016.
- [134] M. Hoefling, F. Iori, S. Corni, and K.-E. Gottschalk. Interaction of Amino Acids with the Au(111) Surface: Adsorption Free Energies from Molecular Dynamics Simulations. *Langmuir*, 26(11):8347–8351, 2010.
- [135] L. J. E. Hofer, E. Sterling, and J. T. McCartney. Structure of Carbon Deposited from Carbon Monoxide on Iron, Cobalt and Nickel. *The Journal of Physical Chemistry*, 59(11):1153–1155, 1955.
- [136] P. Hohenberg and W. Kohn. Inhomogeneous Electron Gas. *Physical Review*, 136(3B):864, 1964.

- [137] H. Hong, T. Gao, and W. Cai. Molecular Imaging with Single-Walled Carbon Nanotubes. *Nano Today*, 4(3):252–261, 2009.
- [138] R. Hong, N. O. Fischer, A. Verma, C. M. Goodman, T. Emrick, and V. M. Rotello. Control of Protein Structure and Function through Surface Recognition by Tailored Nanoparticle Scaffolds. *Journal of the American Chemical Society*, 126(3):739–743, 2004.
- [139] W. G. Hoover. Canonical dynamics: Equilibrium phase-space distributions. *Phys. Rev. A*, 31(3):1695–1697, 1985.
- [140] J. Hu, T. W. Odom, and C. M. Lieber. Chemistry and physics in one dimension: Synthesis and properties of nanowires and nanotubes. *Accounts of Chemical Research*, 32(5):435–445, 1999.
- [141] X. Hu and Q. Zhou. Health and Ecosystem Risks of Graphene. *Chemical Reviews*, 113(5):3815–3835, 2013.
- [142] Y. Huang, J. Lin, Y. Bando, C. Tang, C. Zhi, Y. Shi, E. Takayama-Muromachi, and D. Golberg. BN Nanotubes Coated with Uniformly Distributed Fe₃O₄ Nanoparticles: Novel Magneto-Operable Nanocomposites. *Journal of Materials Chemistry*, 20:1007–1011, 2010.
- [143] Z. E. Hughes and T. R. Walsh. What makes a good graphene-binding peptide? Adsorption of amino acids and peptides at aqueous graphene interfaces. *J. Mater. Chem. B*, 3(16):3211–3221, 2015.

- [144] M. Hyotanishi, Y. Isomura, H. Yamamoto, H. Kawasaki, and Y. Obora. Surfactant-free synthesis of palladium nanoclusters for their use in catalytic cross-coupling reactions. *Chemical Communications*, 47(20):5750–5752, 2011.
- [145] S. Iijima. Helical microtubules of graphitic carbon. *Nature*, 354:56, 1991.
- [146] T. Ikuno, T. Sainsbury, D. Okawa, J. Fréchet, and A. Zettl. Amine-Functionalized Boron Nitride Nanotubes. *Solid State Communications*, 142(11):643–646, 2007.
- [147] Y. Inada and H. Orita. Efficiency of numerical basis sets for predicting the binding energies of hydrogen bonded complexes: Evidence of small basis set superposition error compared to Gaussian basis sets. *Journal of Computational Chemistry*, 29(2):225–232, 2007.
- [148] P. D. Jadzinsky, G. Calero, C. J. Ackerson, D. A. Bushnell, and R. D. Kornberg. Structure of a thiol monolayer-protected gold nanoparticle at 1.1 Å resolution. *Science*, 318(5849):430–433, 2007.
- [149] A. Jain, S. Ranjan, N. Dasgupta, and C. Ramalingam. Nanomaterials in food and agriculture: An overview on their safety concerns and regulatory issues. *Critical Reviews in Food Science and Nutrition*, 58(2):297–317, 2018.
- [150] N. K. Jaiswal, N. Tyagi, A. Kumar, and P. Srivastava. Inducing half-metallicity with enhanced stability in zigzag graphene nanoribbons via fluorine passivation. *Applied Surface Science*, 396:471–479, 2017.

- [151] S.-H. Jhi, D. J. Roundy, S. G. Louie, and M. L. Cohen. Formation and electronic properties of double-walled boron nitride nanotubes. *Solid State Communications*, 134(6):397–402, 2005.
- [152] X. Jia, J. Li, L. Han, J. Ren, X. Yang, and E. Wang. DNA-Hosted Copper Nanoclusters for Fluorescent Identification of Single Nucleotide Polymorphisms. *ACS Nano*, 6(4):3311–3317, 2012.
- [153] C. A. Jiménez-Hoyos, B. G. Janesko, and G. E. Scuseria. Evaluation of range-separated hybrid density functionals for the prediction of vibrational frequencies, infrared intensities, and Raman activities. *Physical chemistry chemical physics : PCCP*, 10(44):6621–6629, 2008.
- [154] C. Jin, F. Lin, K. Suenaga, and S. Iijima. Fabrication of a freestanding boron nitride single layer and Its defect assignments. *Physical Review Letters*, 102(19):3–6, 2009.
- [155] R. Jin. Quantum sized, thiolate-protected gold nanoclusters. *Nanoscale*, 2(3):343–362, 2010.
- [156] R. Jin. Atomically precise metal nanoclusters: stable sizes and optical properties. *Nanoscale*, 7(5):1549–65, 2015.
- [157] R. L. Johnston. Evolving better nanoparticles: Genetic algorithms for optimising cluster geometries. *Dalton Transactions*, (22):4193, 2003.

- [158] C. F. Jones and D. W. Grainger. In vitro assessments of nanomaterial toxicity. *Advanced Drug Delivery Reviews*, 61(6):438–456, 2009.
- [159] R. O. Jones. Density functional theory: Its origins, rise to prominence, and future. *Rev. Mod. Phys.*, 87:897–923, 2015.
- [160] A. K. Kandalam, R. Pandey, M. A. Blanco, A. Costales, J. M. Recio, and J. M. Newsam. First Principles Study of Polyatomic Clusters of AlN, GaN, and InN. 1. Structure, Stability, Vibrations, and Ionization. *The Journal of Physical Chemistry B*, 104(18):4361–4367, 2000.
- [161] Y. Kang, Y. C. Liu, Q. Wang, J. W. Shen, T. Wu, and W. J. Guan. On the spontaneous encapsulation of proteins in carbon nanotubes. *Biomaterials*, 30(14):2807–2815, 2009.
- [162] M. Karplus and R. N. Porter. *Atom and Molecules*. Benjamin-Cummings Pub Co, 1970.
- [163] D. R. Kauffman, D. Alfonso, C. Matranga, H. Qian, and R. Jin. A Quantum Alloy: The Ligand-Protected Au₂₅-xAg_x(SR)₁₈ Cluster. *The Journal of Physical Chemistry C*, 117(15):7914–7923, 2013.
- [164] J. Kaur, P. Singla, and N. Goel. Applied Surface Science Adsorption of oxazole and isoxazole on BNNT surface : A DFT study. *Applied Surface Science*, 328:632–640, 2015.

- [165] A. Kayal and A. Chandra. Orientational order and dynamics of interfacial water near a hexagonal boron-nitride sheet: An ab initio molecular dynamics study. *Journal of Chemical Physics*, 147(16), 2017.
- [166] G. P. Kerker. Non-singular atomic pseudopotentials for solid state applications. *Journal of Physics C: Solid State Physics*, 13(9):L189, 1980.
- [167] F. A. Khan. *Biotechnology Fundamentals*. CRC Press, 2012.
- [168] J. Kim, S.-J. Park, and D.-H. Min. Emerging Approaches for Graphene Oxide Biosensor. *Analytical Chemistry*, 89(1):232–248, 2017.
- [169] A. Kinaci, B. Narayanan, F. G. Sen, M. J. Davis, S. K. Gray, S. K. R. S. Sankaranarayanan, and M. K. Y. Chan. Unraveling the Planar-Globular Transition in Gold Nanoclusters through Evolutionary Search. *Scientific Reports*, 6:1–15, 2016.
- [170] L. Kleinman and D. M. Bylander. Efficacious Form for Model Pseudopotentials. *Phys. Rev. Lett.*, 48(20):1425–1428, 1982.
- [171] J. Klimeš and A. Michaelides. Perspective: Advances and challenges in treating van der Waals dispersion forces in density functional theory. *The Journal of Chemical Physics*, 137(12):120901, 2012.
- [172] W. D. Knight, K. Clemenger, W. A. de Heer, W. A. Saunders, M. Y. Chou, and

- M. L. Cohen. Electronic Shell Structure and Abundances of Sodium Clusters. *Physical Review Letters*, 52(24):2141–2143, 1984.
- [173] H. P. Koch, R. Laskowski, P. Blaha, and K. Schwarz. Adsorption of gold atoms on the h -BN / Rh (111) nanomesh. *Physical Review B*, 245410:1–7, 2011.
- [174] H. P. Koch, R. Laskowski, P. Blaha, and K. Schwarz. Adsorption of small gold clusters on the h -BN / Rh (111) nanomesh. *Physical Review B*, 155404(October):1–7, 2012.
- [175] M. Kociak, D. Taverna, A. Loiseau, and C. Colliex. Electron Energy Loss Spectroscopy Measurement of the Optical Gaps on Individual Boron Nitride Single-Walled and Multiwalled Nanotubes. *Physical Review Letters*, 127601:127601, 2005.
- [176] W. Kohn and L.-J. Sham. Self-Consistent Equations Including Exchange and Correlation Effects. *Physical Review*, 385(1951):1133–1138, 1965.
- [177] J. Kotakoski, C. H. Jin, O. Lehtinen, K. Suenaga, and A. V. Krasheninnikov. Electron knock-on damage in hexagonal boron nitride monolayers. *Physical Review B*, 82:113404, 2010.
- [178] L. P. Kozlowski. Proteome-pI: proteome isoelectric point database. *Nucleic Acids Research*, 45(D1):D1112–D1116, 2017.

- [179] G. Kresse. Efficient iterative schemes for ab initio total-energy calculations using a plane-wave basis set. *Physical Review B*, 54(16):11169–11186, 1996.
- [180] G. Kresse. From ultrasoft pseudopotentials to the projector augmented-wave method. *Physical Review B*, 59(3):1758–1775, 1999.
- [181] G. Kresse and J. Furthmüller. Efficiency of ab-initio total energy calculations for metals and semiconductors using a plane-wave basis set. *Computational Materials Science*, 6(1):15–50, 1996.
- [182] G. Kresse and J. Hafner. Ab initio molecular-dynamics simulation of the liquid-metal–amorphous-semiconductor transition in germanium. *Physical Review B*, 49(20):14251–14269, 1994.
- [183] J. Kresse, G., Hafner. Ab initio molecular dynamics for liquid metals. *Physical Review B*, 47(1), 1993.
- [184] H. W. Kroto, J. R. Heath, S. C. O’Brien, R. F. Curl, and R. E. Smalley. C60: Buckminsterfullerene. *Nature*, 318:162, 1985.
- [185] A. V. Krukau, O. A. Vydrov, A. F. Izmaylov, and G. E. Scuseria. Influence of the exchange screening parameter on the performance of screened hybrid functionals. *The Journal of Chemical Physics*, 125:224106, 2006.
- [186] R. Kurapati, K. Kostarelos, M. Prato, and A. Bianco. Biomedical Uses for 2D

- Materials Beyond Graphene: Current Advances and Challenges Ahead. *Advanced Materials*, pages 6052–6074, 2016.
- [187] C. Lee, W. Yang, and R. G. Parr. Development of the Colle-Salvetti correlation-energy formula into a functional of the electron density. *Physical Review B*, 37(2):785–789, 1988.
- [188] C. H. Lee, S. Qin, M. a. Savaikar, J. Wang, B. Hao, D. Zhang, D. Banyai, J. a. Jaszczak, K. W. Clark, J. C. Idrobo, A. P. Li, and Y. K. Yap. Room-Temperature Tunneling Behavior of Boron Nitride Nanotubes Functionalized with Gold Quantum Dots. *Advanced Materials*, 25(33):4544–4548, 2013.
- [189] C. H. Lee, D. Zhang, and Y. K. Yap. Functionalization, dispersion, and cutting of boron nitride nanotubes in water. *Journal of Physical Chemistry C*, 116(2):1798–1804, 2012.
- [190] J. Lee, S. Mahendra, and P. J. J. Alvarez. Nanomaterials in the Construction Industry: A Review of Their Applications and Environmental Health and Safety Considerations. *ACS Nano*, 4(7):3580–3590, 2010.
- [191] J. H. Lee. A Study on a Boron-Nitride Nanotube as a Gigahertz Oscillator. *J. Korean Phys. Soc.*, 49(1):172–176, 2006.
- [192] J. H. Lee, Y. K. Choi, H. J. Kim, R. H. Scheicher, and J. H. Cho. Physisorption of DNA nucleobases on h-BN and graphene: VdW-corrected DFT calculations. *Journal of Physical Chemistry C*, 117(26):13435–13441, 2013.

- [193] A. L. Lehninger and D. L. Nelson. *Lehninger Principles of Biochemistry*. Worth Publishers, New York, 2000.
- [194] O. Lehtinen, E. Dumur, J. Kotakoski, A. V. Krasheninnikov, K. Nordlund, and J. Keinonen. Production of defects in hexagonal boron nitride monolayer under ion irradiation. *Nuclear Inst. and Methods in Physics Research, B*, 269(11):1327–1331, 2011.
- [195] M. L. Leininger, W. D. Allen, H. F. S. III, and C. D. Sherrill. Is Møller–Plesset perturbation theory a convergent ab initio method? *The Journal of Chemical Physics*, 112(21):9213–9222, 2000.
- [196] M. B. Lerner, J. D’Souza, T. Pazina, J. Dailey, B. R. Goldsmith, M. K. Robinson, and A. T. C. Johnson. Hybrids of a Genetically Engineered Antibody and a Carbon Nanotube Transistor for Detection of Prostate Cancer Biomarkers. *ACS Nano*, 6(6):5143–5149, 2012.
- [197] E. G. Lewars. *Computational Chemistry: Introduction to the Theory and Applications of Molecular and Quantum Mechanics*. Springer Netherlands, 2010.
- [198] N. Lewinski, V. Colvin, and R. Drezek. Cytotoxicity of nanoparticles. *Small*, 4(1):26–49, 2008.
- [199] H.-W. Li, Y. Yue, T.-Y. Liu, D. Li, and Y. Wu. Fluorescence-Enhanced Sensing Mechanism of BSA-Protected Small Gold-Nanoclusters to Silver(I) Ions in

- Aqueous Solutions. *The Journal of Physical Chemistry C*, 117(31):16159–16165, 2013.
- [200] J. Li, X. Fan, Y. Wei, and G. Chen. Penta -B x N y sheet : a density functional theory study of two- dimensional material. *Scientific Reports*, 6(April):1–9, 2016.
- [201] J. Li and J.-J. Zhu. Quantum dots for fluorescent biosensing and bio-imaging applications. *Analyst*, 138:2506–2515, 2013.
- [202] L. Li, L. H. Li, S. Ramakrishnan, X. J. Dai, K. Nicholas, Y. Chen, Z. Chen, and X. Liu. Controlling Wettability of Boron Nitride Nanotube Films and Improved Cell Proliferation. *Journal of Physical Chemistry C*, 116:18334–18339, 2012.
- [203] L. Li, Y. Yu, G. J. Ye, Q. Ge, X. Ou, H. Wu, D. Feng, X. H. Chen, and Y. Zhang. Black phosphorus field-effect transistors. *Nature Nanotechnology*, 9:372, 2014.
- [204] Y. Li, L. Xu, and Y. Li. Chem Soc Rev Graphdiyne and graphyne : from theoretical. *Chem. Soc. Rev.*, 43:2572–2586, 2014.
- [205] Z. F. Li and E. Ruckenstein. Water-Soluble Poly(acrylic acid) Grafted Luminescent Silicon Nanoparticles and Their Use as Fluorescent Biological Staining Labels. *Nano Letters*, 4(8):1463–1467, 2004.
- [206] E. H. Lieb. Thomas-fermi and related theories of atoms and molecules. *Rev. Mod. Phys.*, 53(4):603–641, 1981.

- [207] Y. Lin and J. W. Connell. Advances in 2D boron nitride nanostructures: nanosheets, nanoribbons, nanomeshes, and hybrids with graphene. *Nanoscale*, 4:6908, 2012.
- [208] F. Liu, C. Shen, Z. Su, X. Ding, S. Deng, J. Chen, N. Xu, and H. Gao. Metal-like single crystalline boron nanotubes: synthesis and in situ study on electric transport and field emission properties. *Journal of Materials Chemistry*, 20(11):2197, 2010.
- [209] T. C. Long, N. Saleh, R. D. Tilton, G. V. Lowry, and B. Veronesi. Titanium Dioxide (P25) Produces Reactive Oxygen Species in Immortalized Brain Microglia (BV2): Implications for Nanoparticle Neurotoxicity. *Environmental Science & Technology*, 40(14):4346–4352, 2006.
- [210] R. Longtin. A Forgotten Debate: Is Selenocysteine the 21st Amino Acid? *JNCI: Journal of the National Cancer Institute*, 96(7):504–505, 2004.
- [211] R. Lv and M. Terrones. Towards new graphene materials: Doped graphene sheets and nanoribbons. *Materials Letters*, 78:209–218, 2012.
- [212] N. A. Lvova and O. Y. Ananina. Theoretical study of the adsorption properties of porous boron nitride nanosheets. *Computational Materials Science*, 115:11–17, 2016.
- [213] K. A. Majorek, P. J. Porebski, A. Dayal, M. D. Zimmerman, K. Jablonska, A. J.

- Stewart, M. Chruszcz, and W. Minor. Structural and immunologic characterization of bovine, horse, and rabbit serum albumins. *Molecular Immunology*, 52(3):174–182, 2012.
- [214] D. Malko, C. Neiss, and G. Andreas. Two-dimensional materials with Dirac cones : Graphynes containing heteroatoms. *Physical Review B*, 86:045443, 2012.
- [215] S. S. K. Mallineni, J. Shannahan, A. J. Raghavendra, A. M. Rao, J. M. Brown, and R. Podila. Biomolecular Interactions and Biological Responses of Emerging Two-Dimensional Materials and Aromatic Amino Acid Complexes. *ACS Applied Materials & Interfaces*, 8(26):16604–16611, 2016.
- [216] L. A. Mancera and D. M. Benoit. clusters using the VSCF method †. *Physical Chemistry Chemical Physics*, 18:529–549, 2015.
- [217] A. J. Mannix, X.-F. Zhou, B. Kiraly, J. D. Wood, D. Alducin, B. D. Myers, X. Liu, B. L. Fisher, U. Santiago, J. R. Guest, M. J. Yacaman, A. Ponce, A. R. Oganov, M. C. Hersam, and N. P. Guisinger. Synthesis of borophenes: Anisotropic, two-dimensional boron polymorphs. *Science*, 350:1513–1516, 2015.
- [218] J. M. L. Martin, P. R. Taylor, J. P. Francois, and R. Gijbels. Ab initio study of the spectroscopy, kinteics, and thermochemistry of the BN₂ molecule. *Chemical Physics Letters*, 222, 1994.
- [219] R. Martin. *Electronic Structure*. Cambridge University Press, United Kingdom, 2004.

- [220] O. Matarín and A. Rimola. Influence of Defects in Boron Nitride Nanotubes in B3LYP-D2 * Periodic Simulations. *Crystals*, 6:63, 2016.
- [221] A. Mathew and T. Pradeep. Noble Metal Clusters: Applications in Energy, Environment, and Biology. *Particle & Particle Systems Characterization*, pages 1–37, 2014.
- [222] S. L. Mayo, B. D. Olafson, and W. A. Goddard. DREIDING: A generic force field for molecular simulations. *Journal of Physical Chemistry*, 94(26):8897–8909, 1990.
- [223] S. E. McNeil. In Review: Nanomaterial safety. *Bulletin of the Atomic Scientists*, 65(1):56–61, 2009.
- [224] J. C. Meyer, A. Chuvilin, G. Algara-siller, J. Biskupek, and U. Kaiser. Selective Sputtering and Atomic Resolution Imaging of Atomically Thin Boron Nitride Membranes 2009. *Nano Letters*, 9:2683–2689, 2009.
- [225] K. H. Michel and B. Verberck. Theory of elastic and piezoelectric effects in two-dimensional hexagonal boron nitride. *Physical Review B*, 80:224301, 2009.
- [226] S. Miertus and J. Tomasi. Approximate evaluations of the electrostatic free energy and internal energy changes in solution processes. *Journal of Chemical Physics*, 65(2):239–245, 1982.

- [227] P. Miro, M. Audiffred, and T. Heine. An atlas of two-dimensional materials. *Chem. Soc. Rev.*, 43:6537–6554, 2014.
- [228] J. S. Mohanty, P. L. Xavier, K. Chaudhari, M. S. Bootharaju, N. Goswami, S. K. Pal, and T. Pradeep. Luminescent, bimetallic AuAg alloy quantum clusters in protein templates. *Nanoscale*, 4:4255–62, 2012.
- [229] M. Monthieux and V. L. Kuznetsov. Who should be given the credit for the discovery of carbon nanotubes? *Carbon*, 44(9):1621–1623, 2006.
- [230] F. Mouhat and F.-X. Coudert. Necessary and sufficient elastic stability conditions in various crystal systems. *Physical Review B*, 90:224104, 2014.
- [231] S. Mukhopadhyay, S. Gowtham, R. H. Scheicher, R. Pandey, and S. P. Karna. Theoretical study of physisorption of nucleobases on boron nitride nanotubes: a new class of hybrid nano-biomaterials. *Nanotechnology*, 21:165703, 2010.
- [232] S. Mukhopadhyay, R. H. Scheicher, R. Pandey, and S. P. Karna. Sensitivity of Boron Nitride Nanotubes toward Biomolecules of Different Polarities. *The Journal of Physical Chemistry Letters*, 2:2442–2447, 2011.
- [233] R. J. Needs and C. J. Pickard. Perspective: Role of structure prediction in materials discovery and design. *APL Materials*, 4(5):53210, 2016.

- [234] Y. Negishi, T. Nakazaki, S. Malola, S. Takano, Y. Niihori, W. Kurashige, S. Yamazoe, T. Tsukuda, and H. Ha. A Critical Size for Emergence of Nonbulk Electronic and Geometric Structures in Dodecanethiolate-Protected Au Clusters. *Journal of the American Chemical Society*, 137:1206–1212, 2015.
- [235] A. Nel, T. Xia, H. Meng, X. Wang, S. Lin, Z. Ji, and H. Zhang. Nanomaterial toxicity testing in the 21st century: Use of a predictive toxicological approach and high-throughput screening. *Accounts of Chemical Research*, 46(3):607–621, 2013.
- [236] V. Nicolosi, M. Chhowalla, M. G. Kanatzidis, M. S. Strano, and J. N. Coleman. Liquid Exfoliation of Layered Materials. *Science*, 340(6139), 2013.
- [237] NobelPrize.org. The Nobel Prize in Physics 1918.
- [238] Nobelprize.org. The Nobel Prize in Physics 2010.
- [239] NobelPrize.org. The Noble Prize in Physics 1933.
- [240] Nobelprize.org. The Nobel Prize in Chemistry 1996, 2014.
- [241] Nobelprize.org. The Nobel Prize in Chemistry 1998, 2014.
- [242] S. Nosé. A molecular dynamics method for simulations in the canonical ensemble. *Molecular Physics*, 52(2):255–268, 1984.

- [243] K. S. Novoselov, A. K. Geim, S. V. Morozov, D. Jiang, Y. Zhang, S. V. Dubonos, I. V. Grigorieva, and A. A. Firsov. Electric Field Effect in Atomically Thin Carbon Films. *Science*, 306:666–669, 2004.
- [244] J. F. Nye. *Physical Properties of Crystals*. 1985.
- [245] A. Oberlin, M. Endo, and T. Koyama. Filamentous Growth of Carbon through Benzene Decomposition. *Journal of Crystal Growth*, 32:335–349, 1976.
- [246] Y. Ohno, K. Maehashi, and K. Matsumoto. Label-Free Biosensors Based on Aptamer-Modified Graphene Field-Effect Transistors. *Journal of the American Chemical Society*, 132(51):18012–18013, 2010.
- [247] S. Okada. Atomic configurations and energetics of vacancies in hexagonal boron nitride : First-principles total-energy calculations. *Physical Review B*, 80:161404(R), 2009.
- [248] V. O. Ozcelik and S. Ciraci. Size Dependence in the Stabilities and Electronic Properties of α - Graphyne and Its Boron Nitride Analogue. *Journal of Physical Chemistry C*, 117:2175–2182, 2013.
- [249] J. D. Pack and H. J. Monkhorst. Special points for Brillouin-zone integrations. *Physical Review B*, 16(4):1748–1749, 1976.
- [250] R. K. Pandey, K. Waters, S. Nigam, H. He, S. Pingale, A. C. Pandey, and R. Pandey. A theoretical study of structural and electronic properties

- of alkaline-earth fluoride clusters. *Computation and Theoretical Chemistry*, 1043:24–30, 2014.
- [251] D. Pantarotto, C. D. Partidos, R. Graff, J. Hoebeke, J. P. Briand, M. Prato, and a. Bianco. Synthesis, Structural Characterization, and Immunological Properties of Carbon Nanotubes Functionalized with Peptides. *Journal of the American Chemical Society*, 125(20):6160–6164, 2003.
- [252] J. F. Parker, C. a. Fields-Zinna, and R. W. Murray. The story of a monodisperse gold nanoparticle: Au₂₅L₁₈. *Accounts of chemical research*, 43(9):1289, 2010.
- [253] R. G. Parr and W. Yang. *Density-Functional Theory of Atoms and Molecules*. 1989.
- [254] G. Pastorin, W. Wu, S. Wieckowski, J.-P. Briand, K. Kostarelos, M. Prato, and A. Bianco. Double functionalisation of carbon nanotubes for multimodal drug delivery. *Chemical Communications*, 0(11):1182–1184, 2006.
- [255] M. C. Patterson, B. F. Habenicht, R. L. Kurtz, L. Liu, Y. Xu, and P. T. Sprunger. Formation and stability of dense arrays of Au nanoclusters on hexagonal boron nitride / Rh (111). *Physical Review B*, 205423:1–10, 2014.
- [256] M. C. Payne, M. P. Teter, D. C. Allan, T. A. Arias, and J. D. Joannopoulos. Iterative minimization techniques for ab initio total-energy calculations: Molecular dynamics and conjugate gradients. *Reviews of Modern Physics*, 64(4):1045–1097, 1992.

- [257] R. Peierls. Quelques propriétés typiques des corps solides. *Annales de l'institut Henri Poincaré*, 5(3):177–222, 1935.
- [258] Q. Peng, W. Ji, and S. De. Mechanical properties of the hexagonal boron nitride monolayer : Ab initio study. *Computational Materials Science*, 56:11–17, 2012.
- [259] J. P. Perdew, K. Burke, and M. Ernzerhof. Generalized Gradient Approximation Made Simple. *Physical Review Letters*, 77(18):3865–3868, 1996.
- [260] J. P. Perdew, K. Burke, M. Ernzerhof, and (Errata). Generalized Gradient Approximation Made Simple- ERRATA. *Physical Review Letters*, 77(18):3865–3868, 1996.
- [261] J. P. Perdew, J. A. Chevary, S. H. Vosko, K. A. Jackson, M. R. Pederson, D. J. Singh, and C. Fiolhais. Atoms, molecules, solids, and surfaces: Applications of the generalized gradient approximation for exchange and correlation. *Phys. Rev. B*, 46(11):6671–6687, 1992.
- [262] J. P. Perdew and M. Levy. Physical Content of the Exact Kohn-Sham Orbital Energies: Band Gaps and Derivative Discontinuities. *Phys. Rev. Lett.*, 51(20):1884–1887, 1983.
- [263] J. P. Perdew, A. Ruzsinszky, J. Tao, V. N. Staroverov, G. E. Scuseria, and G. I. Csonka. Prescription for the design and selection of density functional approximations: More constraint satisfaction with fewer fits. *Journal of Chemical Physics*, 123(6), 2005.

- [264] J. P. Perdew, V. N. Staroverov, J. Tao, and G. E. Scuseria. Density functional with full exact exchange, balanced nonlocality of correlation, and constraint satisfaction. *Phys. Rev. A*, 78(5):52513, 2008.
- [265] J. P. Perdew and A. Zunger. Self-interaction correction to density-functional approximations for many-electron systems. *Physical Review B*, 23(10):5048–5079, 1981.
- [266] M. I. Petrescu and M. Balint. Structure and properties modification in boron nitride. Part 1: Direct polymorphic transformations mechanisms. *U.P.B Sci. Bull.*, 69(1):35–42, 2007.
- [267] Z. A. Piazza, H.-S. Hu, W.-L. Li, Y.-F. Zhao, J. Li, and L.-S. Wang. Planar hexagonal B36 as a potential basis for extended single-atom layer boron sheets. *Nature Communications*, 5:1–6, 2014.
- [268] G. Pilania, J. E. Gubernatis, and T. Lookman. Structure classification and melting temperature prediction in octet AB solids via machine learning. *Phys. Rev. B*, 91(21):214302, 2015.
- [269] S. Ping, W. Davidson, A. Jain, G. Hautier, M. Kocher, S. Cholia, D. Gunter, V. L. Chevrier, K. A. Persson, and G. Ceder. Python Materials Genomics (pymatgen): A robust , open-source python library for materials analysis. *Computational Materials Science*, 68:314–319, 2013.

- [270] P. Piquini, R. J. Baierle, T. M. Schmidt, and A. Fazzio. Formation energy of native defects in BN nanotubes : an ab initio study. *Nanotechnology*, 16:827–831, 2005.
- [271] A. Plume. Graphene: ten years of the ‘gold rush’, 2014.
- [272] A. Politano and G. Chiarello. Probing the Young ’ s modulus and Poisson ’ s ratio in graphene / metal interfaces and graphite : A comparative. *Nano Research*, 8(6):1847–1856, 2015.
- [273] M. Prato, K. Kostarelos, and A. Bianco. Functionalized Carbon Nanotubes in Drug Design and Discovery. *Accounts of Chemical Research*, 41(1):60–68, 2008.
- [274] A. Quandt and I. Boustani. Boron Nanotubes. *ChemPhysChem*, 6(10):2001–2008, 2005.
- [275] L. V. Radushkevich and V. M. Lukyanovich. O strukture ugleroda, obrazujucesja pri termiceskom razlozenii okisi ugleroda na zeleznom kontakte. *Zhurnal Fizicheskoi Khimii*, 26:88–95, 1952.
- [276] T. Rangel, D. Caliste, L. Genovese, and M. Torrent. A wavelet-based Projector Augmented-Wave (PAW) method: Reaching frozen-core all-electron precision with a systematic, adaptive and localized wavelet basis set. *Computer Physics Communications*, 208:1–8, 2016.

- [277] D. Rappoport, N. R. M. Crawford, F. Furche, and K. Burke. Approximate Density Functionals: Which Should I Choose? *Encyclopedia of Inorganic Chemistry*, 2009.
- [278] V. A. Rassolov. 6-31G* basis set for third-row atoms. *Journal of Computational Chemistry*, 22(9):976–984, 2001.
- [279] P. C. Ray, H. Yu, and P. P. Fu. Toxicity and environmental risks of nanomaterials: Challenges and future needs. *Journal of Environmental Science and Health - Part C Environmental Carcinogenesis and Ecotoxicology Reviews*, 27(1):1–35, 2009.
- [280] H. Raza. Edge and passivation effects in armchair graphene nanoribbons. *Phys. Rev. B*, 84(16):165425, 2011.
- [281] M. Reibold, P. Paufler, A. A. Levin, W. Kochmann, N. Pätzke, and D. C. Meyer. Carbon nanotubes in an ancient Damascus sabre. *Nature*, 444:286, 2006.
- [282] G. Reiss and A. Hutten. *Handbook of Nanophysics: Nanoparticles and Quantum Dots*. CRC Press, 2010.
- [283] A. Rimola. Intrinsic Ladders of Affinity for Amino-Acid-Analogues on Boron Nitride Nanomaterials: A B3LYP-D2* Periodic Study. *The Journal of Physical Chemistry C*, 119(31):17707–17717, 2015.

- [284] A. Rimola and M. Sodupe. Physisorption vs. chemisorption of probe molecules on boron nitride nanomaterials: the effect of surface curvature. *Physical Chemistry Chemical Physics*, 15(31):13190, 2013.
- [285] A. Rimola and M. Sodupe. Gas-Phase and Microsolvated Glycine Interacting with Boron Nitride Nanotubes. A B3LYP-D2* Periodic Study. *Inorganics*, 2(2):334–350, 2014.
- [286] T. Roman, W. a. Diño, H. Nakanishi, and H. Kasai. Amino acid adsorption on single-walled carbon nanotubes. *The European Physical Journal D*, 38(1):117–120, 2006.
- [287] C. C. J. Roothaan. New Developments in Molecular Orbital Theory. *Reviews of Modern Physics*, 23(2), 1951.
- [288] D. Rossouw, G. A. Botton, E. Najafi, V. Lee, and A. P. Hitchcock. Metallic and Semiconducting Single-Walled Carbon Nanotubes: Differentiating Individual SWCNTs by Their Carbon 1s Spectra. *ACS Nano*, 6(12):10965–10972, 2012.
- [289] A. Rubio, J. L. Corkill, and M. L. Cohen. Theory of graphitic boron nitride nanotubes. *Physical Review B*, 49(7):5081–5084, 1994.
- [290] N. Saikia and R. C. Deka. Density functional study on noncovalent functionalization of pyrazinamide chemotherapeutic with graphene and its prototypes †. *New Journal of Chemistry*, 38:1116–1128, 2014.

- [291] N. Saikia, M. Seel, and R. Pandey. Stability and Electronic Properties of 2D Nanomaterials Conjugated with Pyrazinamide Chemotherapeutic : A First-Principles Cluster Study. *The Journal of Physical Chemistry C*, 120:20323–20332, 2016.
- [292] U. Saikia, N. Saikia, K. Waters, R. Pandey, and S. M. Bora. Electronic Properties of Acetaminophen Adsorbed on 2D Clusters: A First Principles Density Functional Study. *ChemistrySelect*, 2(13):3613–3621, 2017.
- [293] T. Sainsbury, T. Ikuno, D. Okawa, D. Pacile, J. M. J. Frechet, and A. Zettl. Self-Assembly of Gold Nanoparticles at the Surface of Amine- and Thiol-Functionalized Boron Nitride Nanotubes. *Journal of Physical Chemistry C*, 111:12992–12999, 2007.
- [294] T. Sainsbury, A. Satti, P. May, Z. Wang, I. McGovern, Y. K. Gun'ko, and J. Coleman. Oxygen radical functionalization of boron nitride nanosheets. *Journal of the American Chemical Society*, 134(45):18758–18771, 2012.
- [295] C. Samori, H. Ali-Boucetta, R. Sainz, C. Guo, F. M. Toma, C. Fabbro, T. da Ros, M. Prato, K. Kostarelos, and A. Bianco. Enhanced anticancer activity of multi-walled carbon nanotube-methotrexate conjugates using cleavable linkers. *Chemical Communications*, 46(9):1494–1496, 2010.
- [296] E. Sandoz-Rosado, T. D. Beaudet, J. W. Andzelm, and E. D. Wetzel. High

- strength films from oriented, hydrogen-bonded “graphamid” 2D polymer molecular ensembles. *Scientific Reports*, 8(1):3708, 2018.
- [297] S. Sato and M. T. Swihart. Propionic-Acid-Terminated Silicon Nanoparticles: Synthesis and Optical Characterization. *Chemistry of Materials*, 18(17):4083–4088, 2006.
- [298] G. Scalmani and M. J. Frisch. Continuous surface charge polarizable continuum models of solvation. I. General formalism. *Journal of Chemical Physics*, 132(2010), 2010.
- [299] G. Schmid. The relevance of shape and size of Au₅₅ clusters. *Chemical Society Reviews*, 37(9):1909–1930, 2008.
- [300] T. M. Schmidt, R. J. Baierle, P. Piquini, and A. Fazzio. Theoretical study of native defects in BN nanotubes. *Physical Review B*, 67:113407, 2003.
- [301] E. Schroedinger. An Undulatory Theory of the Mechanics of Atoms and Molecules. *Physical Review*, 28(6):1049–1070, 1926.
- [302] P. Schwerdtfeger. The Pseudopotential Approximation in Electronic Structure Theory. *ChemPhysChem*, 12(17):3143–3155, 2011.
- [303] M. Seel and R. Pandey. Proton and hydrogen transport through two-dimensional monolayers. *2D Materials*, 3(2):025004, 2016.

- [304] W. Setyawan and S. Curtarolo. High-throughput electronic band structure calculations: Challenges and tools. *Computational Materials Science*, 49(2):299–312, 2010.
- [305] Q. Shao and C. K. Hall. Binding Preferences of Amino Acids for Gold Nanoparticles: A Molecular Simulation Study. *Langmuir*, 32(31):7888–7896, 2016.
- [306] J. W. Sheldon. Use of the Statistical Field Approximation in Molecular Physics. *Physical Review*, 99(4):1291, 1955.
- [307] C. D. Sherrill. The Born-Oppenheimer Approximation, 2005.
- [308] T. Shin-Ichi, M. Jun, T. D. K., J. Takashi, and I. Yasushi. Fluorescent Platinum Nanoclusters: Synthesis, Purification, Characterization, and Application to Bioimaging. *Angewandte Chemie International Edition*, 50(2):431–435, 2010.
- [309] A. Singh, G. Sinsinbar, M. Choudhary, V. Kumar, and R. Pasricha. Sensors and Actuators B : Chemical Graphene oxide-chitosan nanocomposite based electrochemical DNA biosensor for detection of typhoid. *Sensors & Actuators: B. Chemical*, 185:675–684, 2013.
- [310] S. K. Singhal, V. Kumar, K. Stalin, A. Choudhary, S. Teotia, G. B. Reddy, R. B. Mathur, S. P. Singh, and R. Pasricha. Gold-Nanoparticle-Decorated Boron Nitride Nanosheets: Structure and Optical Properties. *Particle & Particle Systems Characterization*, 30:445–452, 2013.

- [311] P. Singla, M. Riyaz, S. Singhal, and N. Goel. Theoretical study of adsorption of amino acids on graphene and BN sheet in gas and aqueous phase including empirical DFT Dispersion correction. *Physical Chemistry Chemical Physics*, 18:5597–5604, 2016.
- [312] J. C. Slater. Atomic shielding constants. *Physical Review*, 36(1):57–64, 1930.
- [313] J. M. Slocik and R. R. Naik. Probing peptide–nanomaterial interactions. *Chemical Society Reviews*, 39(9):3454, 2010.
- [314] J. C. Snyder, M. Rupp, K. Hansen, K.-R. Müller, and K. Burke. Finding Density Functionals with Machine Learning. *Phys. Rev. Lett.*, 108(25):253002, 2012.
- [315] S. K. Sohaebuddin, P. T. Thevenot, D. Baker, J. W. Eaton, and L. Tang. Nanomaterial cytotoxicity is composition, size, and cell type dependent. *Particle and Fibre Toxicology*, 7, 2010.
- [316] P. J. Stephens, F. J. Devlin, C. F. Chabalowski, and M. J. Frisch. Ab initio calculation of vibrational absorption and circular dichroism spectra using density functional force fields. *Army Research Laboratory*, 1994.
- [317] Y.-P. Sun, B. Zhou, Y. Lin, W. Wang, K. A. S. Fernando, P. Pathak, M. J. Mezziani, B. A. Harruff, X. Wang, H. Wang, P. G. Luo, H. Yang, M. E. Kose, B. Chen, L. M. Veca, and S.-Y. Xie. Quantum-Sized Carbon Dots for Bright

- and Colorful Photoluminescence. *Journal of the American Chemical Society*, 128(24):7756–7757, 2006.
- [318] P. G. Szalay, T. Müller, G. Gidofalvi, H. Lischka, and R. Shepard. Multiconfiguration Self-Consistent Field and Multireference Configuration Interaction Methods and Applications. *Chemical Reviews*, 112(1):108–181, 2012.
- [319] C. Tang, J. Li, Y. Bando, C. Zhi, and D. Golberg. Improved TiO₂ Photocatalytic Reduction by the Intrinsic Electrostatic Potential of BN Nanotubes. *Chemistry - An Asian Journal*, 44:1220–1224, 2010.
- [320] J. Tao, J. P. Perdew, V. N. Staroverov, and G. E. Scuseria. Climbing the Density Functional Ladder: Nonempirical Meta-Generalized Gradient Approximation Designed for Molecules and Solids. *Phys. Rev. Lett.*, 91(14):146401, 2003.
- [321] E. Tasci, G. de la Flor, D. Orobengoa, C. Capillas, J. Perez-Mato, and M. Aroyo. An introduction to the tools hosted in the Bilbao Crystallographic Server. *EPJ Web of Conferences*, 22:9, 2012.
- [322] E. Teller. On the Stability of Molecules in the Thomas-Fermi Theory. *Reviews of Modern Physics*, 34(4):627, 1962.
- [323] A. C. Templeton, W. P. Wuelfing, and R. W. Murray. Monolayer-protected cluster molecules. *Accounts of Chemical Research*, 33(1):27–36, 2000.

- [324] R. Tenne, L. Margulis, M. Genut, and G. Hodes. Polyhedral and cylindrical structures of tungsten disulphide. *Nature*, 360:444, 1992.
- [325] R. Tenne and G. Seifert. Recent Progress in the Study of Inorganic Nanotubes and Fullerene-Like Structures. *Annual Review of Materials Research*, 39(1):387–413, 2009.
- [326] J. A. Thomas and A. J. H. McGaughey. Density, distribution, and orientation of water molecules inside and outside carbon nanotubes. *Journal of Chemical Physics*, 128(8), 2008.
- [327] L. H. Thomas. The calculation of atomic field. *Mathematical Proceedings of the Cambridge Philosophical Society*, 23(5):542–548, 1927.
- [328] R. D. Tilley and K. Yamamoto. The Microemulsion Synthesis of Hydrophobic and Hydrophilic Silicon Nanocrystals. *Advanced Materials*, 18(15):2053–2056, 2006.
- [329] J. N. Tiwari, K. Nath, S. Kumar, R. N. Tiwari, K. C. Kemp, N. H. Le, D. H. Youn, J. S. Lee, and K. S. Kim. Stable platinum nanoclusters on genomic DNA–graphene oxide with a high oxygen reduction reaction activity. *Nature Communications*, 4:2221, 2013.
- [330] G. Tocci, L. Joly, and A. Michaelides. Friction of water on graphene and hexagonal boron nitride from Ab initio methods: Very different slippage despite very similar interface structures. *Nano Letters*, 14(12):6872–6877, 2014.

- [331] A. Togo and I. Tanaka. Scripta Materialia First principles phonon calculations in materials science. *Scripta Materialia*, 108:1–5, 2015.
- [332] S. Tosoni, C. Tuma, J. Sauer, B. Civalleri, and P. Ugliengo. A comparison between plane wave and Gaussian-type orbital basis sets for hydrogen bonded systems: Formic acid as a test case. *The Journal of Chemical Physics*, 127(15):154102, 2007.
- [333] S. Vajda, M. J. Pellin, J. P. Greeley, C. L. Marshall, L. A. Curtiss, G. A. Ballentine, J. W. Elam, S. Catillon-Mucherie, P. C. Redfern, F. Mehmood, and P. Zapol. Subnanometre platinum clusters as highly active and selective catalysts for the oxidative dehydrogenation of propane. *Nature Materials*, 8:213, 2009.
- [334] M. Valiev, E. J. Bylaska, N. Govind, K. Kowalski, T. P. Straatsma, H. J. J. V. Dam, D. Wang, J. Nieplocha, E. Apra, T. L. Windus, and W. A. D. Jong. NWChem : A comprehensive and scalable open-source solution for large scale molecular simulations. *Computer Physics Communications*, 181(9):1477–1489, 2010.
- [335] M. W. van der Kamp and A. J. Mulholland. Combined Quantum Mechanics/Molecular Mechanics (QM/MM) Methods in Computational Enzymology. *Biochemistry*, 52(16):2708–2728, 2013.

- [336] S. van der Walt, S. C. Colbert, and G. Varoquaux. The NumPy Array: A Structure for Efficient Numerical Computation. *Computing in Science & Engineering*, 13(2):22–30, 2011.
- [337] D. Vanderbilt. Soft self-consistent pseudopotentials in a generalized eigenvalue formalism. *Phys. Rev. B*, 41(11):7892–7895, 1990.
- [338] P. Vogt, P. D. Padova, C. Quaresima, J. Avila, E. Frantzeskakis, G. L. Lay, M. C. Asensio, and A. Resta. Silicene : Compelling Experimental Evidence for Graphenelike Two-Dimensional Silicon. *Physical Review Letters*, 108(April):155501, 2012.
- [339] M. Volkmann, M. Meyns, R. Lesyuk, H. Lehmann, and C. Klinke. Attachment of Colloidal Nanoparticles to Boron Nitride Nanotubes. *Chemistry of Materials*, 29:726–734, 2017.
- [340] S. H. Vosko, L. Wilk, and M. Nusair. Accurate spin-dependent electron liquid correlation energies for local spin density calculations: a critical analysis. *Canadian Journal of Physics*, 58(8):1200–1211, 1980.
- [341] H. Vovusha, S. Sanyal, and B. Sanyal. Interaction of nucleobases and aromatic amino acids with graphene oxide and graphene flakes. *Journal of Physical Chemistry Letters*, 4(21):3710–3718, 2013.
- [342] M. Walter, J. Akola, O. Lopez-Acevedo, P. D. Jadzinsky, G. Calero, C. J. Ackerson, R. L. Whetten, H. Grönbeck, and H. Häkkinen. A unified view

- of ligand-protected gold clusters as superatom complexes. *Proceedings of the National Academy of Sciences of the United States of America*, 105(27):9157–62, 2008.
- [343] J. Wang, C. H. Lee, and Y. K. Yap. Recent advancements in boron nitride nanotubes. *Nanoscale*, 2:2028–2034, 2010.
- [344] L. W. Wang. Divide-and-conquer quantum mechanical material simulations with exascale supercomputers. *National Science Review*, 1(4):604–617, 2014.
- [345] Y. Wang, J. Lv, L. Zhu, and Y. Ma. CALYPSO : A method for crystal structure prediction. *Computer Physics Communications*, 183(10):2063–2070, 2012.
- [346] Z. Wang, H. He, W. Slough, R. Pandey, and S. P. Karna. Nature of Interaction between Semiconducting Nanostructures and Biomolecules: Chalcogenide QDs and BNNT with DNA Molecules. *The Journal of Physical Chemistry C*, 119(46):25965–25973, 2015.
- [347] J. H. Warner, A. Hoshino, K. Yamamoto, and R. D. Tilley. Water-Soluble Photoluminescent Silicon Quantum Dots. *Angewandte Chemie International Edition*, 44(29):4550–4554, 2005.
- [348] K. Watanabe, T. Taniguchi, and H. Kanda. Direct-bandgap properties and evidence for ultraviolet lasing of hexagonal boron nitride single crystal. *Nature Materials*, 3:404, 2004.

- [349] K. Waters, R. Pandey, and S. P. Karna. Amino Acid Analogue-Conjugated BN Nanomaterials in a Solvated Phase : First Principles Study of Topology-Dependent Interactions with a Monolayer and a (5,0) Nanotube. *ACS Omega*, 2:76–83, 2017.
- [350] Q. Wei and X. Peng. Superior mechanical flexibility of phosphorene and few-layer black phosphorus. *Applied Physics Letters*, 104(2014):251915, 2014.
- [351] W. Wei, Y. Lu, W. Chen, and S. Chen. One-Pot Synthesis, Photoluminescence, and Electrocatalytic Properties of Subnanometer-Sized Copper Clusters. *Journal of the American Chemical Society*, 133(7):2060–2063, 2011.
- [352] W. Wei, W. Sébastien, P. Giorgia, B. Monica, K. Cédric, B. Jean-Paul, G. Renato, P. Maurizio, and B. Alberto. Targeted Delivery of Amphotericin B to Cells by Using Functionalized Carbon Nanotubes. *Angewandte Chemie International Edition*, 44(39):6358–6362, 2005.
- [353] X. Wei, B. Fragneaud, C. A. Marianetti, and J. W. Kysar. Nonlinear elastic behavior of graphene : Ab initio calculations to continuum description. *Physical Review B*, 80:205407, 2009.
- [354] X. Wen, T. J. Cahill, and R. Hoffmann. Exploring Group 14 Structures: 1D to 2D to 3D. *Chemistry – A European Journal*, 16(22):6555–6566, 2010.
- [355] Q. Weng, X. Wang, X. Wang, Y. Bando, and D. Golberg. Functionalized

- hexagonal boron nitride nanomaterials : emerging properties and applications include the controlled synthesis. *Chemical Society Reviews*, 45:3989–4012, 2016.
- [356] Wikipedia. Atomic units, 2018.
- [357] Wikipedia. Pseudopotential, 2018.
- [358] D. E. Williams and S. R. Cox. Nonbonded potentials for azahydrocarbons: the importance of the Coulombic interaction. *Acta Crystallographica Section B*, 40(4):404–417, 1984.
- [359] L. Wirtz, A. Marini, and A. Rubio. Excitons in Boron Nitride Nanotubes : Dimensionality Effects. *Physical Review Letters*, 96:126104, 2006.
- [360] M. Woińska, S. Grabowsky, P. M. Dominiak, K. Woźniak, and D. Jayatilaka. Hydrogen atoms can be located accurately and precisely by x-ray crystallography. *Science Advances*, 2(5), 2016.
- [361] H. Wolinsky. Nanoregulation. *EMBO reports*, 7(9):858–861, 2006.
- [362] C. Y. Won and N. R. Aluru. Water permeation through a subnanometer boron nitride nanotube. *Journal of the American Chemical Society*, 129(10):2748–2749, 2007.
- [363] C. Y. Won and N. R. Aluru. Structure and dynamics of water confined in a boron nitride nanotube. *Journal of Physical Chemistry B*, 112(6):1812–1818, 2008.

- [364] S. S. Wong, E. Joselevich, a. T. Woolley, C. L. Cheung, and C. M. Lieber. Covalently functionalized nanotubes as nanometre-sized probes in chemistry and biology. *Nature*, 394(6688):52–55, 1998.
- [365] Y. Wu, L. K. Wagner, and N. R. Aluru. Hexagonal boron nitride and water interaction parameters. *Journal of Chemical Physics*, 144(16), 2016.
- [366] T. Xia, N. Li, and A. E. Nel. Potential Health Impact of Nanoparticles. *Annual Review of Public Health*, 30(1):137–150, 2009.
- [367] L. Xiao, B. Tollberg, X. Hu, and L. Wang. Structural study of gold clusters. *The Journal of Chemical Physics*, 114309, 2006.
- [368] L. Xiao and L. Wang. From planar to three-dimensional structural transition in gold clusters and the spin – orbit coupling effect. *Chemical Physics Letters*, 392:452–455, 2004.
- [369] H. J. Xie, Q. F. Lei, and W. J. Fang. Intermolecular interactions between gold clusters and selected amino acids cysteine and glycine: A DFT study. *Journal of Molecular Modeling*, 18(2):645–652, 2012.
- [370] J. Xie, Y. Zheng, and J. Y. Ying. Protein-directed synthesis of highly fluorescent gold nanoclusters. *J. Am. Chem. Soc.*, 131(3):888–9, 2009.
- [371] S.-y. Xie, W. Wang, K. A. S. Fernando, X. Wang, Y. Lin, and Y.-p. Sun.

- Solubilization of Boron Nitride Nanotubes. *Chemical Communications*, pages 3670–3672, 2005.
- [372] N. Yanamala, V. E. Kagan, and A. A. Shvedova. Molecular modeling in structural nano-toxicology: Interactions of nano-particles with nano-machinery of cells. *Advanced drug delivery reviews*, 65(15):2070–2077, 2013.
- [373] C. K. Yang. Exploring the interaction between the boron nitride nanotube and biological molecules. *Computer Physics Communications*, 182(1):39–42, 2011.
- [374] S. Yang, Y. Liu, Y. Wang, and A. Cao. Biosafety and Bioapplication of Nanomaterials by Designing Protein–Nanoparticle Interactions. *Small*, 9(9-10):1635–1653, 2013.
- [375] Y. K. Yap. *B-C-N Nanotubes and Related Structures*. Springer, 1st edition, 2010.
- [376] S. H. Yau, O. Varnavski, and T. Goodson. An Ultrafast Look at Au Nanoclusters. *Accounts of Chemical Research*, 46(7):1506–1516, 2013.
- [377] J. Yin, J. Li, Y. Hang, J. Yu, G. Tai, X. Li, and Z. Zhang. Boron Nitride Nanostructures : Fabrication , Functionalization and Applications. *Small*, (22):2942–2968, 2016.
- [378] M. Yoda, Y. Inoue, and M. Sakurai. Effect of Protein Environment on pKa

- Shifts in the Active Site of Photoactive Yellow Protein. *The Journal of Physical Chemistry B*, 107(51):14569–14575, 2003.
- [379] L. Yuan, Z. Li, J. Yang, and J. G. Hou. Diamondization of chemically functionalized graphene and graphene-BN bilayers. *Phys. Chem. Chem. Phys.*, 14(22):8179–8184, 2012.
- [380] V. A. Zamolo, G. Valenti, E. Venturelli, O. Chaloin, M. Marcaccio, S. Boscolo, V. Castagnola, S. Sosa, F. Berti, G. Fontanive, M. Poli, A. Tubaro, A. Bianco, F. Paolucci, and M. Prato. Highly Sensitive Electrochemiluminescent Nanobiosensor for the Detection of Palytoxin. *ACS Nano*, 6(9):7989–7997, 2012.
- [381] G. Zanti and D. Peeters. Electronic structure analysis of small gold clusters Au_m (m ≤ 16) by density functional theory. *Theoretical Chemistry Accounts*, 132, 2013.
- [382] M. C. Zerner. Perspective on "New developments in molecular orbital theory". *Theoretical Chemistry Accounts*, 103(3-4):217–218, 2000.
- [383] Q. Zhang, J. Q. Huang, W. Z. Qian, Y. Y. Zhang, and F. Wei. The road for nanomaterials industry: A review of carbon nanotube production, post-treatment, and bulk applications for composites and energy storage. *Small*, 9(8):1237–1265, 2013.

- [384] S. Zhang, J. Zhou, Q. Wang, X. Chen, Y. Kawazoe, and P. Jena. Penta-graphene : A new carbon allotrope. *Proceedings of the National Academy of Sciences of the United States of America*, 112(8):2372–2377, 2015.
- [385] Z. Zhang, W. Guo, and Y. Dai. Stability and electronic properties of small boron nitride nanotubes. *Journal of Applied Physics*, 105(8):0–8, 2009.
- [386] J. Zhao, Y. Ding, J. Zhao, and Y. Ding. Theoretical investigation of the divacancies in boron nitride nanotubes : Properties and surface reactivity toward various adsorbates Theoretical investigation of the divacancies in boron nitride nanotubes : Properties and surface reactivity toward variou. *The Journal of Chemical Physics*, 131:014706, 2009.
- [387] Y. Zhao and D. G. Truhlar. Density Functional for Spectroscopy: No Long-Range Self-Interaction Error, Good Performance for Rydberg and Charge-Transfer States, and Better Performance on Average than B3LYP for Ground States. *The Journal of Physical Chemistry A*, 110(49):13126–13130, 2006.
- [388] Y. Zhao and D. G. Truhlar. The M06 suite of density functionals for main group thermochemistry, thermochemical kinetics, noncovalent interactions, excited states, and transition elements: two new functionals and systematic testing of four M06-class functionals and 12 other function. *Theoretical Chemistry Accounts*, 120(1):215–241, 2008.

- [389] C. Zhi, Y. Bando, C. Tang, and D. Golberg. Immobilization of proteins on boron nitride nanotubes. *Journal of the American Chemical Society*, 127(49):17144–17145, 2005.
- [390] C. Zhi, Y. Bando, C. Tang, and D. Golberg. SnO₂ Nanoparticle-Functionalized Boron Nitride Nanotubes Chunyi. *Journal Of Physical Chemistry B*, 110:8548–8550, 2006.
- [391] C. Y. Zhi, Y. Bando, C. C. Tang, Q. Huang, and D. Golberg. Boron Nitride Nanotubes: Functionalization and Composites. *Journal of Materials Chemistry A*, 18:3900–3908, 2008.
- [392] X. Zhong, S. Mukhopadhyay, S. Gowtham, R. Pandey, and S. P. Karna. Applicability of carbon and boron nitride nanotubes as biosensors: Effect of biomolecular adsorption on the transport properties of carbon and boron nitride nanotubes. *Applied Physics Letters*, 102, 2013.
- [393] A. Zobelli, C. P. Ewels, A. Gloter, G. Seifert, O. Stephan, S. Csillag, and C. Colliex. Defective Structure of BN Nanotubes : From Single Vacancies to Dislocation. *Nano Letters*, 6(9):1955–1960, 2006.
- [394] A. Zobelli, A. Gloter, C. P. Ewels, and C. Colliex. Shaping single walled nanotubes with an electron beam. *Physical Review B*, 77:045410, 2008.

Appendix A

Bra-ket Notation

In 1939, Paul Dirac introduced the bra-ket notation (Dirac notation) in an attempt to simplify and aid in the development of quantum mechanics.[72] The "bra" is used to represent a column vector and the "ket" is used to represent the Hermitian conjugate (row vector).

$$\langle \Psi | = \begin{bmatrix} \Psi_1 \\ \Psi_2 \\ \vdots \\ \Psi_n \end{bmatrix} \quad | \Psi \rangle = \begin{bmatrix} \Psi_1 & \Psi_2 & \dots & \Psi_n \end{bmatrix} \quad (\text{A.1})$$

In this notation a inner or scalar product is represented as follows

$$\langle a|\alpha\rangle \tag{A.2}$$

instead of using the previous notation, where the form would look like this.

$$\psi_\alpha\alpha\Psi \tag{A.3}$$

Expectations values of observables also saw a reduction in notation.

$$\psi(q')|\alpha|\Psi(q'') = \langle q'|\alpha|q''\rangle \tag{A.4}$$

When equation 2.57 is expanded into its full form the effort to simplify the notation becomes apparent.

$$E[\Psi] = \frac{\langle\Psi|\hat{H}|\Psi\rangle}{\langle\Psi|\Psi\rangle} = \frac{\int\Psi^*\hat{H}\Psi d\mathbf{x}}{\int\Psi^*\Psi d\mathbf{x}} \tag{A.5}$$

where \mathbf{x} spans some Hilbert space.

Appendix B

Units

B.1 Unit Conversions

Table B.1

Common conversions for units of energy in chemistry and physics. The values were obtained from the Atoms and Molecules by Karplus and Porter [162]

	1 hartree	1 eV	1 kcal/mol	1 kj/mol	1 cm ⁻¹
1 hartree	1	27.211	627.50	2625.5	219470
1 eV	$3.6750 * 10^{-2}$	1	23.061	96.487	8065.7
1 kcal/mol	$1.5936 * 10^{-3}$	$4.3363 * 10^{-2}$	1	4.1840	349.76
1 kj/mol	$3.8088 * 10^{-4}$	$1.0364 * 10^{-2}$	$2.3900 * 10^{-1}$	1	83.593
1 cm ⁻¹	$4.5563 * 10^{-6}$	$1.2398 * 10^{-4}$	$2.8591 * 10^{-3}$	$1.1963 * 10^{-2}$	1

B.2 Atomic Units

Through the body of work atomic units are used for the equations. This allows for terms to cancel and reduce the complexity and bloat in the equations.

$$\hat{H}\Psi(\mathbf{r}) = E\Psi(\mathbf{r}) \quad (\text{B.1})$$

The Hamiltonian can then be split up into three separate operators

$$\hat{H} = \hat{T} + \hat{V}_{Ne} + \hat{V}_{ee} \quad (\text{B.2})$$

$T[\rho(\mathbf{r})]$ is the kinetic energy operator, $V_{Ne}[\rho(\mathbf{r})]$ is the attractive potential operator between the electrons and nuclei and $V_{ee}[\rho(\mathbf{r})]$ is the repulsive potential operator between electrons. They can be expanded into more familiar terms

$$\left[\frac{-\hbar^2}{2m} \nabla^2 + \frac{Ze}{4\pi\epsilon_0\mathbf{R}} + \frac{e^2}{4\pi\epsilon_0\mathbf{r}'} \right] \Psi(\mathbf{r}) = E\Psi(\mathbf{r}) \quad (\text{B.3})$$

Where \mathbf{R} is the distance between the electron and nucleus and \mathbf{r}' is the distance

between electrons. Here is where Table B.2 can be incorporated to simplify the pre-factors of each term. The following terms, m_e , e , \hbar , and $1/4\pi\epsilon_0$, all become one.

Table B.2

Description of the four fundamental constants of Atomic Units (set to unity) and their SI equivalent. Many sources are available, but this table was adapted from Wikipedia.[356] with the units significant figures reduced to the third decimal place. all other Atomic units can be derived from the stated changes in value.

Name	Symbol	SI Value
Electron Rest Mass	m_e	$9.109 * 10^{-31} kg$
Elementary Charge	e	$1.602 * 10^{-19} C$
Reduced Planck's Constant	$\hbar = h/2\pi$	$1.055 * 10^{-34} J * s$
Coulomb Force Constant	$k_e = 1/4\pi\epsilon_0$	$8.988 * 10^9 kg * m^3/s^2 C^2$

With atomic units, the equations now takes the following form

$$\left[\sum_{i=1}^N -\frac{1}{2} \nabla_i^2 + \sum_{i=1}^N \frac{1}{\mathbf{R}_{i\alpha}} + \sum_{i<j}^N \frac{1}{\mathbf{r}_{ij}} \right] \Psi(\mathbf{r}) = E\Psi(\mathbf{r}) \quad (\text{B.4})$$

$\mathbf{R}_{i\alpha}$ is the distance between the i th electron and the nucleus α , \mathbf{r}_{ij} is the distance between the i th and j th electron.

$$\hat{H} = \sum_{i=1}^N \left(-\frac{1}{2} \nabla_i^2 \right) + \sum_{i=1}^N v(\mathbf{r}_i) + \sum_{i<j}^N \frac{1}{r_{ij}} \quad (\text{B.5})$$

Appendix C

List of Selected Publications

1. Metal to Non-metal Conversion of Two-Dimensional Gold Clusters on Boron Nitride Nanotubes
Stability of 3D and 2D Au Clusters on Boron Nitride
S. Bhandari, B. Hao, K. Waters, C. H. Lee, J. C. Idrobo, R. Pandey, D. Zhang, Y. K. Yap
In Preparation
2. Multiscale Modeling of PEEK using Reactive Molecular Dynamics Modeling and Micromechanics
W. A. Pisani, M. S. Radue, S. Chinkanjanarot, B. A. Bednarczyk, E. J. Pineda, K. Waters, R. Pandey, J. A. King, G. M. Odegard
Polymer

Submitted

3. Absorption and Fluorescence Properties of Eight C4 Substituted 7-Aminocoumarins
S. Singh, V. Begoyan, M. Tanasova, K. Waters, M. Seel, R. Pandey
Journal of Physical Organic Chemistry 2018;e3852

4. Dynamics of Self-Assembled Cytosine Nucleobases on Graphene
N. Saikia, F. Johnson, K. Waters, R. Pandey
Nanotechnology, vol. 29, pp. 195601, 2018

5. Stability, elastic and electronic properties of a novel BN₂ sheet with extended hexagons with N-N bonds
K. Waters, R. Pandey
Journal of Physics: Condensed Matter, vol. 30, pp. 135002, 2018

6. Hierarchical Self-Assembly of Noncanonical Guanine Nucleobases on Graphene
N. Saikia, K. Waters, S. P. Karna, R. Pandey
ACS Omega, vol. 2, pp. 3457, 2017

7. Amino-Acid-Conjugated Gold Clusters: Interaction of Alanine and Tryptophan with Au₈ and Au₂₀
M. H. Abdalmonem, K. Waters, N. Saikia, and R. Pandey
J. Phys. Chem. C, vol. 121 pp. 25585-25593, 2017

8. Electronic Properties of Acetaminophen Adsorbed on 2D Clusters: A First Principles Density Functional Study
U. Saikia, N. Saikia, K. Waters, R. Pandey, M. B. Sahariah
ChemistrySelect vol. 2 pp. 3613, 2017
9. Amino Acid Analogue-Conjugated BN Nanomaterials in a Solvated Phase :
First Principles Study of Topology-Dependent Interactions with a Monolayer
and a (5,0) Nanotube
K. Waters, R. Pandey, S. P. Karna
ACS Omega vol. 2, pp. 76-83, 2017
10. Thermoelectric Properties of SnSe Nanoribbons: A Theoretical Aspect
K. Tyagi, K. Waters, G. Wang, D. Haranath, B. Gahtori, R. Pandey
Materials Research Express, vol. 3 pp. 35013, 2016
11. A Theoretical Study of Structural and Electronic Properties of Alkaline-Earth
Fluoride Clusters
R. Pandey, K. Waters, S. Nigam, H. He, S. Pingle, A. Pandey, R. Pandey
Computation and Theoretical Chemistry, vol. 1043, pp. 24-30, 2014

Appendix D

Permission for Chapter 4

Manuscript



Dear Dr. Kevin,

Your permission requested is granted and there is no fee for this reuse. In your planned reuse, you must cite the ACS article as the source, add this direct link <<https://pubs.acs.org/doi/10.1021/acsomega.6b00321>>, and include a notice to readers that further permissions related to the material excerpted should be directed to the ACS.

Please do not hesitate to contact me if you need any further assistance.

Regards,
Jawwad Saeed
ACS Customer Services & Information
<https://help.acs.org>

Appendix E

Permission for BN2 Manuscript

Assignment of copyright and publication agreement

IOP Publishing Limited ("IOP") agrees to publish:

Manuscript Title: Stability, Elastic and Electronic Properties of a novel BN₂ sheet with extended hexagons with N-N bonds. (the "Article") written by

Names of all authors: Waters, Kevin; Pandey, Ravi ("the Named Authors") in the following journal Journal of Physics: Condensed Matter ("the Journal")

Name of copyright owner(s) (if not the Named Author(s) – see Important Information above):

("the Copyright Owner")

IOP Ref: JPCM-110627.R1

Part 1 - Publication on a Subscription basis

1.1 In consideration for acceptance and publication of the Article, the Named Authors of the Article and/or the Copyright Owner hereby assign, where necessary by present assignment of future copyright, to IOP with full title guarantee the entire copyright in all original material published as part of the Article (which expression includes but is not limited to the text, abstract, tables, figures and graphs, related corrigenda or "comments" and multimedia content but excludes any other item referred to as supplementary material and/or any video abstract) throughout the world for the full term of copyright (including any extensions or renewals thereof) for all media and formats, whether known or unknown. Such assignment shall be effective only if the Article (or any resubmission of the Article) is accepted for publication. For the avoidance of doubt, copyright does not subsist in any fundamental data underlying the Article and nothing in this agreement is intended to limit access to or use of such data.

1.2 If the Article, or any part of it, is protected by Crown copyright, in consideration for acceptance and publication of the Article, the relevant Named Authors and the relevant originating department or agency hereby grant IOP a non-exclusive royalty-free worldwide freely-transferrable licence for the full term of copyright (including any extensions or renewals thereof) for all media and formats, whether known or unknown, to do in relation to the Article all acts restricted by copyright worldwide including, but not limited to, the right of action under section 101A of the Copyright Designs and Patents Act 1988. Such licence shall be effective only if the Article is accepted for publication.

1.3 If all the Named Authors are employees of the US Government, they represent and warrant to IOP that the Article was prepared as part of their official duties. In such circumstances, or where the Article was created as part of a work for hire, none of the original content within the Article is subject to copyright protection as it is in the public domain.

1.4 In consideration for acceptance and publication of the Article, the Named Authors and/or the Copyright Owner hereby grant IOP a royalty-free non-exclusive worldwide freely transferrable licence for the full term of copyright (including any extensions or renewals thereof) to do in relation to any supplementary material not deemed to be part of the Article and/or any video abstract all acts restricted by copyright worldwide. This shall include, but not be limited to, making the material available under any licence that IOP deems appropriate for purposes including, but not limited to, the maximisation of visibility and the long term preservation of the content.

1.5 Each of the Named Authors consents to all publication and processing of their personal data by IOP, as that data is displayed on the Article, including, but not limited to, the names and email addresses of the Named Authors. Accordingly, the Named Authors shall not object on data protection grounds to the use of their personal data on the Article wherever IOP chooses to display it, whether itself or via a third party.

Representations and warranties

2.1 The Copyright Owner and/or the Submitting Author on behalf of the Named Authors (as appropriate) represent and warrant that:

2.1.1 the Article is the original work of the Named Authors;

2.1.2 the Article has not been published previously in any form, other than in accordance with our [Preprint pre-publication policy](#);

2.1.3 each of the Named Authors has made a material contribution to the conception and/or writing of the Article, has received the final version of the Article, has agreed to its submission on the terms contained herein and takes responsibility for it and submission has been approved as necessary by the authorities at the establishment where the research was carried out;

2.1.4 the Submitting Author completes and returns this agreement as authorised agent for and on behalf of all the Named Authors and the Copyright Owner (as applicable) and has the full power to enter into this agreement and to make the grants and assignments it contains;

2.1.5 the Article has not been and shall not be submitted to another publisher prior to withdrawal or rejection by IOP;

2.1.6 the Article does not infringe any third party rights, it contains nothing libellous or unlawful, all factual statements are to the best of the Named Authors' knowledge true or based on valid research conducted according to accepted norms and all required permissions have been obtained in writing;

2.1.7 the Article expressly acknowledges any third party funding and/or potential conflicts of interest; and

2.1.8 any supplementary material or video abstract is the original work of the Named Authors, or is the property of the Copyright Owner, or permission has been obtained from its owner(s) for its publication by IOP and permission has been obtained for the inclusion of any third party content.

2.2 The Named Authors and/or the Copyright Owner (as appropriate) indemnify and will keep indemnified IOP against all costs and expenses suffered or incurred by IOP as a result of and/or arising out of any breach of the representations and/or warranties in this section 2.

The Named Authors' rights

3.1 IOP grants the Named Authors the rights specified in paragraphs 3.2 and 3.3. All such rights must be exercised solely for non-commercial purposes. Where possible, any use should display citation information and IOP's copyright notice, and, for electronic use, best efforts must be made to include a link to the online abstract in the Journal.

Exercise of the rights in paragraph 3.2 may use the peer reviewed, edited, formatted and typeset version of the Article including any tagging, indexing and other enhancements published by IOP and/or its licensors ("Final Published Version").

Exercise of the rights referred to in paragraph 3.3 must not use the Final Published Version and extend only to the version of the Article accepted for publication including all changes made as a result of the peer review process, and which may also include the addition to the article by IOP of a header, an article ID, a cover sheet and/or an 'Accepted Manuscript' watermark, but excluding any other editing, typesetting or other changes made by IOP and/or its licensors (the "Accepted Manuscript") and must be accompanied by the following statement of provenance:

"This is the Accepted Manuscript version of an article accepted for publication in Journal of Physics: Condensed Matter.

IOP Publishing Ltd is not responsible for any errors or omissions in this version of the manuscript or any

version derived from it. The Version of Record is available online at [insert DOI].'

3.2 The rights are:

3.2.1 To make copies of the Final Published Version of the Article (all or part) for teaching purposes;

3.2.2 To include the Final Published Version of the Article (all or part) in a research thesis or dissertation provided it is not then published commercially;

3.2.3 To make oral presentation of the Final Published Version of the Article (all or part) and to include a summary and/or highlights of it in papers distributed at such presentations or in conference proceedings; and

3.2.4 To use original figures and text from the Final Published Version of the Article falling within the quota outlined in and subject to the STM Permissions Guidelines ([http://www.stm-
assoc.org/permissions-guidelines/](http://www.stm-
assoc.org/permissions-guidelines/)) at the relevant time in force.

For the avoidance of doubt, the Named Authors retain all proprietary rights in the Article other than copyright.

3.3 Additional rights of the Named Authors are to:

3.3.1 Use the Accepted Manuscript (all or part) without modification in personal compilations of the Named Authors' own works (provided not created by a third party publisher); and

3.3.2 Include the Accepted Manuscript (all or part) on the Named Authors' own Personal Website(s), institutional website(s), repositories, Scientific Social Networks and third party websites provided that this is fully in accordance with the Author Rights set out at the following url legal.ioppublishing.org/author-rights on the date of submission of the agreement.
Miscellaneous

4. To the extent that there are moral rights in the Article, all the Named Authors expressly reserve and assert their moral rights to be identified as the authors of the Article.

5. The Named Authors and/or the Copyright Owner shall execute such further documents, and take such actions and do such things, as may be requested by IOP at IOP's reasonable expense to give full effect to the terms of the agreement.

6. For the avoidance of doubt, the grants and assignment envisaged herein shall become effective only upon acceptance of the Article for publication. In the event that the Article is withdrawn prior to acceptance, or is rejected, this agreement shall have no effect and no party shall be bound by it.

7. The agreement shall be governed by English Law and subject to the non-exclusive jurisdiction of the English courts.

Confirmation

8. By selecting to publish on a subscription basis, the Submitting Author is responsible for ensuring that, where relevant all Named Authors, who are affiliated to a university/institution which has an open access policy which is incompatible with IOP's green open access policy, obtain a waiver for the Article from their institution or university's open access policy and retain such waiver as evidence of compliance. These Named Authors agree that they shall obtain such waivers and provide them to IOP promptly on request.

9. By typing the Submitting Author's name into the box at Part 3 below and clicking "Submit", the Named Authors agree to these terms. The Authorised Signatories of any third party Copyright Owner(s) and/or the Submitting Author agree, on behalf of such Copyright Owner(s), to these terms by typing the Copyright Owner's name into the "Copyright Owner" box at the top of the page.

Part 2 - Publication on a Gold Open Access basis

1.1 In consideration for acceptance and publication of the Article, the Named Authors of the Article and/or the Copyright Owner hereby assign, where necessary by present assignment of future copyright, to IOP with full title guarantee the entire copyright in all original material published as part of the Article (which expression includes but is not limited to the text, abstract, tables, figures and graphs, related corrigenda or "comments" and multimedia content but excludes any other item referred to as supplementary material and/or any video abstract) throughout the world for the full term of copyright (including any extensions or renewals thereof) for all media and formats, whether known or unknown. Such assignment shall be effective only if the Article (or any resubmission of the Article) is accepted for publication. For the avoidance of doubt, copyright does not subsist in any fundamental data underlying the Article and nothing in the agreement is intended to limit access to or use of such data.

1.2 If the Article, or any part of it, is protected by Crown copyright, in consideration for acceptance and publication of the Article, the relevant Named Authors and/or the relevant originating department or agency hereby grant IOP a non-exclusive royalty-free worldwide licence for the full term of copyright (including any extensions or renewals thereof) for all media and formats, whether known or unknown, to do in relation to the Article all acts restricted by copyright worldwide.

1.3 If all the Named Authors are employees of the US Government, they represent and warrant to IOP that the Article was prepared as part of their official duties. In such circumstances, or where the Article was created as part of a work for hire, none of the original content within the Article is subject to copyright protection as it is in the public domain.

1.4 In consideration for acceptance and publication of the Article, the Named Authors and/or the Copyright Owner hereby grant IOP a royalty-free non-exclusive worldwide freely transferrable licence for the full term of copyright (including any extensions or renewals thereof) to do in relation to any supplementary material not deemed to be part of the Article and/or any video abstract all acts restricted by copyright worldwide. This shall include, but not be limited to, making the material available under any licence that IOP deems appropriate for purposes including, but not limited to, the maximisation of visibility and the long term preservation of the content.

1.5 Each of the Named Authors consents to all publication and processing of their personal data by IOP, as that data is displayed on the Article, including, but not limited to, the names and email addresses of the Named Authors. Accordingly, the Named Authors shall not object on data protection grounds to the use of their personal data on the Article wherever IOP chooses to display it, whether itself or via a third party.

1.6 Each of the Named Authors and, where relevant, the Copyright Owner consents to the publication of the Article under the Creative Commons Attribution 3.0 Unported licence (CC BY 3.0) (<https://creativecommons.org/licenses/by/3.0/>) or any successor to that licence.

Representations and warranties

2.1 The Copyright Owner and/or the Submitting Author, on behalf of the Named Authors (as appropriate) represent and warrant that:

2.1.1 the Article is the original work of the Named Authors;

2.1.2 the Article has not been published previously in any form, other than in accordance with our [Preprint pre-publication policy](#);

2.1.3 each of the Named Authors has made a material contribution to the conception and/or writing of the Article, has received the final version of the Article, has agreed to its submission on the terms contained herein and takes responsibility for it and submission has been approved as necessary by the authorities at the establishment where the research was carried out;

2.1.4 the Submitting Author completes and returns the agreement as authorised agent for and on

behalf of all the Named Authors and Copyright Owner (as applicable) and has the full power to enter into the agreement and to make the grants and assignments it contains;

2.1.5 the Article has not been and shall not be submitted to another publisher prior to withdrawal or rejection by IOP;

2.1.6 the Article does not infringe any third party rights, it contains nothing libellous or unlawful, all factual statements are to the best of the Named Authors' knowledge true or based on valid research conducted according to accepted norms and all required permissions have been obtained in writing;

2.1.7 the Article explicitly acknowledges any third party funding and/or potential conflicts of interest; and

2.1.8 any supplementary material or video abstract is the original work of the Named Authors, or is the property of the Copyright Owner, or permission has been obtained from its owner(s) for its publication by IOP and permission has been obtained for the inclusion of any third party content.

2.2 The Named Authors and/or the Copyright Owner indemnify and will keep indemnified IOP against all costs and expenses suffered or incurred by IOP as a result of and/or arising out of any breach of the representations and/or warranties in this section 2.

The Named Authors' rights

3.1 The Named Authors and all third parties will have the rights to use the Article as described in the licence applied to the Article pursuant to paragraph 1.6, above, which shall include the right to copy, distribute and display the published version of the Article and create derivative works, subject to appropriate attribution.

3.2 Where the Article is used in accordance with paragraph 3.1 above, the following attribution shall be included subject to any additional terms of the licence under which the Article was published:

Article title
Named Author(s)
DOI
Journal citation
Name of the licence with a link to that licence
Indication if any changes were made

Miscellaneous

4. To the extent that there are moral rights in the Article, all the Named Authors expressly reserve and assert their moral rights to be identified as the authors of the Article.

5. The Named Authors and/or the Copyright Owner shall execute such further documents, and take such actions and do such things, as may be requested by IOP at IOP's reasonable expense to give full effect to the terms of the agreement.

6. For the avoidance of doubt, the grants and assignment envisaged herein shall become effective only upon acceptance of the Article for publication. In the event that the Article is withdrawn prior to acceptance, or is rejected, the agreement shall have no effect and no party shall be bound by it.

7. The agreement shall be governed by English Law and subject to the non-exclusive jurisdiction of the English courts.

Confirmation

8. By selecting to publish Gold Open Access, the Submitting Author is responsible for ensuring that the Article Publication Charge of the Journal is paid in full to IOP, pursuant to IOP's payment terms, unless otherwise agreed in writing with IOP.

9. By typing the Submitting Author's name into the box at Part 3 below and clicking "Submit", the Named Authors agree to all these terms. Authorised Signatories of any third party Copyright Owner(s) and/or the Submitting Author agree, on behalf of such Copyright Owner(s), to these terms by typing the Copyright Owner's name into the "Copyright Owner" box at the top of the page.

Part 3 – Confirmation and Execution

Please tick the appropriate boxes in section A, section B and section C below.

Section A - Please tick one of the boxes below to confirm how you would like the Article published (if it is accepted):

Subscription – Part 1 Applies

Section B - Please tick one of the boxes below to confirm the following:

For Subscription. Please tick this box to confirm that each Named Author, who is affiliated to a university/institution which has an open access policy which is incompatible with IOP's green open access policy, has obtained a waiver for the Article from their institution or university's open access policy. For more information refer to this [page](#).

Section C - Please ALSO tick one of the boxes below to confirm the basis upon which you are granting IOP the right to publish the article (if it is accepted):

Standard transfer of copyright (assignment) – please select this box unless one of the exceptions below applies to the Article.

Type your name here:

Kevin
Waters (the "Submitting Author")

Date:

02-Feb-2018

By clicking "Submit" and typing your name above, you shall be assumed to have read and understood all of the terms and conditions of the relevant part of the agreement and you will be agreeing to all of the terms and conditions and assignment (as the case may be) detailed above.

LAST UPDATED September 2017